MODELING AND CONTROL OF Nd:YAG LASER PERCUSSION DRILLING OF NICKEL-BASED SUPER ALLOYS

MARTIN RUTHANDI MAINA

MASTER OF SCIENCE
(Mechatronic Engineering)

JOMO KENYATTA UNIVERSITY OF AGRICULTURE AND TECHNOLOGY

2014

Modeling and Control of Nd:YAG Laser Percussion Drilling of Nickel-Based Super Alloys

Martin Ruthandi Maina

A thesis submitted in partial fulfillment for the of Degree of Master of Science in Mechatronic Engineering in the Jomo Kenyatta University of Agriculture and Technology

2014

DECLARATION

This thesis is my original work and has not been presented for a degree in any other University.

Signature:..... Date.....

Martin Ruthandi Maina

This thesis has been submitted with our approval as the University Supervisors.

Signature:..... Date.....

Eng. Prof. B. W. Ikua

JKUAT, Kenya

Signature:..... Date.....

Prof. G.N. Nyakoe

JKUAT, Kenya

Signature:..... Date.....

Dr. J.N. Keraita

DeKUT, Kenya

DEDICATION

I dedicate this work to my entire family. They have always been there to lift me up when I fall, and to celebrate with me when I succeed.

ACKNOWLEDGEMENT

First, I would like to thank the Almighty God for giving me a chance to pursue and complete this course successfully. Secondly, I would like to acknowledge my supervisors, Prof. Eng. Ikua B. W, Prof. Nyakoe G. N and Dr. Keraita J. N for their invaluable guidance and advice throughout my studies.

I would like to thank Jomo Kenyatta University of Agriculture and Technology for granting me the scholarship throughout my studies. My heartfelt appreciation goes to my course mates, L. Wanja and B. Wairimu for their encouragement, positive criticism and good co-existence especially during my course work.

I express my sincere thanks to all members of staff and all postgraduate students in Mechanical and Mechatronic Engineering departments for their input to my work during postgraduate seminars through their comments and suggestions.

Finally, I express my appreciation to my mum Mrs. Lucy W. Maina, and the entire family for their prayers, encouragement, guidance and love which kept me going.

TABLE OF CONTENTS

LIST OF TABLES

LIST OF FIGURES

LIST OF APPENDICES

LIST OF ABBREVIATIONS

ANFIS	Adaptive neuro-fuzzy inference system
ANN	Artificial Neural Network
ANOVA	Analysis of Variancek
BPL	Back propagation Learning
CW	Continuous Wave
DMD	Direct metal deposition
DOE	Design of Experiments
EBD	Electron Beam Drilling
ECD	Electro-chemical Drilling
EDM	Electro-Discharge Machining
FAM	Fuzzy Associative Memories
FDM	Finite Difference Method
FEM	Finite Element Method
FF	Feed Forward
FIS	Fuzzy Inference System
FLC	Fuzzy Logic Controller
FPP	Focal Plane Position
GUI	Graphics User Interface
HAZ	Heat Affected zone
KBS	Knowledge Based System
L-M	Lonberg-Marcoitte
LSE	Least Squares Estimate
Nd:YAG	Neodymium: Yttrium Aluminium Garnet
NNDF	Neural Network-Driven Fuzzy

PLD	Pulsed Laser Deposition
RL	Reinforcement Learning
RN	Recurrent Networks
RSM	Response Surface Method
TBC	Thermal Barrier Coating
TDNN	Time Delayed Neural Networks
UL	Unsupervised Learning

NOMENCLATURE

$\boldsymbol{A}$	Absorptivity
$\boldsymbol{A_{lq}}$	Absorptivity of liquid
$\boldsymbol{A_{wp}}$	Absorptivity of solid workpiece
$\boldsymbol{c_e}$	effective heat capacity $[JKg^{-1}K^{-1}]$
$\boldsymbol{c_p}$	specific heat capacity$[JKg^{-1}K^{-1}]$
$\boldsymbol{c_{pl}}$	specific heat of liquid $[JKg^{-1}K^{-1}]$
$\boldsymbol{c_{ps}}$	specific heat of solid $[JKg^{-1}K^{-1}]$
$\boldsymbol{d}$	beam diameter$[m]$
$\boldsymbol{d_{ent}}$	hole entrance diameter $[m]$
$\boldsymbol{d_{exit}}$	hole exit diameter $[m]$
$\boldsymbol{d_s}$	minimum spot diameter $[m]$
$\boldsymbol{E}$	Laser energy $[J]$
$\boldsymbol{E_1}$	Energy state 1 $[J]$
$\boldsymbol{E_2}$	Energy state 2 $[J]$
$\boldsymbol{f}$	Focal length $[m]$
$\boldsymbol{f_r}$	Frequency $[Hz]$
$\boldsymbol{\Delta f}$	Depth of focus $[m]$
$\boldsymbol{g}$	gravitational acceleration $[ms^{-2}]$
$\boldsymbol{H_f}$	Photon energy $[J]$
$\boldsymbol{I_0}$	incident laser intensity $[Wm^{-2}]$
$\boldsymbol{I_{abs}}$	absorbed laser intensity $[Wm^{-2}]$
$\boldsymbol{k}$	thermal conductivity$[Wm^{-1}k^{-1}]$
$\boldsymbol{k_{lq}}$	thermal conductivity of liquid $[Wm^{-1}k^{-1}]$
$\boldsymbol{k_{wp}}$	thermal conductivity of solid $[Wm^{-1}k^{-1}]$

$\boldsymbol{L_m}$	latent heat of melting $[JKg^{-1}]$
$\boldsymbol{L_v}$	latent heat of vaporisation $[JKg^{-1}]$
$\boldsymbol{m_v}$	mass of vapour $[kg]$
$\boldsymbol{\dot{m}_m}$	molten liquid ejection rate $[kgs^{-1}]$
$\boldsymbol{\dot{m}_s}$	solid melting rate $[kgs^{-1}]$
$\boldsymbol{\dot{m}_v}$	vaporisation rate $[kgs^{-1}]$
$\boldsymbol{M_m}$	molar mass $[kgmol^{-1}]$
$\boldsymbol{n}$	input-output data
$\boldsymbol{n_c}$	Checking data set
$\boldsymbol{n_t}$	Training data set
$\boldsymbol{O}$	output
$\boldsymbol{p_v}$	vapour pressure $[pa]$
$\boldsymbol{p_o}$	incident laser power $[w]$
$\boldsymbol{r}$	radial distance $[m]$
$\boldsymbol{R_g}$	specific gas constant $[JKg^{-1}K^{-1}]$
$\boldsymbol{R_u}$	universal gas constant $[8.314Jmol^{-1}K^{-1}]$
$\boldsymbol{R_f}$	reflectivity
$\boldsymbol{t}$	time $[s]$
$\boldsymbol{t_m}$	time required to initiate melting $[s]$
$\boldsymbol{t_w}$	workpiece thickness $[m]$
$\boldsymbol{T}$	temperature $[K]$
$\boldsymbol{T_{bl}}$	boiling temperature $[K]$
$\boldsymbol{T_{lq}}$	temperature of liquid $[K]$
$\boldsymbol{T_{lo}}$	melt surface temperature $[K]$
$\boldsymbol{T_m}$	melting temperature $[K]$
$\boldsymbol{T_{wp}}$	temperature of solid $[K]$

$\boldsymbol{T_0}$	ambient temperature $[K]$
$\boldsymbol{W_p}$	pth rule firing strength
$\boldsymbol{X}$	Input
$\boldsymbol{z}$	vertical distance from the workpiece surface $[m]$
$\boldsymbol{z_m}$	melting front $[m]$
$\boldsymbol{z_{m0}}$	melting front at the hole centre $[m]$
$\boldsymbol{z_v}$	vaporisation front $[m]$
$\boldsymbol{z_{v0}}$	vaporisation front at the hole centre $[m]$
$\boldsymbol{\alpha}$	thermal diffusivity $[m^2 s^{-1}]$
$\boldsymbol{\alpha_{lq}}$	thermal diffusivity of liquid $[m^2 s^{-1}]$
$\boldsymbol{\alpha_{wp}}$	thermal diffusivity of solid $[m^2 s^{-1}]$
$\boldsymbol{\lambda}$	Wavelength $[m]$
$\boldsymbol{\theta}$	Taper angle $[degree]$
$\boldsymbol{\theta_b}$	beam divergence angle $[degree]$
$\boldsymbol{\mu}$	Universe of discourse
$\boldsymbol{\mu_f}$	Heat flux $[Wm^{-2}]$
$\boldsymbol{\rho_{ql}}$	density of liquid $[kgm^{-3}]$
$\boldsymbol{\rho_{wp}}$	density of solid $[kgm^{-3}]$
$\boldsymbol{\rho_{th}}$	thermal energy density $[Jm^{-3}]$

ABSTRACT

Non-Conventional methods have recently been employed in the drilling of materials such as super alloys which are hard to machine using mechanical conventional methods. These materials are mainly used in turbines in the power generation and aerospace industries. One of the recently developed non-conventional methods for drilling is using pulsed lasers whereby a laser beam is focused to a spot equal in diameter to the hole to be drilled. Pulsed lasers such as Nd:YAG are mainly employed for this process.

Laser percussion drilling is commonly employed to produce holes with small diameters, usually less than 1mm. With percussion drilling, the control of hole parameters such as taper, entrance and exit hole variation and roundness is difficult and these parameters are of utmost importance for small holes. Selection of machining parameter combinations for obtaining optimum circularity at entry and exit and minimum hole taper is a challenging task owing to the presence of a large number of process variables. There is therefore need to develop a control system that is able to adjust the various process parameters to the optimum values and hence control the drilling process.

The main aim of this study was to model the laser percussion drilling process and to develop a control system for optimizing the process by controlling the laser power and pulse duration based on the hole diameters and taper. A neuro-fuzzy strategy for control of machining parameter settings for the generation of the maximum circularity at entry and exit and minimum hole taper was adopted. A controller based on adaptive neural fuzzy inference system (ANFIS) was developed for the laser percussion drilling process.

In this study, the effects of laser machining parameters, namely laser power and pulse

duration, were successfully investigated. These have been proven to bear a great influence on the laser drilling process. A model for predicting the optimal laser parameters for quality drilling of Nickel-based super alloy-Inconel 718 was successfully developed. Inconel 718 was chosen since it is one of the commonly employed nickel alloys in the turbines. The model satisfactorily predicted the hole tapers and diameters, given inputs of laser power and pulse duration. The results showed that both laser power and pulse duration have great influence on the hole geometric parameters. Hole taper reduces with increase in both laser pulse duration and laser power. Hole diameters increase with increase in both laser power and pulse duration. A neuro-fuzzy controller was then developed based on $MATLAB^R$ and $LabVIEW^R$ platforms. The controller was used to control the laser percussion drilling by simulating a drilling environment. It was demonstrated that a neuro-fuzzy based controller effectively controls the hole diameters and taper through in-process adjustments of laser power and pulse duration. While using the controller, the diameters increase with increase in peak power and pulse duration upto an optimum level beyond which the peak power and pulse duration remain constant. The hole taper decreases with increase in peak power and pulse duration upto an optimum level beyond which the peak power and pulse duration remain constant. The ANFIS based neuro-fuzzy contoller read the input values from a spreadsheet file. Using the learning capabilty of artificial neural networks, the controller was able to compute the optimum values for laser peak power and pulse duration. Artificial neural networks have excellent capabality for approximation of process performance. Thus, the controller helps maintain the peak power and pulse duration at optimum levels.

CHAPTER ONE

1.0 INTRODUCTION

1.1 Background

Super alloys are commonly used in turbine engines in regions that are subject to high temperatures, which require high strength, high temperature creep resistance, fatigue life, phase stability, as well as corrosion resistance. Modern turbine stage inlet temperatures exceed the melting point temperatures of turbine blade materials. To combat and avert failure of turbine blades in turbine engines resulting from these excessive operating temperatures, film cooling has been incorporated into blade designs. In film cooling, cool air is bled from the compressor stage, ducted to the internal chambers of the turbine blades, and discharged through small holes in the blade walls. This air provides a thin, cool, insulating blanket along the external surface of the turbine blade [1].

Cooling holes can be produced by methods such as electro-chemical drilling (ECD), electron beam drilling (EBD), electro-discharge machining (EDM) and laser drilling [1]. Compared to laser drilling, these methods have various disadvantages. EDM process uses discrete discharges to drill the hole. It is substantially slower than laser drilling and it is not suited to the production of holes at high or variable incidence angles where multiwire heads cannot be used. More so, it requires relatively complex consumables tooling and electrolyte fluids, both of which contribute adversely to cost of hole production. ECD is slow and as a side effect it produces a lot of waste. EBD requires use of a vacuum chamber which makes it complex [2].

Laser beam machining is based on the conversion of electrical energy into light energy and then into thermal energy. All types of lasers emit an intense, coherent, highly collimated beam of single wavelength light. This narrow beam is focused by an optical lens to project a small, intense spot of light on the workpiece surface. Optical energy is converted into heat energy upon incidence and temperatures generated can be high enough to melt or vaporize any material [3]. Laser drilling offers ability to produce small diameter holes with high aspect ratios. It is a non-contact process which leads to no tooling wear or breakage, and minimal material distortion. It leads to highly accurate and consistent results with precise control of heat input. More so, it offers ease of programming and ready adaptability to automation [2].

Laser Percussion drilling is used for drilling relatively small holes; less than 1.0 mm diameter. While holes less than 6.5 mm deep can be percussively drilled with high power systems, the maximum material thickness for small holes is limited. The qualities of a hole produced by laser drilling are judged on a number of different characteristics. The geometric factors are hole roundness, hole taper and variation in hole entrance diameter. Various laser parameters have varying effects on the geometric factors of the hole [4]. The laser parameters include peak power, pulse width, pulse frequency, number of pulses, assist gas pressure, assist gas nozzle diameter, focal plane position, and the stand-off distance [5]. Owing to the complexity of this process and also the number of parameters involved, modeling is useful since the process is unfeasible to study through experiments only.

Machining systems that employ artificial intelligence reduce the machining time and increase the accuracy of the machining process, hence lowering the cost of production [6]. Fuzzy logic control systems have benefits of replicating all desired features of human input, while maintaining all the advantages of closed-loop automation control. One of

the major problems in the use of the fuzzy logic control is the difficulty of choice and design of membership functions to suit a given problem. A systematic procedure for choosing the type of membership function and the ranges of variables in the universe of discourse is still not available. Tuning of the fuzzy controller by trial and error is often necessary to get a satisfactory performance. However, the neural networks have the capability of identifying the characteristic features of a system that can be extracted from the input-output data. This learning capability of the neural network can be combined with the control capabilities of a fuzzy logic system resulting in a neuro-fuzzy inference system [7].

1.2 Problem Statement

Super-alloy development has relied heavily on both chemical and process innovations and has been driven primarily by the aerospace and power generation industries. Super-alloy products that are subjected to high working temperatures and corrosive atmosphere are coated with various types of coatings [8]. This makes them even more difficult to machine using other methods hence necessitating laser application. One such super alloy is nickel based Inconel 718 which finds great application in the manufacture of turbine parts. The small size of the holes (usually less than 1 mm diameter) required in the turbines renders mechanical methods inappropriate. High quality drilling of super-alloys can be achieved by application of diode pumped solid state Q-switched Nd:YAG laser at fundamental wavelength of 1064 nm [3].

Hole tapering is one of the inherent manufacturing problems associated with laser percussion drilling. When a series of laser pulses are delivered to a point on a workpiece, the incident laser energy due to the laser pulses leads to vaporization of the molten

material and hence generation of recoil pressure which is responsible for ejection of molten material in the form of droplets. Also affected is the hole circularity at the entry and exit [4]. These imperfections affect airflow over the surface of the component which in turn affects the lifespan of the component. The Nd:YAG laser parameters namely, laser power and pulse length, bear a great influence on the quality of the drilled holes. These should be carefully controlled to produce good quality holes for the various applications [9]. There is, therefore, the need for research on the set of optimum laser drilling parameter combinations, and also the need for development of a control system that is able to adjust the various process parameters to the optimum values.

1.3 Objectives

The main objective was to model and develop a control system for the laser percussion drilling process. To achieve this objective, the following specific objectives were accomplished;

1. Development of a model for predicting the optimal laser process parameters for laser percussion drilling using finite element method.
2. Validation of the model through comparison with experimental data.
3. Application of the model to investigate the effects of laser parameters on desired quality attributes in drilling of Nickel-based Super alloys.
4. Development of a Neuro-fuzzy controller for the laser percussion drilling process and investigation of its performance on the process.

1.4 Justification of the study

Super-alloys exhibit excellent mechanical strength and creep resistance at high temperatures, good surface stability, and corrosion resistance. These are hard-to machine materials. They find great application in the power generation and aerospace industries. To enhance functionality of the super alloys, they are coated with various types of coating. This may make them even more difficult to machine hence necessitating laser application for machining. Laser Percussion drilling is a very important enabling technology within these industries as it allows for the drilling cycle times to be reduced when producing cooling holes [9]. Tapering and non-circularity of the holes result during this drilling process. These have adverse effects on the airflow over the surface of the component affecting the lifespan of the component [4]. These imperfections can not be avoided but they can be minimized by selecting the appropriate laser parameter combinations for the laser drilling process. Selection of these combinations is a challenging task owing to the presence of large number of parameters involved. This research sought to model the laser drilling process and to develop a neuro-fuzzy control system to help predict parameter combinations for the process and control the entire process to reduce the taper and enhance circularity of the drilled holes.

1.5 Outline of thesis

This thesis contains five chapters. The first chapter provides an introduction to the research by highlighting the existing problem, the objective and the justification of the research work. Chapter 2 provides a literature review on laser drilling process and the various approaches employed in the modeling and control of the process. It also

provides a literature review on artificial intelligence specifically the aspects employed in this work. In Chapter 3, the approaches employed to develop the laser drilling model and the neuro fuzzy controller are discussed. Chapter 4 discusses the results obtained and finally, Chapter 5 outlines the conclusion and recommendations.

CHAPTER TWO

2.0 LITERATURE REVIEW

2.1 Overview

Producing macro or micro holes of high aspect ratio in super alloys is beyond the capabilities of conventional machining processes. High tool wear and excessive heat generation have rendered mechanical drilling unsuitable [10]. Past studies have shown that laser drilling is well suited for the drilling of thermal barrier coated (TBC) super-alloys since both the ceramic and metallic layers can be processed [8–12]. In comparison, the competing technology of electrical discharge machining is limited to conducting substrates and therefore cannot machine TBC coated components [11]. An example of such is Nickel based Inconel 718. Nickel based super-alloys have mainly been employed in steam turbines for power generation and jet engines [9].

High machining rate of the laser percussion drilling action makes it a prime candidate for drilling such components as combustion chambers, which have between 40,000 to 50,000 holes. Other components such as turbine and guide vanes contain fewer holes, typically 50 to 200, but given the total numbers of components involved, percussion drilling still has the potential to provide significant cost-benefit [12]. The determination of efficient laser process and laser beam parameters for the drilling process is a major challenge for the power generation and aerospace industry [8]. Research on the application of lasers in drilling is thus gaining increasing interests.

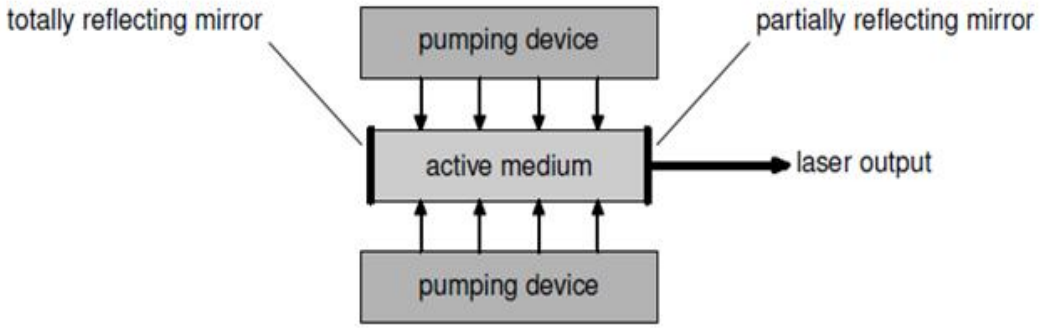

Figure 2.1: A schematic diagram of a laser

2.2 Laser fundamentals

Figure 2.1 shows a schematic diagram of a laser. Laser is an acronym for Light Amplification by Stimulated Emission of Radiations. The basic laser consists of two mirrors which are placed in parallel to each other to form an optical resonator, that is a chamber in which light would oscillate back and forth between the mirrors forever, if not prevented by some mechanism such as absorption. One of the two mirrors is partially transparent to allow some of the oscillating power to emerge as the operating beam. The other mirror is totally reflecting. Between the mirrors an active medium resides which is capable of amplifying the light oscillations by the mechanism of stimulated emission [2, 3].

There is a change from one energy level to another when light radiation interacts with matter. This energy difference between the levels must be balanced by the emission or absorption of radiant energy and the relevant relation is given by [3]:

$$H_f = hf = \frac{hc}{\lambda} = E_2 - E_1 \tag{2.1}$$

where h is Planck's constant, f is the frequency, c is the speed of light, λ is the wavelength, E_2 and E_1 are the energies of the two states involved and H_f is the photon energy.

There are three different ways in which light radiation interact with energy levels namely, fluorescence, absorption, and stimulated emission [2, 3, 13]. These processes are shown schematically in Figure 2.2. The wavy arrows represent photons while the horizontal straight lines represent energy levels. Transition of the electron from one level to another is represented by the vertical arrows [2, 3].

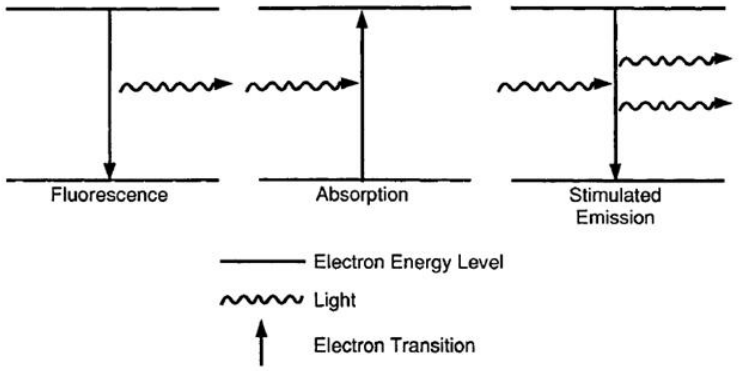

Figure 2.2: Schematic diagram of the interaction of light with electronic energy levels

During fluorescence, a molecule in an upper energy level spontaneously decays to a lower energy level, emitting the energy in form of a photon with the appropriate frequency. For absorption, light of frequency f and wavelength λ interacts with a molecule in a low energy level raising it to a higher level. The light energy is hence absorbed by the molecule [2]. For stimulated emission, a molecule in an upper energy level interacts with incoming light of frequency f. The molecule is stimulated to drop to a lower energy level emitting the energy difference as light. This is the process responsible for laser operation [2].

A laser needs a material with a suitable set of energy levels called the active medium

for the laser. This active medium can be a solid, liquid, or gas. There are various types of lasers that are commonly used for laser material processing [13]. These include gas lasers, solid state lasers, semiconductor lasers and liquid dye lasers. In gas lasers the active laser medium is gas. Semiconductor lasers use semiconductor materials as active medium and they are based on radiative recombination of charge carriers. For liquid dye lasers, liquid solution consisting of an organic dye dissolved in liquid solvent acts as the laser active medium [2, 15].

In solid state lasers, a crystalline solid host is doped with ions that provide the required energy states. The transition metal ions are the the ions. The oxides or fluorides are used as the host crystals [3]. Nd:YAG laser which has a wavelength of 1064 nm is the most widely used solid state laser. The laser beam is generated through a combination of the YAG host crystal and the Nd^{3+} ions. Nd^{3+} ions improves the laser efficiency while undoped pure yttrium-aluminium garnet gives high thermal conductivity and good optically isotropic property [2, 13].

Nd:YAG lasers operate in continuous wave or pulsed modes. The pumping source may be a lamp or semiconductor diode laser [14]. These lasers are used for applications such as drilling, welding and cutting. Nd:YAG lasers are also employed in medical treatment. In drilling applications, Nd:YAG lasers are widely used for drilling shaped holes of aircraft turbine blades to improve the cooling efficiency in the film cooling process. In welding applications, the pulsed beam is delivered to the workpiece through an optical fibre to improve the system flexibility [15]. Nd:YAG lasers are also used in high precision cutting of reflective materials or cutting process where the delivery of the laser beam through an optical fibre is required. In comparison with the CO_2 gas laser, Nd:YAG lasers give lower beam power but higher peak power when operating in pulsed mode, hence allowing machining of thicker workpieces [9, 15].

2.3 Laser drilling mechanisms

Laser drilling is a complex process involving several thermal and physical mechanisms. A high intensity laser beam is focused into a small on a workpiece. Laser energy is absorbed and conducted into the workpiece. This results in heating, melting and vaporisation of material. Mass removal in the form of liquid or vapour leads to formation of a hole. Further irradiation of laser beam may cause ionization of the vapour trapped in the cavity leading to the formation of the plasma [10, 13].

When a laser beam is focussed onto the workpiece surface, it may be absorbed and/or reflected and in case of transparent materials, transmitted. Absorptivity and reflectivity indicate the ability to absorb laser energy of material. Several factors affect the absorptivity. These include laser wavelength, incident angle and polarization of the laser beam, temperature of material, surface roughness of material, and oxide formed on the surface [14]. Opaque material have negligible transmissivity [13]. The absorptivity, A, can be expressed as:

$$A = 1 - R_f \tag{2.2}$$

where R_f is the reflectivity of material.

Laser drilling process can be divided into four phases namely; surface heating, surface melting, vaporisation, and melt ejection [5]. Figure 2.3 shows the material removal mechanisms in laser drilling.

The initial stage is the surface heating phase whereby the laser energy heats up the

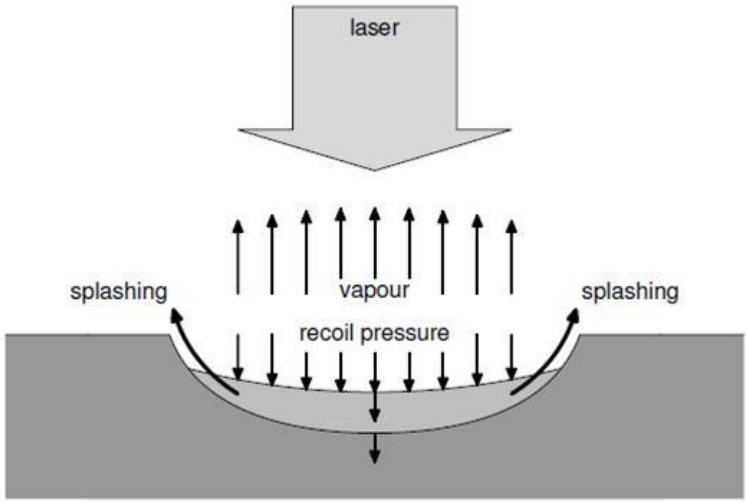

Figure 2.3: Schematic diagram of the material removal mechanisms in laser drilling

solid from ambient temperature to the melting point. A series of multiple pulses are employed in case of laser percussion drilling. Each successive laser pulse is separated by a pulse off time. There is no laser beam-substrate interaction during the pulse off time, hence leading to a temperature drop [13, 14].

Melting begins when the energy of the laser beam incident on the solid surface is sufficient. The melting occurs dominantly in the vertical direction [15]. With the beam still incident on the substrate, the temperature rises upto to the boiling point and vaporisation begins. The combined effects of the vaporisation and liquid expulsion leads to cavity formation [15].

The significant material removal mechanisms during laser drilling are vaporization and the physical expulsion of the melt. The dominant mechanism depends on the irradiation conditions and material properties. Holes drilled with purely evaporative material removal mechanisms are generally marked with clean surface and sharp boundaries without recast layer, spatter, and associated dross. On the other hand, material removal by melt expulsion is an energetically efficient mechanism. Generally, the energy

required to remove the material via melt expulsion is about one quarter of that required to vaporize the same volume [13, 15].

Melt expulsion during the drilling process may be due to pressure generated from inside the melt (explosive melt expulsion) or from outside the melt (hydrodynamic melt expulsion). Explosive melt expulsion can take place in some of the following cases [13, 14]:

1. Increase in the volume of the chemical decomposition reaction products due to subsurface overheating.
2. Vaporization of the lowest melting point components in a multicomponent system while the other components are still in molten state.
3. Increase in volume of the dissolved contaminant gases at high temperature at subsurface layer of metallic systems.

Hydrodynamic melt expulsion takes place along the surface of the laser-drilled hole towards the periphery of laser spot and is due to differential vapor (plasma) plume pressure on the molten surface [13, 14].

Analysis of melt expulsion process shows that the molten material flowing along the wall of the hole breaks up into discrete droplets while leaving the hole due to surface tension effects. At the end of the drilling process, the molten material which could not be ejected in form of droplets form a thin layer of recast material at the periphery of hole [13].

2.4 Laser Percussion drilling technique

There are three common techniques for laser drilling namely; single pulse drilling, trepanning drilling and percussion drilling [2]. Of interest in this study is the percussion drilling technique.

Single pulse drilling is used for drilling narrow (less than 1 mm) holes through thin (less than 1 mm) plates. High pulse energies are supplied in drilling with single pulse because the irradiated energy levels must be sufficient to vaporize the material in single pulse. Examples of its application are drilling of the sieves and filters. Drilling on-the-fly process, in which laser beam or workpiece or both are moved relatively, may be incorporated into the single pulse drilling technique in order to increase the production rate.

In trepanning, wider holes (less than 3 mm) in thicker plates (less than 10 mm) are produced by drilling a series of overlapping holes around a circumference of a circle so as to cut a contour out of the plate. Trepanning can be performed by translating either the workpiece or the focusing optic. The process is much similar to contour cutting and can be performed by the laser operating in the continuous wave (CW) or pulsed mode. CO_2 and Nd:YAG lasers are most commonly used in trepanning.

In percussion drilling, a series of short pulses (10^{-12} to 10^{-3} s) separated by longer time periods (10^{-2} s) are directed on the same spot to form a through hole. Each laser pulse contributes to the formation of hole by removing a certain volume of material. Pulsed Nd:YAG lasers are most commonly used for percussion drilling because of their higher energy per pulse. Percussion drilling is used to produce narrow holes (less than 1.3 mm) through relatively thicker (up to 25 mm) metal plates. High speed of

the percussion drilling makes it the most cost-effective method in applications such as drilling of combustion chambers having 40,000-50,000 holes and other applications such as drilling of turbine and guide vanes having 50-200 holes, given the large number of total components involved [2, 15]. Figure 2.4 shows the percussion drilling technique.

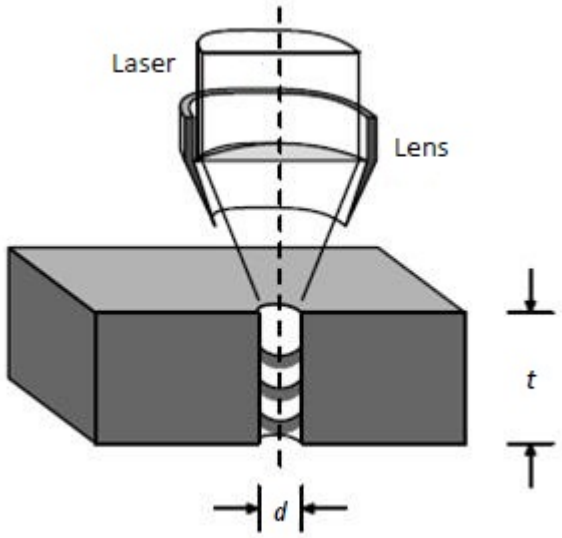

Figure 2.4: Percussion drilling

Percussion drilling can operate at lower beam energy which enables drilling of the high aspect ratio holes i.e., up to approximately 1:100 for through holes and 1:20 for blind holes. Although the recommended maximum thickness of material to be laser drilled is 50 mm, this aspect ratio implies that laser percussion drilling can produce a hole in material with thickness greater than 50 mm [2, 15].

The physical processes occurring during laser percussion drilling can be split up into three stages. Initially a thin region of molten material is formed by absorption of laser energy at the target surface. After some time the surface of this melt pool reaches vaporization temperature. The sudden expansion of the vapor evaporating from the surface eventually leads to the splashing stage when the melt pool is pushed radially out by the recoil pressure. Melt expulsion occurs when the pressure gradients on the

surface of the molten layer are sufficiently large to overcome the surface tension forces and expel molten material from the hole. On its way of escaping out some part of this molten material may resolidify at the walls. The timescales for these three stages are between 10^{-5} and 10^{-4} s for melting and 10^{-5} s for splashing and solidification [2,14,15].

Since laser drilling requires the temperature of the target to be raised above boiling point, lasers with pulse lengths in the region of several hundred microseconds, or even less, are most commonly used in laser drilling applications. In addition, the holes with smaller diameter and larger aspect ratio require the laser with shorter wavelengths. This makes the CO_2 and Nd:YAG lasers primary candidates for laser drilling. The range of hole diameters possible for typical thicknesses of metal, with Nd:YAG laser is 0.001-0.060 in., whereas with CO_2 laser the range is 0.005-0.050 in [14].

Low *et al* [17] compared the hole drilled by a linearly increasing inter-pulse with that produced by a normal pulse delivery pattern. When a modulated pulse train was used, the spatter accumulated around the hole entrance was reduced while the material ejected from the hole exit was increased. Using a linearly increasing inter-pulse train improved the hole taper. This was attributed to the attenuation of laser intensity at the hole exit which resulted from multiple reflections and better absorption along the hole wall.

Peters *et al* [18] carried out an investigation of Nd:YAG laser percussion drilling process using high speed filming with the aim of determining dominant factors for the process. They noted that with percussion drilling process, there are a large number of factors which can potentially affect this process, so it is important to know which ones are critical, and therefore need to be well-controlled. They used experimental design techniques to carry out their work. In order to understand how changes in these

dominant factors affect the process, they used a high speed camera operating at up to 40,000 frames per second, which gave 40 frames within the 1 ms second drilling laser pulse. The laser used for drilling in this experiment was a Lumonics 704 TR which has a beam quality M2 of 24, for laser pulse lengths from 0.3-1.0 ms, and peak powers from 4-33 kW. The workpiece material used was a nickel-based super alloy C263, with a thickness of 3 mm. Drilling events were recorded both with and without, an assist gas in order that its effect on the process could be observed. Laser percussion drilling mechanism in Nickel alloys with pulse energies of up to 30 J in 1 ms was studied in this experiment. They concluded that the process consisted of three stages namely: Initial coupling of the laser into the surface, breaking down its reflectivity, and giving rise to a plasma plume above the workpiece. This was followed by majority material removal and finally continued hole development.

They noted that pulse shaping can improve hole quality, with the most successful being split into two parts, with the first half at relatively low power. During this part no plasma is produced, and only a small amount of material is removed. The majority of the material is instead removed during the second half of the pulse. It is thought that the pre-heat provided by the first half of the pulse provides a more controlled coupling into the material.

Ghoreishi et al [19] developed a statistical model for laser percussion drilling for hole taper and circularity control. They studied various variables in an attempt to understand the possibility of controlling simultaneously the two important characteristics of a laser drilled hole: taper and circularity. Six variables, namely the peak power, pulse width pulse frequency, number of pulses, assist gas pressure and focal plane position, were selected as independent controllable factors. Response surface method was used to statistically analyse the process. For each variable, five levels were considered and

the experiments were performed based on a central composite design. A fibre-optic delivered Nd:YAG laser was used to drill mild steel sheets with a thickness of 2.5 mm. The entrance diameter, the taper and the ratio of maximum to minimum Feret diameter for the hole entrance (circularity) were considered as responses/outputs in order to evaluate the process performance in terms of hole taper and circularity. Statistical modeling was carried out to develop mathematical models to relate the responses (outputs) to the six independent variables through multiple regression. A complete analysis of variance (ANOVA) was performed to test the significance of the obtained. The developed models were verified by experiments. The work showed that the pulse width and peak power have significant effects on the hole diameter, hole taper and hole circularity. However, the pulse frequency has no effect on these three hole characteristics. The number of pulses has no significant effect on hole diameter and circularity but has a significant effect on hole taper.

2.5 Influence of laser and process parameters on percussion drilling process

Although laser percussion drilling offers advantages such as high processing speed, high tolerance, and repeatability, a percussion drilled hole suffers from some drawbacks which include resolidified material, hole taper, and non-circularity of the hole as shown in Figure 2.5 [15]. In addition, barrelling, heat affected zone (HAZ), and microcracking may also be observed in pulsed drilled holes.

Recast layer refers to the resolidified material deposited on the hole wall. If the resolidified material is found at the hole entrance and exit, it is refered to as spatter and dross, respectively. Hole taper represents the decrease of hole diameter with hole depth. Hole

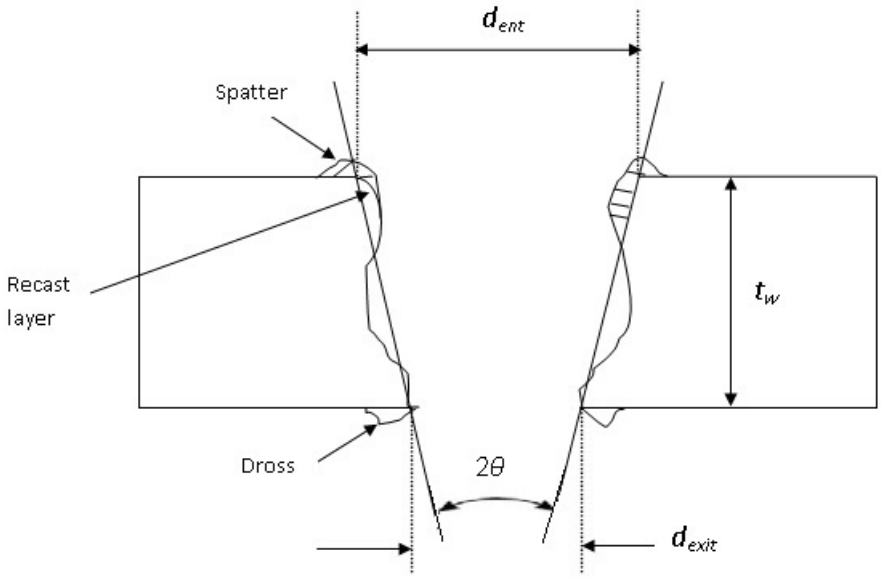

Figure 2.5: Illustration of laser drilled hole

circularity is defined as the ratio of the maximum to minimum diameters of the hole. Expression for the hole taper (θ) is given as follows [2, 15]:

$$\theta = tan^{-1}(\frac{d_{ent} - d_{exit}}{2t_w}) \tag{2.3}$$

where d_{ent} , d_{exit} , and t_w are diameter at hole entrance, diameter at hole exit, and thickness of material, respectively.

These defects are unavoidable during the laser drilling process but can be minimized through selection of the appropriate operating conditions. Various laser parameters and process parameters are found to have influence on the laser drilled hole characteristics [15].

Laser parameters involved include pulse shape, laser wavelength, transverse modes,

pulse energy, pulse duration, pulse repetition frequency and beam divergence. Material parameters include superalloy properties, ceramics properties, surface reflectivity and thickness. Environmental parameters include humidity and temperature. Assist gas parameters include the type of gas, gas pressure and also the nozzle design for the gas delivery. Focussing lens setting parameters include the lens focal length and focal position [3, 15].

2.5.1 Assist gas

Assist gas facilitates the material removal, blowing out the resolidified material, protecting the optics from the debris ejected and providing additional cooling to the substrate [2]. Various assist gases such as compressed air, oxygen, argon, and nitrogen have been used for drilling different materials. Inert gases are used as assist gas when the laser-drilled holes free from oxide layer are desired. Air can also produce acceptable quality holes in some metals such as aluminum [2, 3].

Assist gas affects material removal and drilling rate. The gas flows coaxially in tandem with the laser beam. Therefore, the pressure of the assist gas would disturb the laser beam profile irradiating the workpiece thereby scattering or blocking some incident energy. This results to a non-linear drilling profile hence enlargement of the drilled hole [3].

Due to exothermic reactions and oxidation reactions involved during the drilling process, the type of assist gas used bears a great influence on the final drilled hole quality. Exothermic energy is normally added to the process when using oxygen, hence it is widely used as an assist gas to increase the material removal rate. The oxide formed at the surface reduces the viscosity of the liquid metal. This promotes the melt ejection.

Oxygen assist gas also causes a change in the absorptivity, and a change in the melting temperature of the material [2, 3].

In addition to the type of assist gas and gas supply pressure, the geometry and quality of laser-drilled holes is also affected by nozzle design, nozzle-material standoff. Nozzle designs differ significantly for various laser drilling setups, but typical orifice openings range from 2.5 to 6.0 mm and 0.75 to 2.5 mm for percussion drilling and trepanning, respectively. Nozzle-material standoff is the distance between the nozzle tip and the surface of the workpiece and often equals the nozzle-focal point standoff when the beam is focused on the surface of the workpiece. Nozzle-materials standoff depends on the laser type, nozzle type, and gas flow rates and often range from 4 to 40 mm and 0 to 15 mm for percussion drilling and trepanning, respectively. Nozzle stand-off with Nd:YAG laser is about 5 mm. In gas-assisted laser drilling, the hole depth is found to be decreased with decreasing the nozzle-material standoff. For best laser drilling results the nozzles must be aligned coaxially with the focused laser beam [15].

Khan *et al.* [16] studied the effects of the assist gas type and nozzle size on the nanosecond laser percussion drilling of 316L stainless steel. Experiments were performed using oxygen, air and also with no assist gas. There was a reduction in the drilling velocity when assist gas was employed. With oxygen assist gas, lowest drilling rate was achieved. However, the diameter and taper of the hole drilled with the assist gas were larger compared to those obtained from drilling without assist gas. Nozzle diameter was also found to have impact on hole quality in that drilling with the smallest gas nozzle produced the thinnest recast layer.

Low *et al.* [20] studied the influence of assist gas on spatter accumulated during laser percussion drilling of Nimonic 263 alloy. They considered four gases namely; argon,

nitrogen, compressed air and oxygen. It was found that oxygen assist gas gave the lowest spatter thickness with the weakest spatter bonding strength.

It can be concluded that the type of assist gas used bears a great influence on the final drilled hole quality due to exothermic reactions and oxidation reactions involved during the drilling process. Exothermic energy is normally added to the process when using gases such as oxygen. This leads to an increase the material removal rate. The oxide formed at the surface reduces the viscosity of the liquid metal. This promotes the melt ejection. Assist gas also causes a change in the absorptivity, and a change in the melting temperature of the material. For this study laser drilling without assist gas was considered and hence the effects of the various assist gases were not included in the modeling stage.

2.5.2 Laser machining parameters

Laser parameters include: laser peak power, pulse duration, pulse frequency, pulse energy, number of laser pulses, and pulse shape. Past research work has shown relationship between these laser parameters, hole geometry, and metallurgical quality. For any laser machine, pulse peak power, pulse width and pulse energy are normally interdependent [15].

As peak power increases, more energy is transferred into the material creating more vapour above the workpiece surface. The large amount of vapour then causes a large recoil pressure above the melt liquid layer and enhances the liquid removal. High peak power can be achieved by either increasing the pulse energy or by reducing the pulse width. However, if a lower peak power is required, then it is recommended to adjust pulse energy rather than pulse width. At high laser pulse energy the exit diameter

increases due to pressure exerted by the vaporization of the material in the hole [15,21].

Pulse width/duration bears a significant influence on the hole properties. Longer pulse results in larger diameter and the deeper holes. However, too long pulse duration may be unable to produce the through hole. Previous studies [5, 19, 25] have revealed that drilling with a short pulse duration reduces the severity of micro-cracking and the recast layer thickness, improves hole circularity and process repeatability, and causes less heat affected zones (HAZ) defects. However, for nanosecond and femtosecond pulse drilling, HAZ does not depend on pulse width setting [15, 21].

Ghoreishi [19] investigated the effects of pulse frequency in laser percussion drilling process. Ghoreishi used the response surface method in order to study the relationship between various parameters. It was found that laser frequency had minimal effect on the process, specifically on geometrical parameters of the drilled hole. Pulse frequency had no significant effect on the maximum drill depth. However, the interaction time to reach the maximum drilling depth varied depending on the pulse frequency [3, 15, 21].

Han and Pryputniewicz [22] investigated the effect of pulse duration on laser drilling of stainless steel. They found out that too long pulse duration may be unable to produce the through hole. As the pulse width was extended to more than 1.75 ms, no through hole was achieved for stainless steel 304 with a thickness of 30 mm. They attributed this to the occurrence of the laser-supported absorption (LSA) at high laser pulse energy.

In case of percussion laser drilling, the numbers of laser pulses are delivered successively at the same spot and the material is removed after each pulse. The number of pulses has significant influence on the hole depth. During the initial pulses, drilling rate

increases rapidly which may be due to an effective mass removal mechanism. As the number of pulses increase, the drilling rate decreases. At very high number of pulses, the defocusing of the laser beam at the bottom of the drilling front leads to inefficient material removal and hence significant increase in the depth may not be observed with further increase in the number of pulses [21].

Roos [23] studied the effect of pulse shaping on laser drilling. Roos compared the hole quality drilled by the normal continuous pulse and the short spiked pulse train with the same laser energy. It was found that the pulse train configuration provides a better hole quality without clogging due to molten material.

Tan [24] also investigated the effect of pulse shaping on laser drilling of silicon. In an attempt to improve the hole wall deformation, Tan employed the pulse train, called multi-bursts in his work for drilling a silicon workpiece with an aspect ratio up to 1:10. Initially, a series of low energy pulses interacted with the workpiece and produced a through hole with minimal deformation after which a series of high energy pulses were delivered to enlarge the hole diameter. This was done until the required dimension was obtained. Using a pulse train with increasing laser energy for each successive pulse improved the straightness of the wall.

Laser pulse shaping strongly affects material removal mechanism. In case of drilling with normal pulse, the hole made by the relaxation oscillations in the beginning of the pulse gets immediately clogged by the molten material generated in the later part of the pulse. Hence, for efficient laser drilling, it is preferable to use a pulse having spikes along the whole width of the pulse [3].

2.5.3 Focusing Conditions

The divergence angle for most laser beams is quite small and it can be adjusted and focused to a small spot using a simple lens system [25]. The focusing optics determines the focal length, depth of focus, and focal spot size. The size of the single pulse and percussion laser-drilled holes is highly determined by the spot size of the laser beam on the surface of the workpiece [2,13]. Figure 2.6 shows the focal pattern of converging lens.

The minimum spot diameter (d_s) depends on the focal length of the lens (f) and is given by;

$$d_s = f\theta_b \tag{2.4}$$

where θ_b is the total beam divergence angle.

In addition, the beam diameter along the length of the beam is given by the beam divergence. The depth of focus (Δf) is given by [2, 15];

$$\Delta f = \frac{2d_s f}{d} = \frac{2\theta_b f^2}{d} \tag{2.5}$$

where d is the unfocused beam diameter.

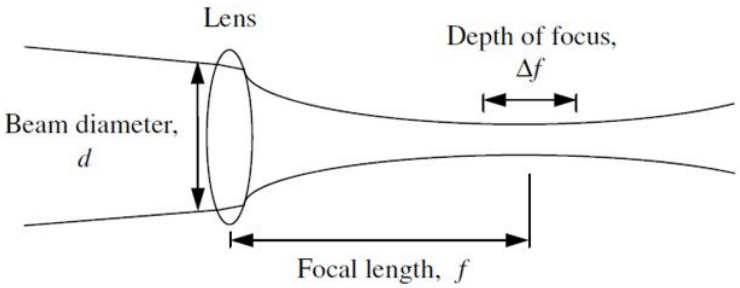

Figure 2.6: Schematic of focal pattern of converging lens

Smaller focal spot diameter can be obtained by reducing the focal length, thus increasing the laser energy density (intensity). Higher laser energy density increases the material removal rates, thus increasing the drilling speed. However, reduction in focal length is also associated with decrease in depth of focus, which may undesirably affect the flatness and perpendicularity of the laser-drilled holes. The smaller depth of focus may also lead to disruption of the process if the workpiece to be drilled is not flat. Hence, longer depth of focus is desired to allow the workpiece to be positioned more easily [13, 15].

Focal plane position (FPP) is given based on relative position to the workpiece surface. This maybe zero FPP, positive FPP, or negative FPP. For zero FPP, the focal plane position is located exactly on the workpiece surface. For positive FPP, the focal plane position is set above the workpiece surface, and for negative FPP, the focal plane position is set below the workpiece surface [2]. In order to obtain a hole with small diameter, good circularity, and low taper, a negative FPP should be employed. [15].

Semak [26] investigated the effects of focal plane positions during laser machining. The relationship between beam focus position and penetration depth in contionous wave laser machining was studied numerically and experimentally for different machining conditions. Calculations were performed using a transient hydrodynamic model that

incorporates the effect of evaporation recoil pressure and the associated melt expulsion. The model results were compared with experimental results. Semak concluded that maximum penetration occurs with a specific location of the beam focus, with respect to the original sample surface, and that this relationship depends on the processing conditions. In particular, beam absorption in the plasma has a significant effect on the relationship between penetration and focus position. When the process parameters result in strong beam absorption in the plasma, the maximum penetration will occur when the laser focus is at or above the sample surface. In a case of weak absorption however, the penetration depth reaches its maximum value when the beam focus is located below the sample surface.

Lazare and Tokarev [27] studied the issue of beam divergence in laser drilling. They developed a mathematical model for predicting the drill depth as a function of laser pulse energy and beam divergence. It was found that deeper holes can be drilled with a low divergence laser with high brilliance (laser pulse energy/divergence angle).

Leigh *et al.* [28] investigated the effects of four controllable variables on the metallurgy and geometry of acute (30° to surface) laser percussion drilled holes in 2 mm thick flat pieces of nickel based super-alloy CMSX 4. Assist gas pressure, nozzle stand-off distance, focal plane position (FPP), and number of pulses were chosen as the independent process variables. It was found that a positive FPP and high nozzle stand -off gave the minimum entrance oxide layer thickness whereas the recast layer was minimized for a zero FPP and high pulse number.

Kamalu and Byrd [29] carried out statistical design of laser drilling experiments to study drilling performance under a variety of parametric combinations. The investigation was mainly concerned with the effects of parameters upon hole diameters and the

focal position was found to be more significant than laser energy input.

2.5.4 Material properties and environment

Naeem and Wakeham [8], investigated laser percussion drilling of high quality holes for the aerospace market with a new low cost high peak power up to 20 kW and high beam quality pulsed Nd:YAG laser specially developed for aerospace market. Holes were drilled with various laser and processing parameters on coated and uncoated nickel based super-alloy material to examine the hole quality in terms of recast layer, taper, oxidised layer and cracking etc. The drilling tests carried out with this high beam quality driller showed that good quality holes were achieved with both coated and uncoated materials. It was very easy to produce holes of different sizes without affecting the taper and the recast layer by varying the laser and processing parameters. The reduced taper was attributed to better depth of focus due to good beam quality whereas the low consistent recast layer was due to very round beam profile of the laser. Laser drilling through TBCs was seen to cause no cracking of the coating and at the bond coat/substrate interface. Significant improvement was due to the advanced GUI software control of the laser which allowed drilling of holes with different parameters for both ceramic coating and the metallic substrate.

Material properties which affect the quality of drilled hole include reflectivity, absoptivity and thermal properties. Environmental parameters include humidity and temperature. As the temperature of the substrate increases due to laser heating, absorptivity of materials rises accordingly. As a result, strong vaporisation induced at the liquid-vapour interface enhances the beam scattering and hence absorption at the interface. Dust, oxides and other impurities deposited on the surface also contribute

to an increase in the absorption coefficient. If plasma is formed in the process, it can absorb part of the laser energy and subsequently transfer it to the substrate [2].

Bandyopadhyay et al [30], carried out an experimental study on laser drilling of Inconel 718 and Ti-6Al 4V. They investigated the effect of material and its thickness on the geometrical and metallurgical aspects of laser drilled holes. The results showed that that increasing the material thickness leads to less hole taper whereas spatter, recast layer and HAZ increase with material thickness.

In laser drilling, the melt depth for the same interaction time for different material, varies according to the differences in material properties. workpiece geometry also affects the process performance. The thickness of the material plays a role on the final drilled hole quality. Increasing the material thickness leads to a lowering of the hole taper whereas spatter, recast layer and HAZ increase with material thickness. Other variables which have impact on the laser performance include vibration of the machine, dust, oil vapour, ambient temperature, and humidity [15].

2.6 Control and optimization approaches for laser drilling process

Various control and optimization techniques may be employed to ensure efficient and effective laser drilling. These include techniques to predict the various hole parameters in order to adjust drilling parameters accordingly. Modeling is useful where it is unfeasible to study through experiments. Work has been done in an attempt to develop models to predict the attributes of laser drilled work. Research has shown that using an experimental design technique and statistical modeling, it is possible to analyse the

interactive effects between various process parameters of the laser percussion drilling process, which are otherwise difficult to detect using a conventional experimentation method and analysis [1, 31].

Sivarao *et al* [32] used design of experiment (DOE) based statistical approaches in modeling of laser processing. They developed a mathematical model through experimental runs. DOE provides the opportunity to optimize and predict possible output based on the parameters setting. In this study, a review was done on DOE techniques that have been employed for laser beam process optimization by other researches. The study predominantly focused on the usage of response surface methodology, Taguchi's method and factorial design in laser beam machining. They concentrated mainly on material removal rate, kerf width, surface roughness, and heat affected zones (HAZ). They found out that pulse frequency, pulse energy, pulse width and cutting speed have significant effect on these parameters.

Joonghan [33] carried out a study on measurement and numerical simulation of high temperature laser material processing with the aim of controlling laser drilling process in aerospace industry. The study looked at three representative processes with three different interactions of plasma namely; pulsed laser deposition (PLD) process for thin coating deposition where material deposit occurs via plasma and vapor, drilling process for material removal to create shaped holes for efficient cooling, and direct metal deposition (DMD) process (very weak plasma) to clad a thick layer.

Laser drilling experiments were carried out to generate cooling holes in an aerospace material, Inconel 718. The effect of the process parameters and different drilling methods on the hole qualities were comprehensively investigated. A numerical simulation for pulsed laser drilling was also carried out to provide the fundamental understanding

of the high power density laser process and to investigate the effect of pulse format on the drilling performance.

It was found that a modulated beam using a short pulse width and high beam intensity yielded better drilling performance than the conventional pulsed laser under the same average power. Spectroscopic studies during laser drilling and DMD were carried out for the purpose of process diagnostics by employing the optical emission spectroscopy. The results indicated that plasma parameters can be used to monitor the drilling depth during laser drilling and the elemental composition created during the DMD.

Ranga *et al.* [34] developed a thermal model for laser drilling and cutting of engineering materials to determine the number of laser pulses required to drill a hole of required depth and diameter and also perform heat affected zone (HAZ) calculations for different materials.

Thermal aspects of laser drilling and cutting process were modeled using the Jaeger's heat source method. The laser beam was considered as a circular moving plane disc heat source. The resulting equation was a general solution, in that it can be used for transient as well as quasi-steady state conditions. It could be used with different laser beam distributions, such as normal, bimodal, and uniform. Simpson 1/3 numerical integration method was used to solve the heat source equation and programmed using Visual Basic.NET.

Temperature rise at any time and at any location in the workpiece drilled or cut was determined using the laser beam parameters and the thermal properties of work materials, such as AISI-1036 steel, and CP-titanium. Fusion and evaporation temperatures of the work materials were used to calculate the amount of material removed by each

laser pulse for a given laser beam parameters. The effect of latent heat of fusion and evaporation were considered. Effect of different laser beam parameters, such as energy density, beam radius, and pulse duration on the profile of laser drilled hole and cut materials were investigated. Mass and energy balance were done for the laser machining process. The model satisfactorily predicted the number of laser pulses for a given depth of hole and also was able to perform HAZ calculations for different materials.

Wei [4], carried out a computational and experimental investigations of laser drilling and welding for microelectronic packaging. More specifically, the studies were focused on development of a consistent set of equations representing interaction of the laser beam with materials solution of these equations by finite difference method (FDM) and finite element method (FEM), experimental demonstration of laser micromachining, and correlation of the results. The contribution of this work included among other things:

1. Development of a finite difference method (FDM) code which has the capability of adjusting the laser power distributions, coefficient of energy absorption, and nonlinear material properties of the workpiece as functions of temperature, and can be extended to calculate the profiles of laser micromachined workpieces.
2. Detailed investigations of the effect of laser operating parameters on the results of the profiles and dimensions of the laser microdrilled workpiece, which provide the guideline and advance currently existing laser micromachining processes.
3. Detailed considerations of absorption of laser beam energy, effect of thermal and aerodynamic conditions due to shielding gas, and the formation of plasma and its effect on laser micromachining processes.

The results of this work facilitated improvements and optimizations of the laser micro-

machining techniques.

One way to reduce uncertainty in problem solving and decision making is by seeking the advice of an expert in related field. When computers are used to reduce uncertainty, the computer itself can become an expert in a specific field through a variety of methods. One such method is machine learning, which involves computer algorithm to capture hidden knowledge from data. Artificial Neural network (ANN) has an ability to derive meaning from complicated data, can be used to extract patterns and detect trends that are too complex to be noticed by either humans or other computer techniques [35, 36].

2.7 Neuro-fuzzy learning and control

Some researchers have employed neural networks and fuzzy logic systems in their work. Nakhjavani et al [43], optimized laser percussion drilling by using neural network. They integrated the neural network method with the Lonberg-Marcoitte(L-M). To begin with,optimum input parameters of the process were obtained in order to optimize every single output parameters (responses). ANN method was used to create an experimental model of the process based on the experimental results. Then optimum input parameters (peak power, pulse width, pulse frequency, number of pulses, assist gas pressure and focal plane position) were determined by Lonberg-Marcoitte. The output parameters include the hole entrance diameter, circularity of hole entrance and hole exit circularity, and hole taper. The tests were conducted on Stainless steel 304 sheets, with 2.5 mm thickness. The sheets were drilled by a 400 W pulsed Nd: YAG laser emitting at 1.06 μm wavelength. Oxygen was used as assist gas. They concluded that modeling with neural networks gives excellent results compared to other methods.

In another study, Sivarao and Brevern [44], studied neural network modeling and val-

idation for micro quality evaluation in Laser processing. Three significant design parameters were used in this research; namely cutting speed, gas pressure and power. Prediction of laser machining cut quality, namely surface roughness was carried out using machine learning techniques based on Quick Back Propagation Algorithm (BPL) using ANN. Experimentally observed responses were used to train, map and optimize the network algorithms before the best architecture was selected. Ten different architectures and models were tested and finally the best model was finalized. The model was then fed with new sets of machining parameters to experimentally validate the model's ability in predicting the cut quality. The findings were very promising and yielded excellent accuracies for both model and experimental validation reaching almost 88% and 92% respectively.

Neuro-fuzzy systems represent a newly developed class of hybrid intelligent systems combining the main features of artificial neural networks with those of fuzzy logic systems [6]. The main aim is to circumvent difficulties encountered in applying fuzzy logic for systems represented by numerical knowledge (data sets), or conversely in applying neural networks for systems represented by linguistic information (fuzzy sets). Neither fuzzy reasoning systems nor neural networks are by themselves capable of solving problems involving at the same time both linguistic and numerical knowledge [7, 41].

The integration of fuzzy logic systems with neural networks reduces the limitations of fuzzy systems in terms of lack of learning while strengthening the neural network features in terms of explicit knowledge representation.

Neuro-fuzzy systems (NFS) can be divided into three major types according to their topologies and functionalities [6, 38]. These are; cooperative neuro-fuzzy systems, neu-

ral network-driven fuzzy reasoning systems (NNDF) and hybrid neuro-fuzzy systems. Of interest in this study is the hybrid neuro-fuzzy systems.

Cooperative neuro-fuzzy systems has as its main task the optimization and tuning of the neural networks involved in the architecture. The idea is to optimize and tune the fuzzy inferencing structure using some sort of learning mechanism. This type of NFS structure lacks parallelism, in that both the neural network and the fuzzy system operate virtually independently of each other. As such, while the learning takes place in the neural network at a certain level, the fuzzy inference system remains unchanged during this stage. In cooperative neuro-fuzzy systems, the combination of neural networks and fuzzy inferencing aims at optimizing the structure of a given fuzzy system through learning provided by a neural network. This can be achieved by utilizing a neural network to determine certain parameters of the fuzzy system, a process that can be carried out either off line or on line.

Takagi and Hayashi developed the Neural network-driven fuzzy reasoning system. This scheme is proposed to solve problems pertaining to systems where techniques other than heuristic approaches are needed to design the membership function and ystems where reasoning must be adaptable to changes in the environment. The basic idea of the Takagi-Hayashi method is to implement the membership functions in the antecedent in the inference functions of the consequent. To implement this scheme, a suitable neural network is used.

Hybrid neuro-fuzzy systems are based on an architecture which integrates in an appropriate parallel structure a neural network and a fuzzy logic-based system. The fuzzy logic system and the neural network work as one synchronized entity, [7].

Hybrid neuro-fuzzy systems have a parallel architecture, and exploit similar learning paradigms, as is the case for neural networks. The parallelism of the system can be viewed as a mapping of the fuzzy system into a neural network structure. Each functional module of the fuzzy logic system corresponds to a particular layer of the neural network. The resulting system can be interpreted either as a neural network or a fuzzy logic system. Figure 2.7 depicts the mapping from a fuzzy logic system to a neural network structure [38].

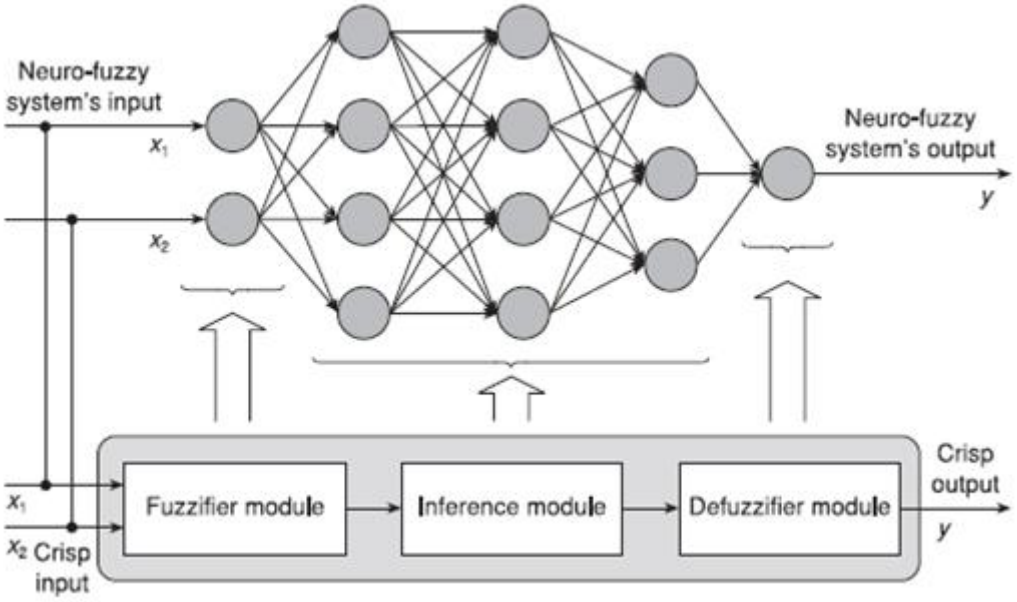

Figure 2.7: Mapping from a fuzzy logic system to a neural network structure

Hybrid neuro-fuzzy systems have the same architecture as that of traditional fuzzy systems except that a layer of hidden neurons performs each of the tasks of the fuzzy inference system. As such, a fuzzy logic inference system can be implemented as a five-layer neural network. This type of architecture is the most commonly used among neuro-fuzzy inference systems, and it uses the Sugeno-type fuzzy inferencing. The structure of the system can be described layer by layer as follows [7, 38]:

Layer 1: Fuzzification–This layer consists of a set of linguistic variables. The crisp

inputs x_1 and x_2 are fuzzified through mapping into membership functions of the linguistic variables, which usually take triangular, trapezoid, or bell-shaped membership functions.

Layer 2: Rule nodes–This layer contains one node per each fuzzy if-then rule. Each rule node performs a connective operation within the rule antecedent (*if* part). Usually, the minimum or the dot product is used as the T-norm operator to represent the connective AND. The union OR connective is usually represented using the maximum operation or any other T-conorm operator.

Layer 3: Normalization–In this layer, the firing strengths of the fuzzy rules are normalized. The normalized firing strength is given by;

$$\overline{w}_p = \frac{w_p}{\sum_{i=1} w_i} \tag{2.6}$$

where w_p is the firing strength of the p-th rule.

Layer 4: Consequent layer–This layer is related to the consequent of the fuzzy rule. The values of the consequent (*then* part) are multiplied by normalized firing strengths according to:

$$\overline{O}_p = \overline{w}_p O_p \tag{2.7}$$

where $\overline{O}_p$ is the consequent layer output and O_p is the normalization layer output.

Layer 5: Summation–This layer computes the overall output as the summation of the incoming signals:

$$O^* = \sum_p \overline{O}_p \tag{2.8}$$

where O^* is the overall output.

A common example of a hybrid neuro-fuzzy system is the Adaptive-Neuro-Fuzzy Inference System (ANFIS), which can be represented in a four or five layer architecture [7, 40, 42].

Hybrid learning rules combines the gradient method and the least squares estimate (LSE) to identify parameters. Each epoch of the hybrid learning procedure is composed of a forward pass and backward pass. In the forward pass, input data is supplied and functional signals go forward to calculate each node output. The consequent parameters are identified by least square estimator method. After identifying the parameters, the functional signals keep going forward till the error measure is calculated. In the backward pass, the error rates (derivative of the error measure with respect to each node output) propagate from the output end towards the input and the premise parameters are updated by gradient method [38, 42].

There are two learning algorithms for adaptive networks. These are batch learning/off-line learning and pattern learning/on-line learning. With batch learning or off-line learning, the update action takes place only after the whole training data set has been presented, i.e., only after each epoch or sweep. For pattern learning, also called on-line

learning, parameters are updated after each data presentation. This learning paradigm is vital to the on-line parameter identification for systems with changing characteristics. For the sequential least squares formula to account for the time-varying characteristics of the incoming data, the effects of old data pairs as new data pairs become available are decayed [7, 42].

Modeling with neural network has a considerable capability for approximation of the process performance. Accordingly, this method is preferred for modeling compared to the other methods of modeling approximation such as Response Surface Method (RSM) [43]. The present work aims at combining the important aspects of fuzzy logic control and artificial neural networks to come up with a neuro-fuzzy system that will be used to ensure improved quality of the laser drilled holes. The neural network should learn and train the fuzzy logic controller based on some expert knowledge. A hybrid neuro-fuzzy system, ANFIS, is employed.

2.8 Summary

This chapter has provided a literature review on laser drilling process and the various approaches employed in the modeling and control of the process. It also provides a literature review on artificial intelligence specifically the aspects employed in this work. The review has shown that research work in laser drilling and artificial intelligence is gaining interests and considerable progress has been made.

There exists several defects during laser percussion drilling process. These include hole tapering, recast layer formation, hole non-circularity and micro-cracks. Laser parameters and process parameters have been proven to bear the greatest impact on these defects. The control of the laser drilling process is still a challenge due to the

large number of parameters involved. The following gaps were identified:

1. No control system has been developed so far to address the challenge of laser parameter combinations.
2. Assist gas bears considerable effects on the laser drilling process. These defects are yet to be fully investigated experimentally.
3. Little work has been done on femto-second pulse drilling on aerospace materials. This can be seen to improve the drilled hole qualities due to reduction in micro-cracking and HAZ regions.
4. Most models developed were statistical. Little modeling work has been done based on soft computing techniques such as artificial neural networks.
5. Very minimal work has been done on adaptive control techniques for the laser percussion drilling process. This could be due to the complexity of the process.

The present work aims at modeling the laser percussion drilling process and combining the aspects of artificial neural networks and fuzzy logic in order to come up with a neuro-fuzzy controller.

CHAPTER THREE

3.0 METHODOLOGY

In this chapter the approaches employed to develop a laser percussion drilling model and a Neuro-fuzzy controller are discussed.

3.1 Model Development

Finite element method (FEM) was employed for the model development. In this section a mathematical formulation for the laser drilling process and the approach employed for the FEM implementation, model validation and simulations are discussed.

3.1.1 Mathematical formulation of laser drilling

The analysis of laser drilling process is divided into three phases namely; solid heating phase, melting phase and vaporization phase [45–49].

3.1.1.1 Solid heating phase

This refers to the heating of the material from room temperature to melting point. Figure 3.1 shows solid plate subjected to a laser heat beam at the surface.

For one-dimensional transient heat conduction, the heat conduction equation is given by:

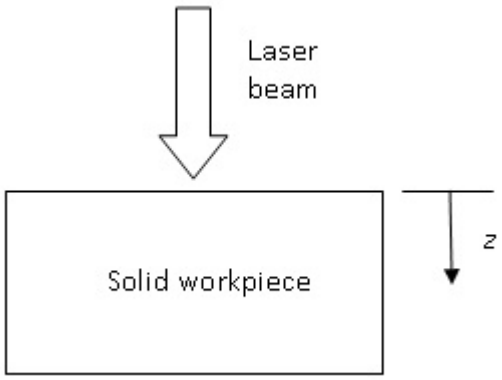

Figure 3.1: Schematic diagram of solid heating phase

$$\frac{\partial^2 T_{wp}}{\partial z^2} = \frac{1}{\alpha_{wp}} \frac{\partial T_{wp}}{\partial t} \tag{3.1}$$

where T_{wp}, t , z , and α_{wp} are the temperature in solid, time, vertical distance, and thermal diffusivity of the solid, respectively.

The boundary and initial conditions are;

$$T_{wp}(z, 0) = T_o \tag{3.2}$$

$$I_{abs} = -k_{wp} \frac{\partial T_{wp}}{\partial z}_{z=0} \tag{3.3}$$

where k_{wp} is the thermal conductivity of the solid workpiece, T_0 is the ambient temperature, and I_{abs} is the absorbed laser intensity.

$$I_{abs} = (1 - R_f)I_o = A_{wp}I_o \tag{3.4}$$

3.1.1.2 Melting phase

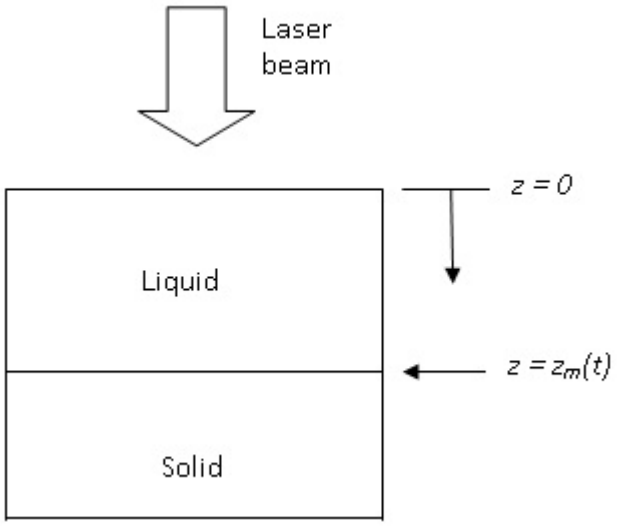

Figure 3.2: Schematic diagram of melting phase

Melting begins when the energy of the laser beam incident on the solid surface is sufficient enough to melt the material. This leads to the solid-liquid interface being formed and it propagates into the solid [13, 49, 50].

The heat conduction equations are given by:

$$\frac{\partial^2 T_{lq}(z,t)}{\partial z^2} = \frac{1}{\alpha_{lq}} \frac{\partial T_{lq}(z,t)}{\partial t}; 0 \leq z < z_m \tag{3.5}$$

$$\frac{\partial^2 T_{wp}(z,t)}{\partial z^2} = \frac{1}{\alpha_{wp}} \frac{\partial T_{wp}(z,t)}{\partial t}; z_m \leq z < \infty \tag{3.6}$$

with boundary and initial conditions:

$$-k_{lq} \frac{\partial T_{lq}(z,t)}{\partial z} = A_{lq} I_o; z = 0 \tag{3.7}$$

$$T_{wp}(z,t) = T_{lq}(z,t) = T_m; z = z_m(t) \tag{3.8}$$

$$\rho_{wp} L_m \frac{dz_m(t)}{dt} = k_{wp} \frac{\partial T_{wp}(z,t)}{\partial z} - k_{lq} \frac{\partial T_{lq}(z,t)}{\partial z}; z = z_m(t) \tag{3.9}$$

$$T_{wp}(z,t) = T_o; z \to \infty \tag{3.10}$$

$$z_m(t_m) = 0; t = t_m \tag{3.11}$$

where T_{lq} (z, t) and T_{wp} (z, t) are the temperature profiles in liquid and solid, k_{lq}, ρ_{wp} and α_{lq} are the thermal conductivity of liquid, density of solid, and thermal diffusivity

of the liquid, L_m, t_m , and $z_m(t)$ are the latent heat of melting, the time required to initiate melting, and the melting front location, respectively.

Expressions for the melt depth and the melting front velocity are derived by substituting the assumed temperature profiles in the heat conduction equations [46–54].

3.1.1.3 Vaporisation phase

When temperature of the liquid layer reaches the boiling point, vaporization takes place. This leads to the formation of the liquid-vapour interface which propagates into the liquid layer. The solid-liquid interface created due to melting propagates into the solid. The combined effects of the vaporisation and liquid expulsion leads to cavity formation [55, 56].

Considering one-dimensional model as given in Figure 3.3; Heat conduction equations in the solid and liquid are given by:

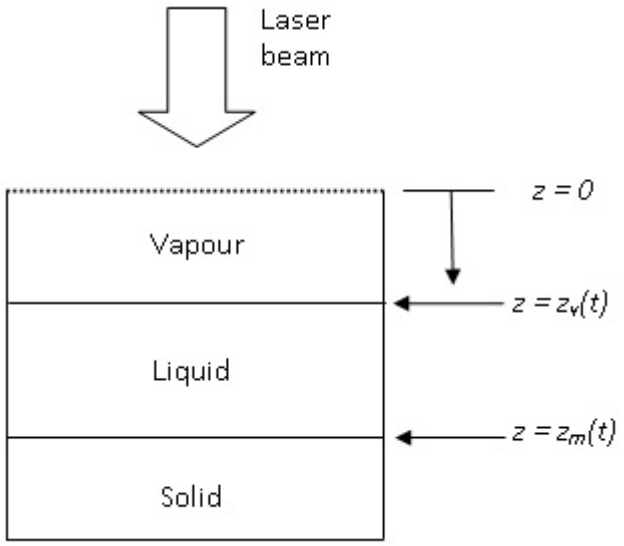

Figure 3.3: Schematic diagram of vaporisation phase

$$\frac{\partial^2 T_{lq}(z,t)}{\partial z^2} = \frac{1}{\alpha_{lq}} \frac{\partial T_{lq}(z,t)}{\partial t}; 0 \leq z < z_m(t) \tag{3.12}$$

$$\frac{\partial^2 T_{wp}(z,t)}{\partial z^2} = \frac{1}{\alpha_{wp}} \frac{\partial T_{wp}(z,t)}{\partial t}; z_m(t) \leq z < \infty \tag{3.13}$$

Boundary conditions at the solid-liquid and liquid-vapour interfaces are given as:

$$\rho_{wp} L_m \frac{dz_m(t)}{dt} = k_{wp} \frac{\partial T_{wp}(z,t)}{\partial z} - k_{lq} \frac{\partial T_{lq}(z,t)}{\partial z}; z = z_m(t) \tag{3.14}$$

$$T_{wp}(z_m(t),t) = T_{lq}(z_m(t),t) = T_m; z = z_m(t) \tag{3.15}$$

$$\rho_{lq} L_v \frac{dz_v(t)}{dt} = I_{abs} + k_{lq} \frac{\partial T_{lq}(z,t)}{\partial z}; z = z_v(t) \tag{3.16}$$

$$T_{lq}(z_v(t),t) = T_{l0}; z = z_v(t) \tag{3.17}$$

where L_v is the latent heat of vaporisation and T_{lo} is the melt surface temperature.

The melt surface temperature T_{lo} is a function of vapour pressure. The vapour pressure (P_v) is given by:

$$P_v = P_o exp\left[\frac{L_v}{R_g}\left(\frac{1}{T_{bl}} - \frac{1}{T_{l0}}\right)\right] \tag{3.18}$$

where p_0 and T_{bl} are atmospheric pressure and boiling point, and R_g is the specific gas constant defined by $R_g = R_u/M_m$, where R_u is the universal gas constant (8.314 J/(mol.K)) and M_m is the molar mass. Therefore, if P_v is known, T_{l0} can be calculated.

$$T_{l0} = I_{abs}\sqrt{\frac{4t}{\pi \rho_{lq} c_e k_{lq}}} \tag{3.19}$$

where c_e is the effective heat capacity and is defined as:

$$c_e = c_{ps} + \frac{L_m}{T_m} \tag{3.20}$$

where c_{ps}, L_m and T_m are specific heat of solid, latent heat of melting, and melting temperature of the material.

The liquid-vapour and solid-liquid interfaces are formed respectively at:

$$z = z_v(r, t) \tag{3.21}$$

$$z = z_m(r, t) \tag{3.22}$$

It should be noted that the auxiliary equations to enable solve heat equations are established from the conservation of mass and momentum [57–60]. The mass of the solid melt at the solid-liquid interface is equal to the total mass removed due to melt ejection and vaporisation. If the melt ejection is taken into consideration, the mass balance can be written as:

$$\dot{m}_s = \dot{m}_m + \dot{m}_v \tag{3.23}$$

where m_s, m_m, and m_v are solid melting rate, molten liquid ejection rate, and vaporization rate, respectively.

3.1.1.4 Three-Dimensional Heat Conduction

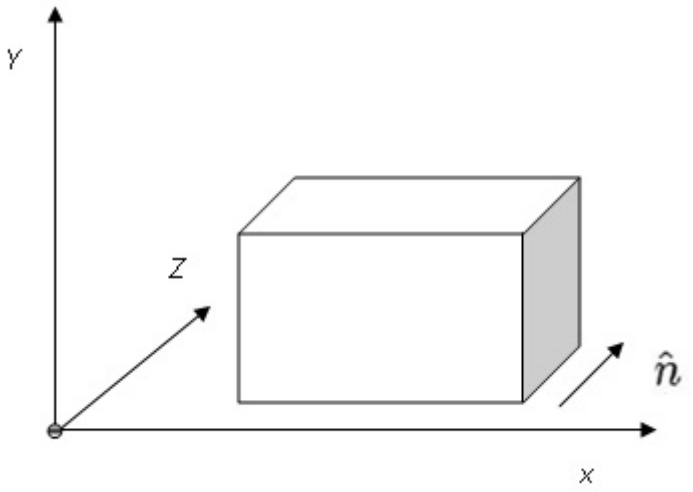

Figure 3.4: Solid in a Three dimensional Space

Considering a solid in a three-dimensional space with a volume (V) and surface area (S) as shown in Figure 3.4, the Fourier's law of heat conduction is given by;

$$\mu_f = -k\nabla T.\hat{n} \tag{3.24}$$

where ∇ is a function of $(\frac{\partial}{\partial x}, \frac{\partial}{\partial y}, \frac{\partial}{\partial Z})$, T is the temperature, k is thermal conductivity, and μ_f is the heat flux.

From law of conservation of energy;

$$\frac{d}{dt}\int_V \rho_{th} dV = -\int_S \mu_f dS + \int_V Q_s dV \tag{3.25}$$

where ρ_{th} is the thermal energy density, and Q_s is the heat source.

Thermal energy density is given by;

$$\rho_{th} = C_p \rho T \tag{3.26}$$

where C_p is the specific heat capacity of the material and $C_p\rho$ is a measure of volumetric heat capacity.

Equation (3.25) can be simplified further as;

$$\int_V C_p \rho \frac{\partial T}{\partial t} = \int_S k \nabla T . \hat{n} dS + \int_V Q_s dV \tag{3.27}$$

Thus;

$$C_p \rho \frac{\partial T}{\partial t} = k \nabla^2 T + Q_s \tag{3.28}$$

The measure of thermal diffusivity, α, is given by;

$$\alpha = \frac{k}{C_p \rho} \tag{3.29}$$

Equation (3.28) can be simplified as;

$$\nabla^2 T + Q = \frac{1}{\alpha}\frac{\partial T}{\partial t} \tag{3.30}$$

where Q and α are constants.

For the solid heating phase, the three-dimensional transient heat conduction equation is given by;

$$\frac{\partial^2 T_{wp}}{\partial x^2} + \frac{\partial^2 T_{wp}}{\partial y^2} + \frac{\partial^2 T_{wp}}{\partial Z^2} + Q = \frac{1}{\alpha_{wp}}\frac{\partial T_{wp}}{\partial t} \tag{3.31}$$

where x, y, and z are spatial variables. $T(x, y, z, t)$ is a function of the spatial variables and time.

The heat conduction equation can be re-written as:

$$\nabla^2 T_{wp} + Q = \frac{1}{\alpha_{wp}}\frac{\partial T_{wp}}{\partial t} \tag{3.32}$$

The boundary and initial conditions are;

$$T_{wp}(x, y, z, 0) = T_o \tag{3.33}$$

$$I_{abs} = -k_{wp}\nabla^2 T_{wp} \tag{3.34}$$

For the melting phase, the three-dimensional transient heat conduction equations are given by;

$$\nabla^2 T_{lq}(x, y, z, t) + Q = \frac{1}{\alpha_{lq}} \frac{\partial T_{lq}(x, y, z, t)}{\partial t}; 0 \leq z < z_m, 0 \leq r < r_m \tag{3.35}$$

$$\nabla^2 T_{wp}(x, y, z, t) + Q = \frac{1}{\alpha_{wp}} \frac{\partial T_{wp}(x, y, z, t)}{\partial t}; z_m \leq z < \infty, r_m \leq r < \infty \tag{3.36}$$

where z_m is the melting front location, r is the melt radius and is equal to variables x and y, and r_m is the radius at the melting front location.

The boundary and initial conditions are given by:

$$-k_{lq}\nabla T_{lq}(x, y, z, t) = A_{lq} I_o; z = 0, r = 0 \tag{3.37}$$

$$T_{wp}(x,y,z,t) = T_{lq}(x,y,z,t) = T_m; z = z_m(t), r = r_m(t) \tag{3.38}$$

$$\rho_{wp} L_m \frac{dz_m(t)}{dt} = k_{wp} \frac{\partial T_{wp}(z,t)}{\partial z} - k_{lq} \frac{\partial T_{lq}(z,t)}{\partial z}; z = z_m(t) \tag{3.39}$$

$$\rho_{wp} L_m \frac{dr_m(t)}{dt} = k_{wp} \frac{\partial T_{wp}(r,t)}{\partial r} - k_{lq} \frac{\partial T_{lq}(r,t)}{\partial r}; r = r_m(t) \tag{3.40}$$

$$T_{wp}(r,z,t) = T_o; (r,z) \to \infty \tag{3.41}$$

$$z_m(t_m) = 0; t = t_m \tag{3.42}$$

The following were the assumptions made when formulating the governing equations to help simplify the equations:

1. The temperature distribution in the liquid layer is linear.
2. The temperature distribution in the solid, starting from the solid-liquid interface to the thermal diffusion depth is linear.
3. The moving speeds for the solid-liquid interface and liquid-vapour interface are constant and equal.

3.1.2 FEM Implementation and Model Validation

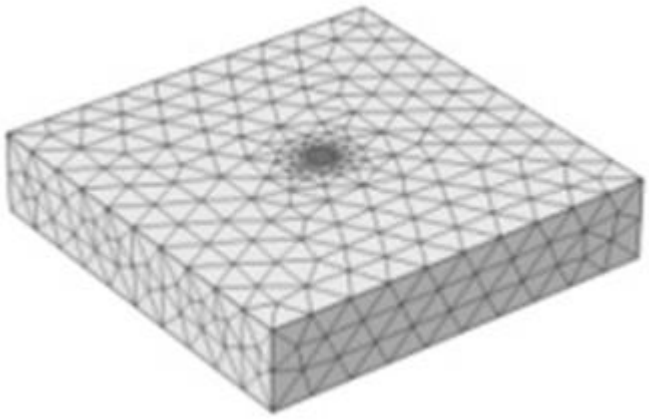

Figure 3.5: Representation of a mesh generated by $COMSOL^R$

Finite element method (FEM) is employed in this study. The model developed is based on $COMSOL^R$, which is a Finite Element Analysis software package that allows the user to develop 3D models with associated boundary conditions. A fine mesh is used for the entire model. This is as shown in Figure 3.5. The type of mesh used affects the computing time but has no significant effect on the accuracy of the results. The mesh type employed in this study was tetrahedral with a total of 2338 elements.

A stationary Q-switched Nd:YAG laser is employed. With this type of laser, high laser power in the order of Kilowatts can be achieved. It is also possible to obtain modulated laser pulses in the range of milliseconds.

An image analyzer, was used to analyze the images generated from $COMSOL^R$. The data from the images was used to construct graphs illustrating the taper and hole diameters predictions.

Several assumptions were made when implementing the FEM model on COMSOL platform. The major assumptions on which the model is based are as follows:

1. The laser beam has a Gaussian distribution in pulsed mode.
2. The beam divergence angle is small. Incident laser energy is directional and collimated.
3. The stress strain relationship for the work-piece is linear.
4. The work-piece is free from any residual stresses.

Figure 3.6 shows a representation of the work piece orientation. In the three-dimensional case, convection effects are treated most efficiently as boundary conditions. Convective boundary conditions are be used at the top of the surface where both laser heating and ambient air cooling take place. The remaining boundaries are thermally insulated.

Simulations were carried out in order to investigate the effects of laser peak power and pulse duration on laser drilling of 304 Stainless steel with a thickness of 2.4 mm. The results from these simulations were compared with experimental ones as reported by Wei [4] in order to validate the model. The conditions for the experimental work by Wei [4] is summarized in Table 3.1.

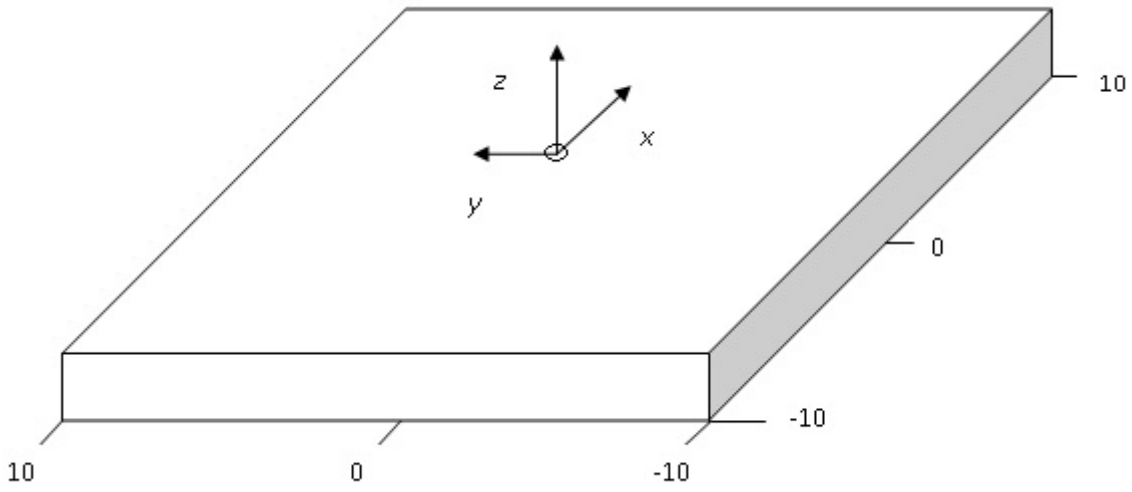

Figure 3.6: Representation of the workpiece orientation

Table 3.1: Machining conditions for experimental work

Machining condition	**Description**
Material	304 Stainless steel
Material thickness	2.4 mm
Laser equipment	Pulsed Nd:YAG laser
Laser wavelength	1.06 μm
Laser peak power	1.5-4 kW
Laser energy per pulse	1.75-4 J
Pulse frequency	1-10 Hz
Pulse width	0.5-2 ms
Lens focal length	100 mm
Beam spot size	80 μm

3.1.3 Investigation of the effects of various laser parameters on drilled hole geometry

Table 3.2: Thermophysical properties for Nickel-based Inconel 718

Thermophysical property	**Value**
Density	8.19g/cc
Specific heat capacity	0.435J/g-degC
Thermal conductivity	11.4W/m-k
Melting point	1260-1336degC
Solidus	1260degC
Liquidus	1336degC
Tensile Strength,Yield at elevated temperature	980MPa

The material employed in this study was Nickel-based super alloy, Inconel 718 whose Thermophysical properties are given in Table 3.2. The model was used to simulate the effects of laser peak power and pulse duration on laser drilling of Inconel 718 sheets with a thickness of 3 mm.

For the simulations to determine the effects of laser peak power on drilled hole geometry, the peak power was varied from 1 kW to 6 kW with a constant pulse duration of 2 ms.

For simulations to determine the effects of pulse duration on the drilled hole geometry, the pulse duration was varied from 1 ms to 3.5 ms, with a constant peak power of 3 kW. The machining time was maintained at 5 pulses with a laser spot diameter of 0.4 mm.

3.2 Development of Neuro-Fuzzy Controller

This section outlines the procedure used to develop the neuro-fuzzy controller. The controller is ANFIS based.

3.2.1 ANFIS Model

It is proposed to use Sugeno inference mechanism for the ANFIS due to its ability to model non-linear systems [36, 38]. In this type of inference mechanism, the output is a function of the inputs and is a fuzzy singleton. ANFIS involves three major steps namely: Identification of inputs, outputs and their ranges; design of membership functions and rule base; and mapping of fuzzy outputs to corresponding crisp values.

3.2.1.1 Identification of inputs, outputs and their ranges

The inputs to the ANFIS model are the taper angle and diameter at hole exit. The values of these inputs are derived from experimental work as reported by Joonghan Shin and Satapathy [33, 61]. Joonghan carried out Laser drilling of Inconel 718. The laser used was a high average power diode-pumped solid state Nd:YAG laser operated at 1064 nm. Drilling was carried out on Inconel 718 plates 3 mm thick, 5 mm wide, and 25 mm long. Satapathy carried out laser drilling on a medium carbon steel specimen,

100mm long, 10mm wide, and 8mm thick. A pulsed Nd-YAG laser system was used with a rated average power of 100W. The set of data obtained from these experiments was used to train and test the ANFIS for this work.

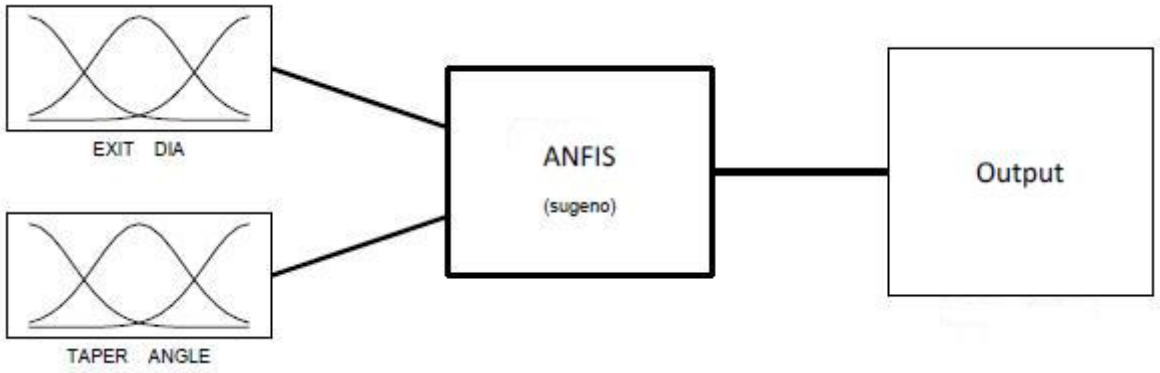

Figure 3.7: Block representation of ANFIS

Figure 3.7 shows the block representations of ANFIS. The inputs into the ANFIS are diameters at the exit and hole taper angles. The outputs are laser peak power and pulse durations.

3.2.1.2 Design of membership functions and rule base

The design of membership functions is achieved as follows: Figure 3.8 shows the ANFIS editor. A set of training data, which constitutes the laser drilling conditions and the expected output, is presented to the ANFIS. The ANFIS is generated by use of grid partitioning, which is a method for grouping data into clusters based on their similarity. The ANFIS is then trained by use of hybrid learning rule. The hybrid learning rule combines the gradient method and the least squares estimate (LSE).

The ANFIS is then tested against a set of testing data. Different sets of data are presented to the ANFIS, and based on the input-output relationship of the ANFIS, the membership functions are constructed. The membership functions for the two inputs

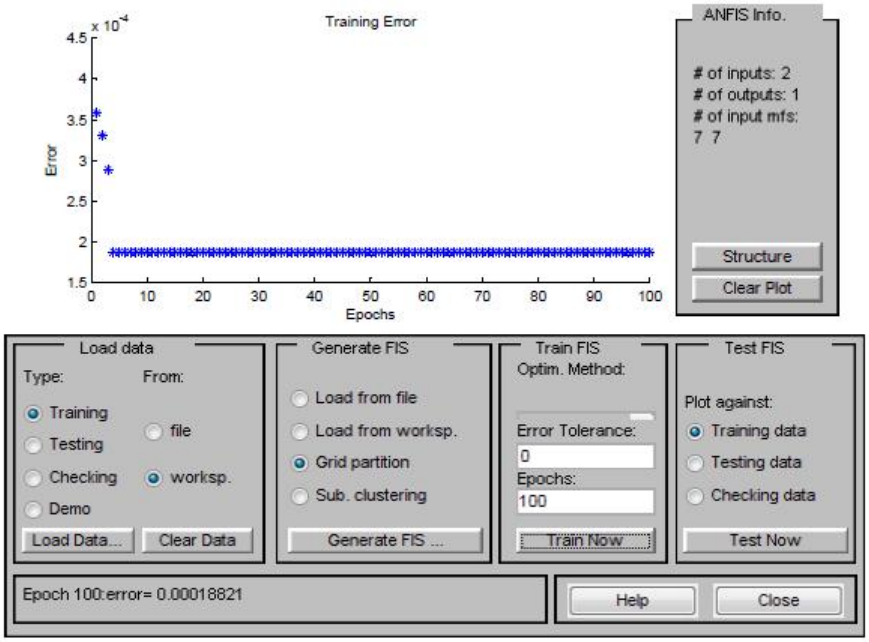

Figure 3.8: ANFIS editor

are similar but with different universe of discourse (μ). The membership functions for the diameter at the exit are shown by Figure 3.9.

Gaussian type membership functions are used for the two inputs because they represent the non-linear nature of the problem in a better way than triangular or trapezoidal membership functions. The membership function definitions are as shown in Table 3.3.

The rule base for the FLC is generated based on the execution of the ANFIS. ANFIS automatically generates its own rule base depending on its set of training data. Figure 3.10 shows some of the rules generated for laser peak power.

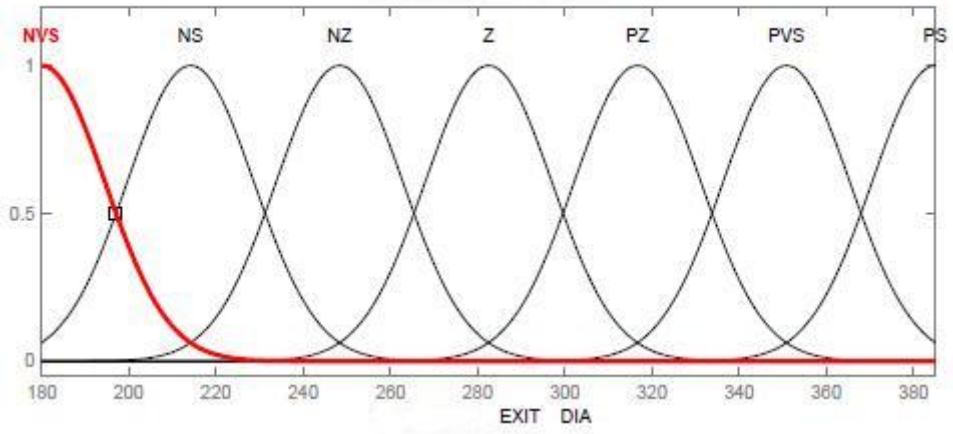

Figure 3.9: Membership functions for hole diameter at the exit

Table 3.3: Membership functions definition

Symbol	**Meaning**
NVS	Negative very small
NS	Negative small
NZ	Negative zero
Z	Zero
PZ	Positive zero
PVS	Positive very small
PS	Positive small

3.2.1.3 Mapping of fuzzy outputs to corresponding crisp values

Figure 3.11 shows a diagrammatic representation of some of the rules for the ANFIS. It shows the crisp output (laser power) of 3.22 kW with diameter at the exit being 283 μm and taper angle of 2.38°. There are a total of 49 rules. If one or both input values are changed, then the output changes as per the rules to give the optimum laser power.

The structure for ANFIS is shown in Figure 3.12. The ANFIS was presented with different input sets so as to simulate a machining situation. The results were used in the design of the input and output membership functions as well as in the generation of the rules for the Fuzzy Logic Controller.

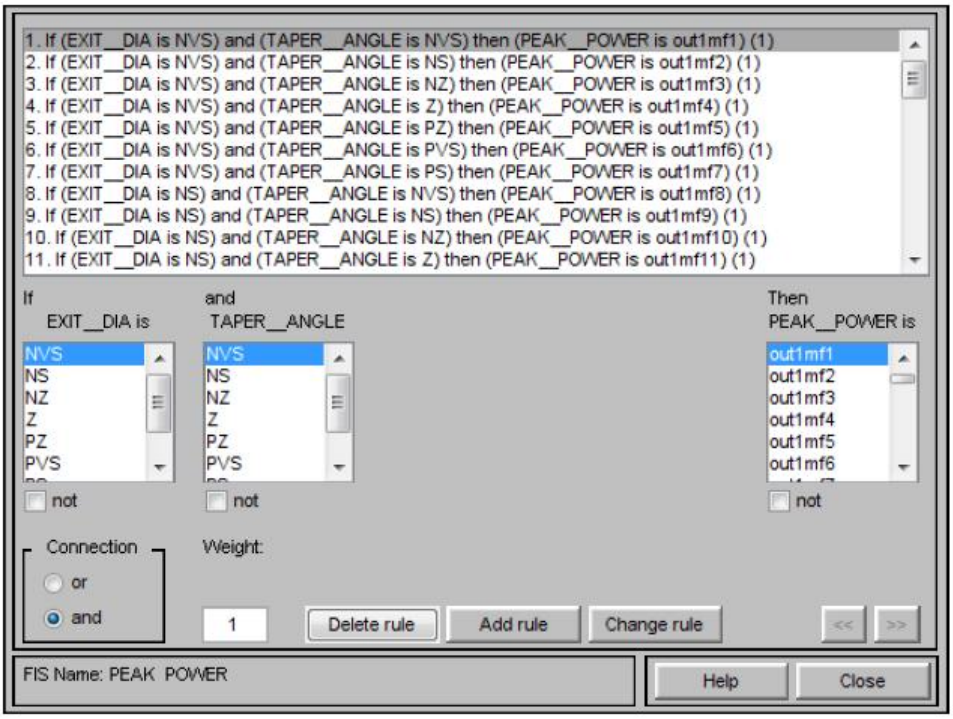

Figure 3.10: Rules generated by ANFIS for laser power

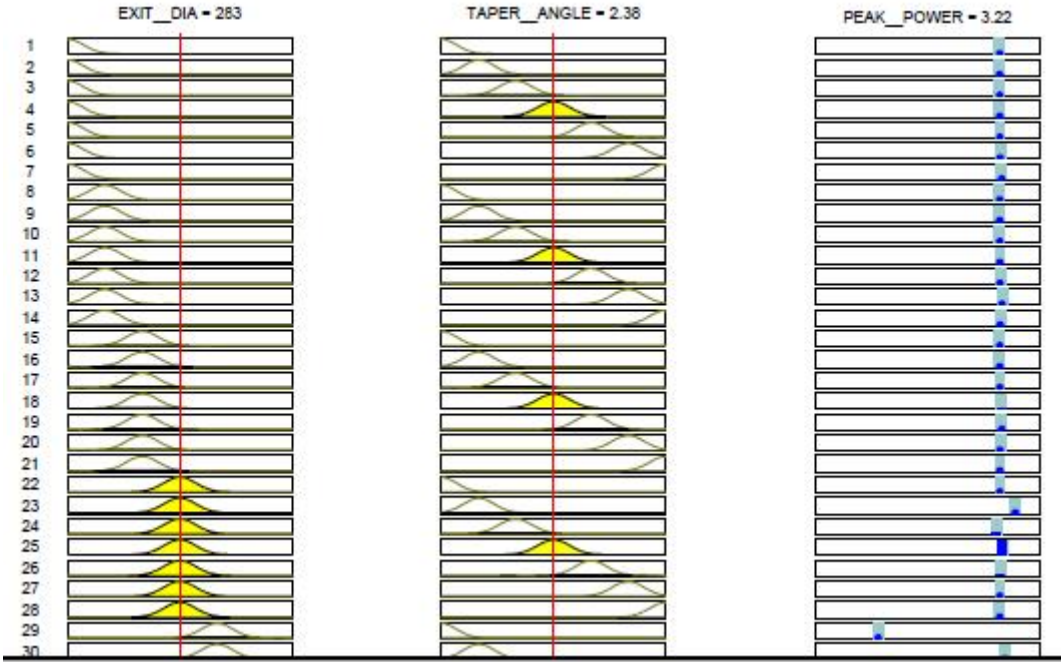

Figure 3.11: Diagrammatic representation of some of the rules for the ANFIS

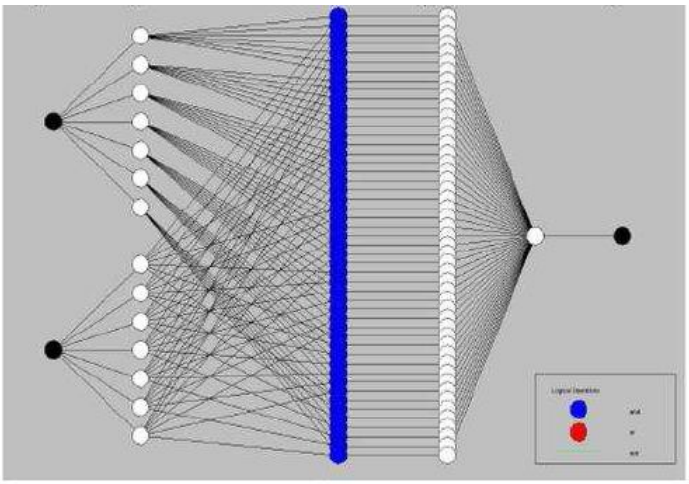

Figure 3.12: Structure for ANFIS

3.2.2 Design of Fuzzy Logic Controller

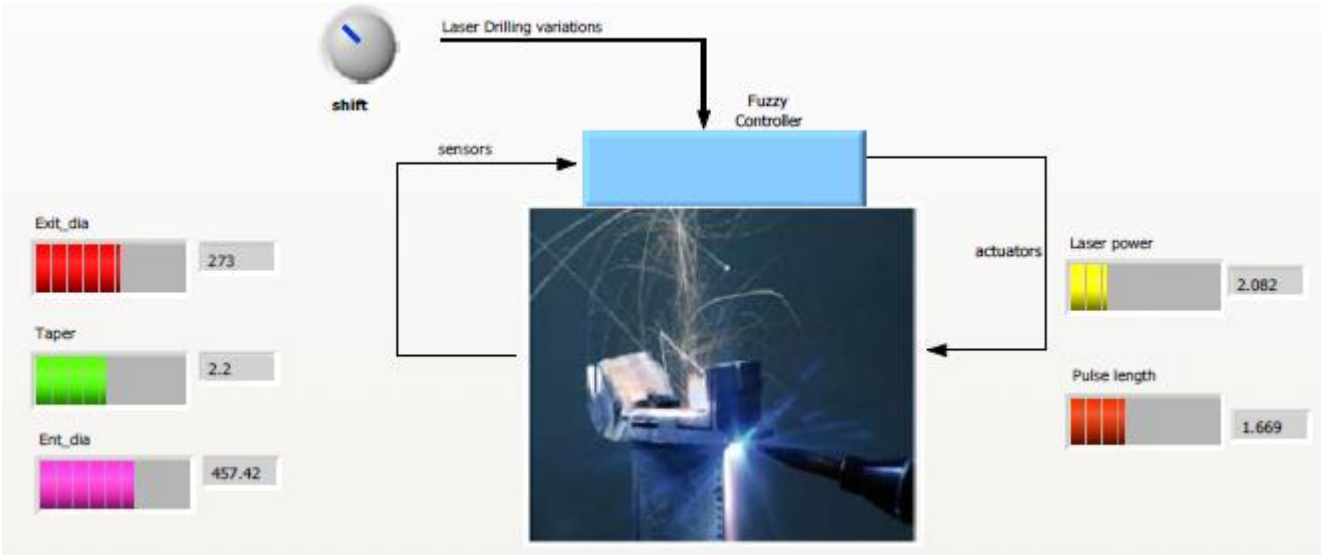

Figure 3.13: Fuzzy logic controller front panel

Figure 3.13 shows the front panel for the controller, displaying some controller outputs. *LabVIEW* software was used to develop the fuzzy logic controller.

Implementation of the FLC involved referencing a fuzzy system designed on *LabVIEW* and saved as a $.fs$ file, and reading of input data from a spreadsheet file. The input data included values of hole diameters at the exit and taper angles derived from the laser

drilling model. The controller computed values for the diameter at the hole entrance. Input values were recorded as the controller run.

Fuzzy Logic control was then performed based on the information received on the shift register. The initial information came from the $.fs$ file. The output values were then computed based on the control action. The output parameters were laser power and the pulse duration. These output values were recorded as the controller runs.

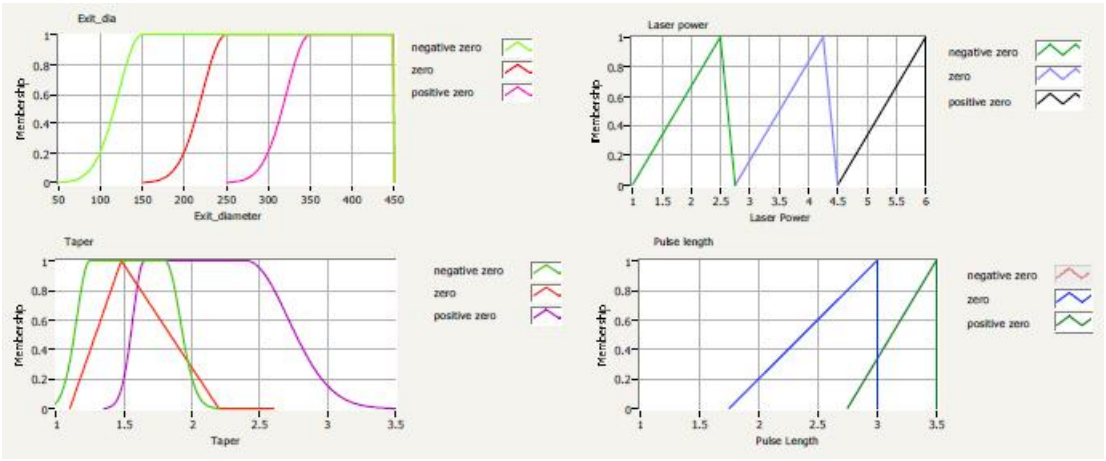

Figure 3.14: Typical membership functions

The controller checked if the control had a different value from the previous loop iteration. The controller then got the membership functions points of the input and output variables, and changed the values using a simple shifting algorithm. The controller then set the membership function points with the new values and displayed them in graphs to show how they were affected. Typical membership functions were as shown in Figure 3.14 while Figure 3.15 shows the fuzzy logic controller.

3.3 Summary

This chapter has discussed the approaches employed to develop the laser drilling model and the Neuro-fuzzy controller. The effects of laser machining parameters, namely laser power and pulse duration, were successfully investigated. A model for predicting the optimal laser parameters for quality drilling of Inconel 718 was successfully developed. Finite Element Method was used to evaluate the temperature distribution. Using mathematical formulations for the laser drilling process, a simulation model was developed on $COMSOL$ platform and analysis done using an image analyzer. A neuro-fuzzy controller was then developed based on $MATLAB$ and $LabVIEW$ platforms. The controller was used to control the laser percussion drilling by simulating a drilling environment.

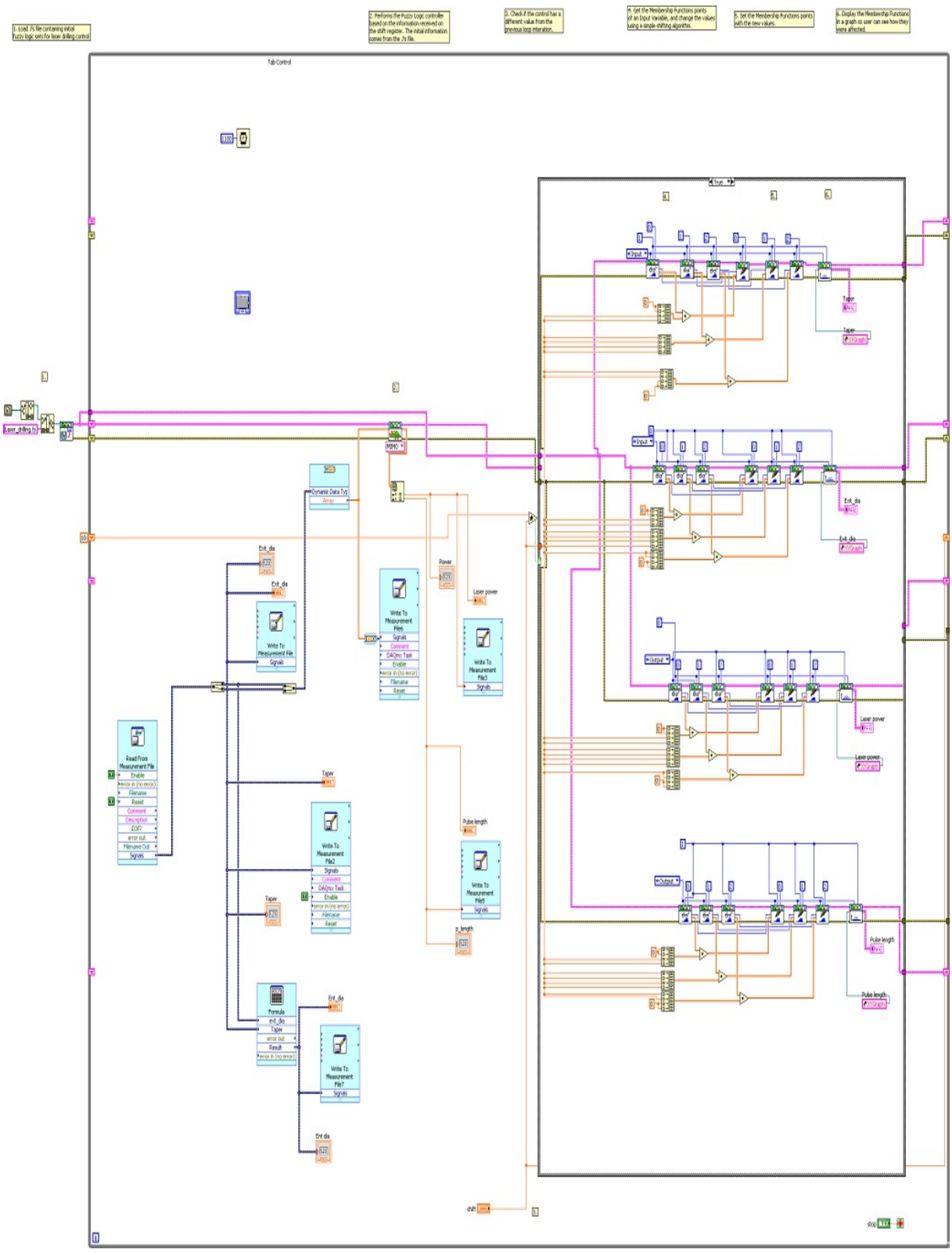

Figure 3.15: Fuzzy logic controller

CHAPTER FOUR

4.0 RESULTS AND DISCUSSION

In this chapter, detailed results from model simulations and neuro-fuzzy controller are discussed. The parameters under study were laser peak power and laser pulse duration. Simulations results from the model are discussed under sections 4.1 and 4.2 while those from the neuro-fuzzy controller are discussed under section 4.3.

4.1 Model validation results

Comparison is made for the simulation results with experimental data obtained from drilling of 304 Stainless steel sheets as reported by Wei [4] in order to validate the model. The stationary Q-switched Nd:YAG pulsed laser parameters used for the simulations are listed in Table 4.1.

Table 4.1: Laser parameters used in simulations on 304 Stainless steel

Laser parameter	**Description**
Laser type	Q-switched Nd:YAG
Pulse duration range	1-3.5 ms
Spot diameter	80 μm
Peak power range	1-6 kW

4.1.1 Peak power simulations

Peak power was varied from 1 kW to 6 kW at a constant pulse duration of 2 ms. Temperature distribution along the material thickness varies depending on the amount of laser peak power. Figure 4.1 shows the temperature profile along the material thickness for the various laser peak powers.

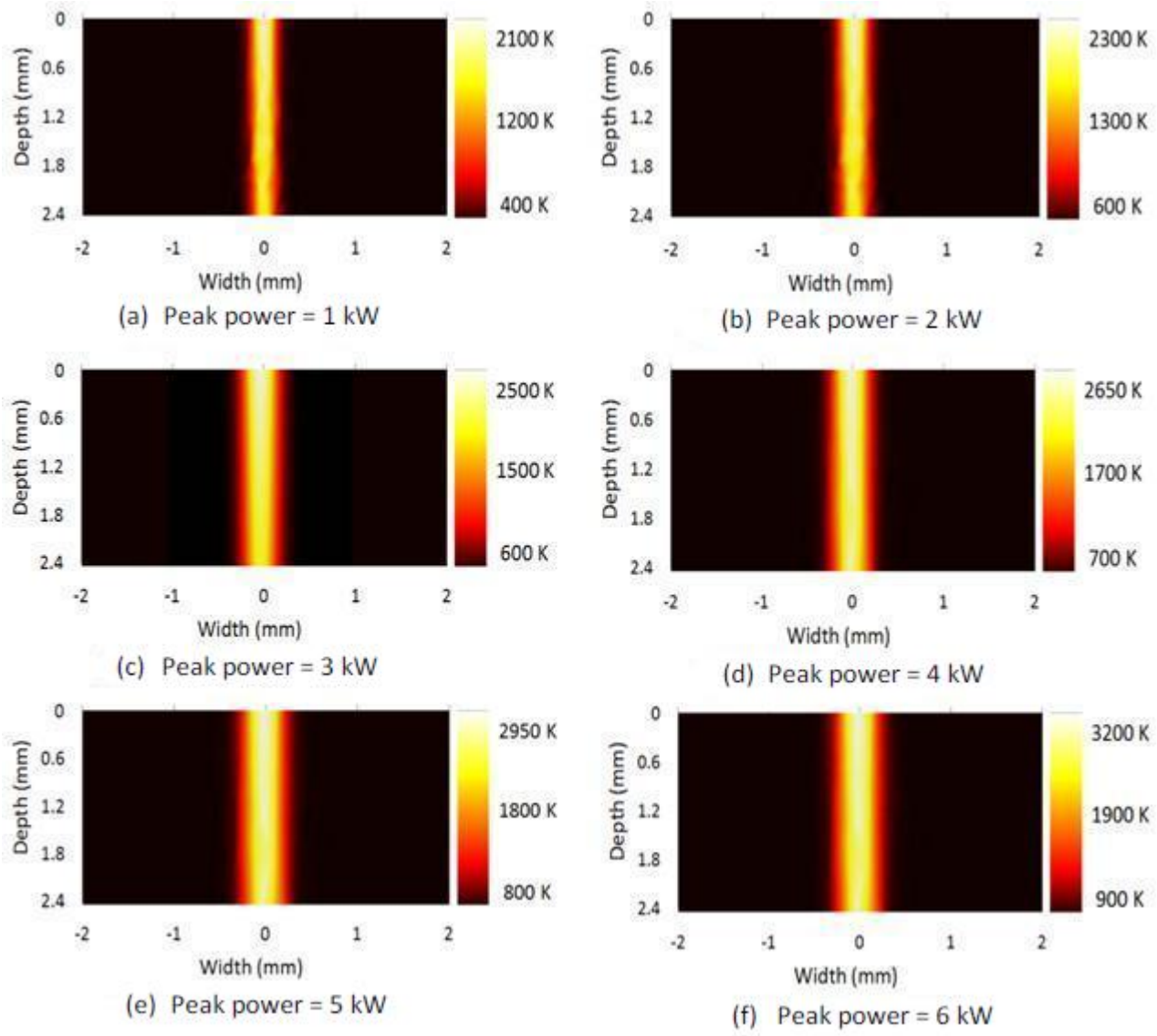

Figure 4.1: Temperature distribution along the material thickness (304 Stainless steel) for different laser peak powers

For the peak power of 6 kW, Figure 4.1(f), the temperature of the material below the heating zone reaches over 3200 K. The whole depth of the material below the heating zone is molten. The HAZ closest reaches temperature of 1900 K. These two zones experience melting since the temperatures reached here surpass the 304 Stainless steel melting point of 1723 K. The HAZ farthest reaches 900 K, and would not experience melting. For all the simulations carried out, the laser cut through the material depth.

4.1.1.1 Effect of laser peak power on taper angle and diameters

Comparison is made for the simulated taper angles with experimental ones reported by Wei [4], as shown in Figures 4.2 and 4.3. In both cases, it can generally be seen that taper angles decreased with increase in laser drilling peak power while the diameters increased with increase in peak power. The taper angle is a function of both entrance and exit diameters. During the drilling process, the hole is created as more material is molten and ejected by recoil pressure due to the vaporization of some of the molten material. With increase in peak power, the exit hole diameter therefore increases at a higher rate than the entrance diameter thereby reducing the hole taper. Increasing peak power at a constant pulse duration leads to an increase in incident laser intensity leading to more material removal.

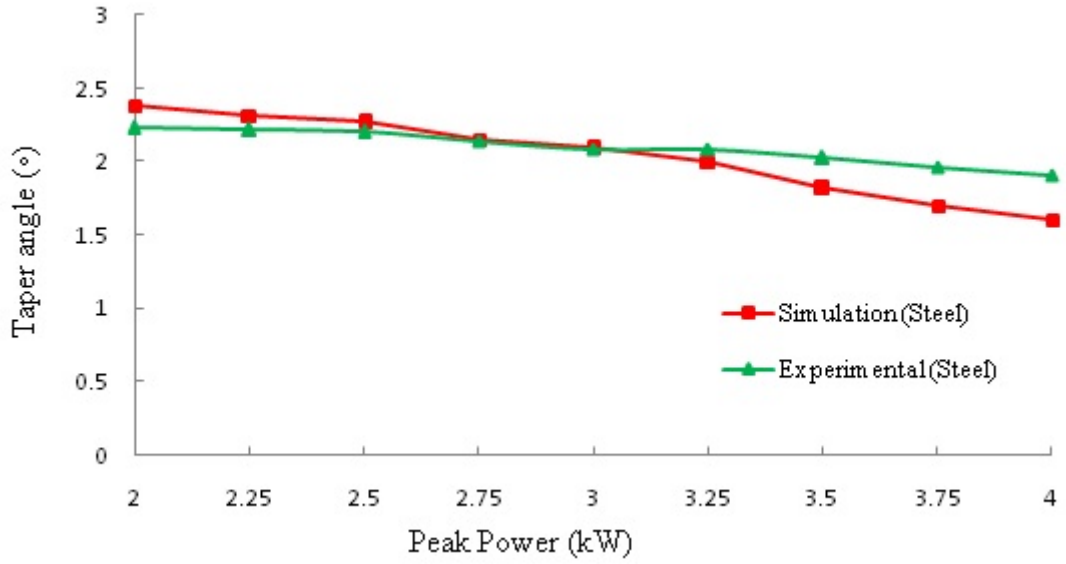

Figure 4.2: Influence of laser peak power on taper angles

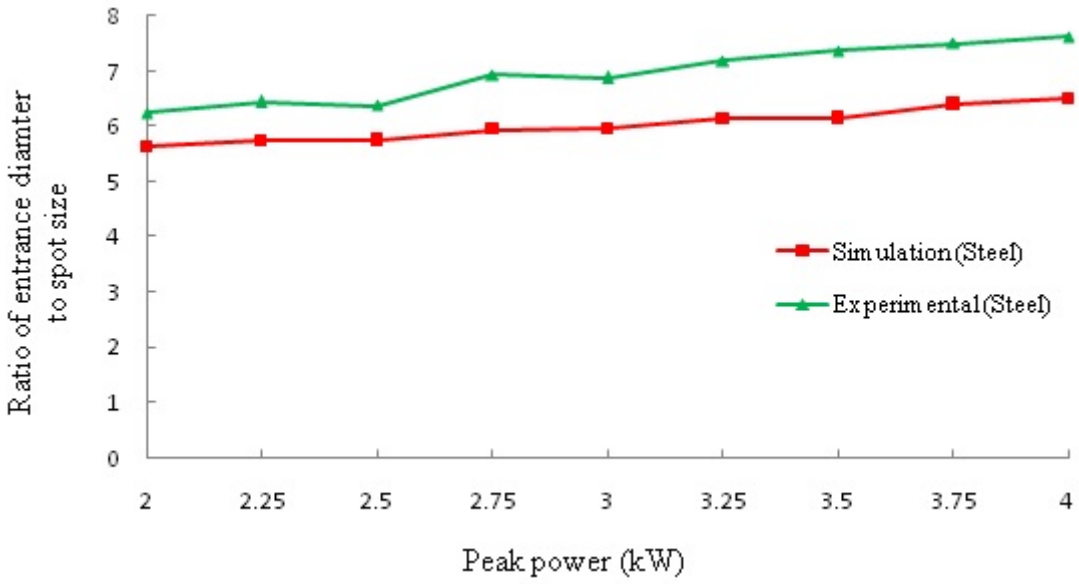

Figure 4.3: Influence of laser peak power on hole entrance diameters

4.1.2 Pulse duration simulations

Figure 4.4 shows the temperature profile along the material thickness for the various laser pulse durations. Pulse duration was varied from 1 ms to 3.5 ms at a constant peak power of 3 kW.

Figure 4.4(f) shows the temperature profile for the pulse duration of 3.5 ms. The temperature of the material below the heating zone reaches over 3250 K. The whole depth of the material below the heating zone is molten. The HAZ closest reaches temperature of 1950 K .These two zones experience melting since the temperatures reached here surpass the 304 stainless steel melting point of 1723 K. The HAZ farthest reaches 900 K and would not experience melting. The laser cuts through the material depth. The exit hole would be smaller than the entry hole. For all the simulations the laser cut through the material depth.

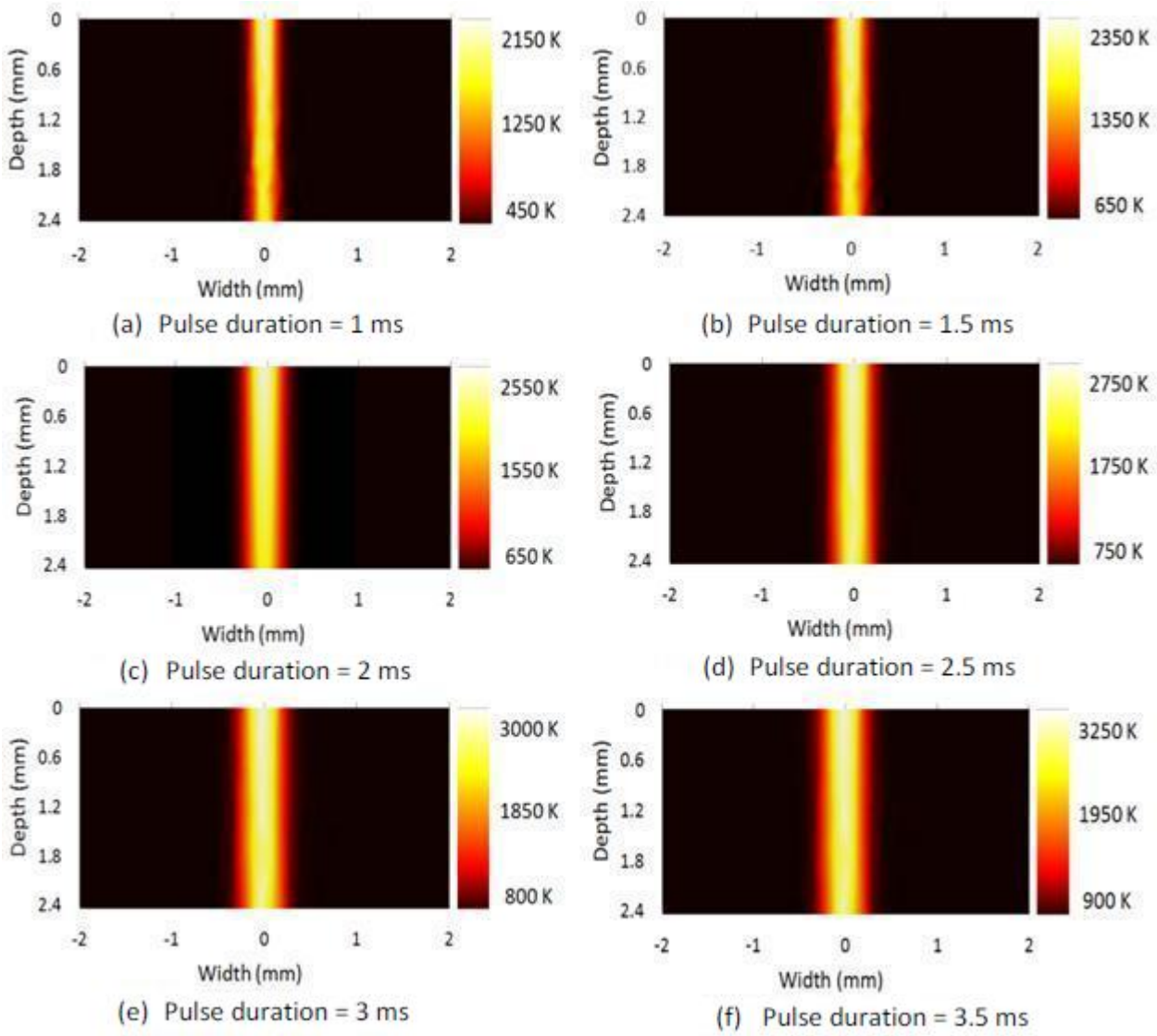

Figure 4.4: Temperature distribution along the material thickness (304 Stainless steel) for different pulse durations

4.1.2.1 Effect of laser pulse duration on taper angle and diameters

Comparison is made for the simulated taper angles with experimental ones reported by Wei [4] as shown in Figures 4.5 and 4.6. It can generally be seen that taper angles reduced with an increase in laser drilling pulse width while the diameters increased with an increase in laser pulse duration. Increasing laser pulse duration at a constant peak power increases energy per pulse hence leading to more material removal.

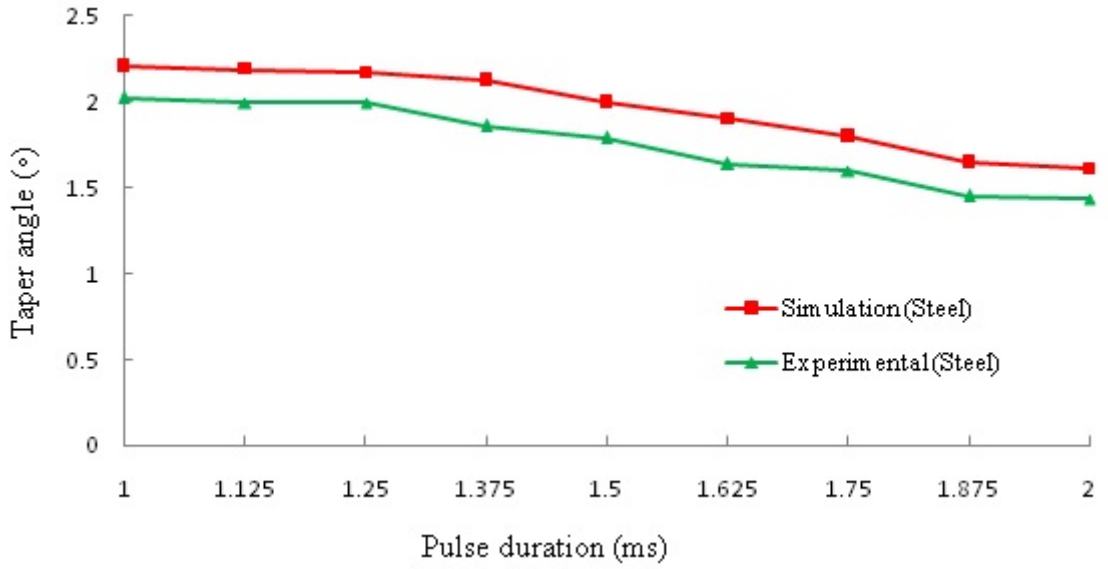

Figure 4.5: Influence of laser pulse duration on taper angles

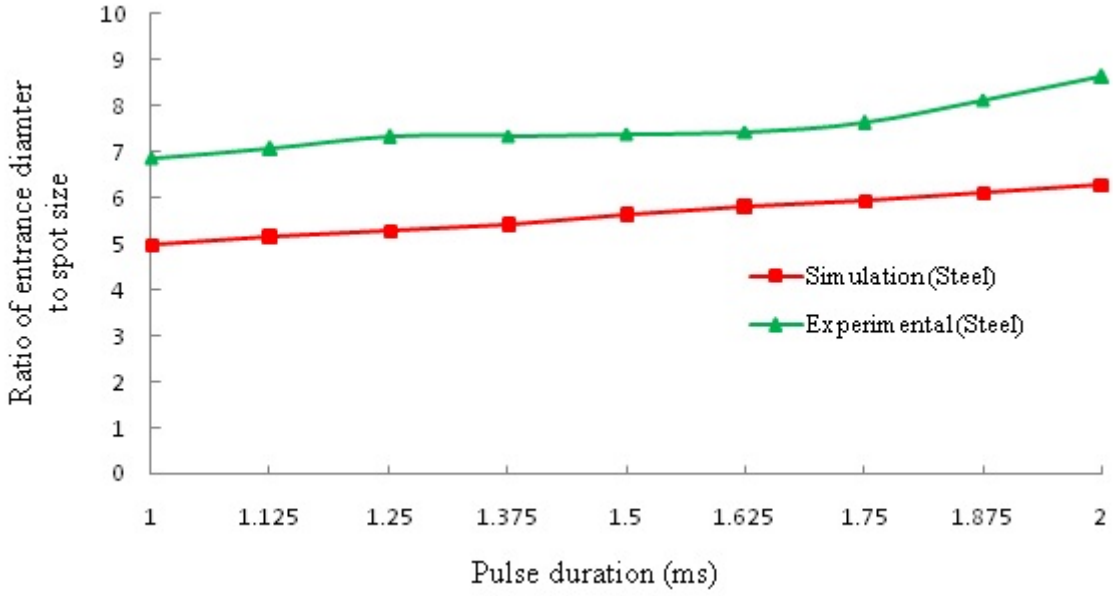

Figure 4.6: Influence of laser pulse duration on hole entrance diameters

The discrepancies in the graph magnitudes could be attributed to external factors not considered in the model, such as the plume/vapor screening effect of laser drilling. The vapor attenuates the intensity of incident laser radiation. The laser drilling model developed was based on laser drilling without any assist gas. Therefore, the effects

of assist gas on the laser drilling process were not considered and these bear a great influence on the drilled hole quality. These include the cooling effect, and exothermic and endothermic reactions due to the gas used. Assist gas affects material removal and drilling rate. The gas flows coaxially in tandem with the laser beam. Therefore, the pressure of the assist gas would disturb the laser beam profile irradiating the workpiece thereby scattering or blocking some incident energy. This results to a non-linear drilling profile hence enlargement of the drilled hole

The type of assist gas used bears a great influence on the final drilled hole quality due to exothermic reactions and oxidation reactions involved during the drilling process. Exothermic energy is normally added to the process when using gases such as oxygen. This leads to an increase the material removal rate. The oxide formed at the surface reduces the viscosity of the liquid metal. This promotes the melt ejection. Assist gas also causes a change in the absorptivity, and a change in the melting temperature of the material. Moreover, the model assumed a linear temperature distribution in the solid, starting from the solid-liquid interface to the thermal diffusion depth.

4.2 Effects of Laser parameters on drilled hole geometry

Simulations were carried out on laser drilling of Nickel-based super alloy, Inconel 718 with a thickness of 3 mm. The parameters studied were laser peak power and laser pulse duration.

4.2.1 Effect of laser peak power on hole geometry

Figure 4.7 shows the temperature profile along the material thickness for the various laser peak powers. Peak power was varied from 1 kW to 6 kW at a constant pulse duration of 2 ms.

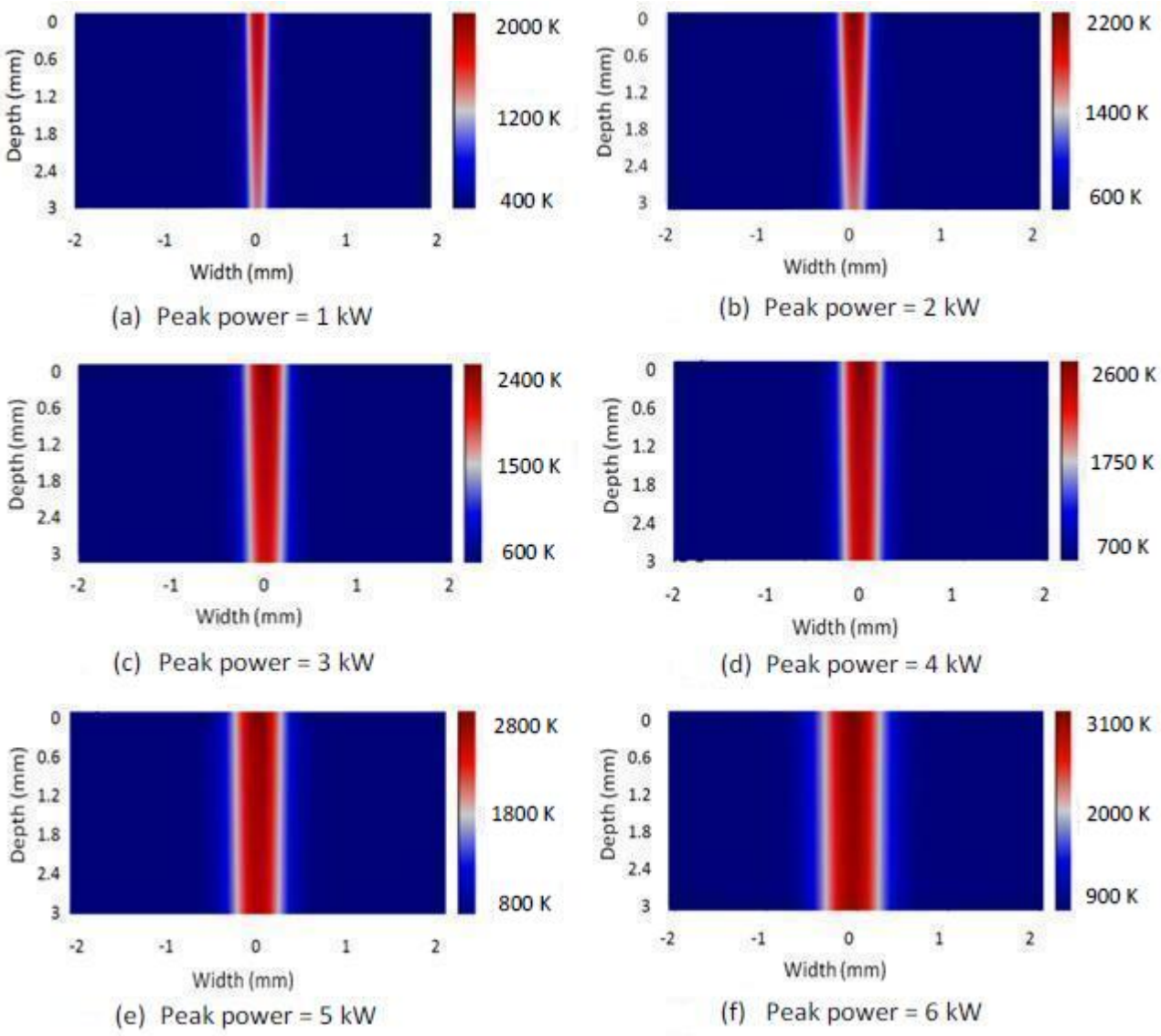

Figure 4.7: Temperature distribution along the material thickness (Inconel 718) for different laser peak powers

Figure 4.7(a) shows the temperature profile for 1 kW peak power. The temperature

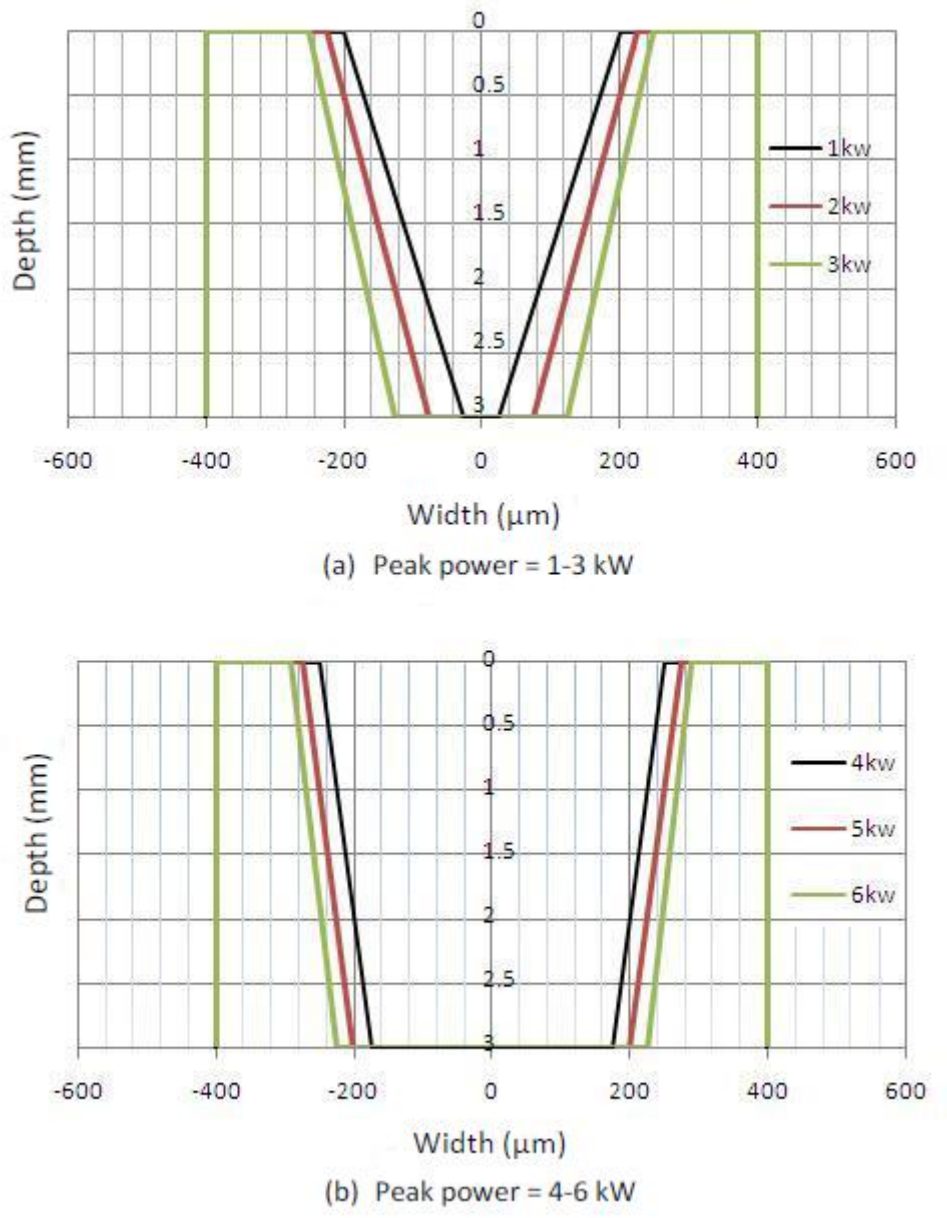

Figure 4.8: Hole profile along material thickness (Inconel 718) for different laser peak powers

of the material below the beam spot (heating zone) reaches over 2000 K. The whole depth of the material below the heating zone is molten. This zone therefore experiences melting since the temperatures reached here surpass the Inconel 718 melting point of 1610 K. The HAZ closest reaches temperature of 1200 K, while the HAZ farthest

reaches 400 K. These two zones do not experience melting.

For the peak power of 2 kW, Figure 4.7(b), the temperature of the material below the heating zone reaches over 2200 K. The whole depth of the material below the heating zone is molten. This zone therefore experiences melting since the temperatures reached here surpass the Inconel 718 melting point of 1610 K. The HAZ closest reaches temperature of 1400 K, while the HAZ farthest reaches 600 K. These two zones do not experience melting.

Figure 4.7(c) shows the temperature profile for 3 kW peak power. The temperature of the material below the heating zone reaches over 2400 K. The whole depth of the material below the heating zone is molten. This zone therefore experiences melting since the temperatures reached here surpass the Inconel 718 melting point of 1610 K. The HAZ closest reaches temperature of 1500 K, while the HAZ farthest reaches 600 K. These two zones do not experience melting.

For the peak power of 4 kW, Figure 4.7(d), the temperature of the material below the heating zone reaches over 2600 K. The whole depth of the material below the heating zone is molten. The HAZ closest reaches temperature of 1750 K. These two zones experience melting since the temperatures reached here surpass the Inconel 718 melting point of 1610K. The HAZ farthest reaches 700 K, and would not experience melting.

Figure 4.7(e) shows the temperature profile for 5 kW peak power. The temperature of the material below the heating zone reaches over 2800 K. The whole depth of the material below the heating zone is molten. The HAZ closest reaches temperature of 1800 K. These two zones experience melting since the temperatures reached here

surpass the Inconel 718 melting point of 1610 K. The HAZ farthest reaches 800 K, and would not experience melting.

For the peak power of 6 kW, Figure 4.7(f), the temperature of the material below the heating zone reaches over 3100 K. The whole depth of the material below the heating zone is molten. The HAZ closest reaches temperature of 2000 K. These two zones experience melting since the temperatures reached here surpass the Inconel 718 melting point of 1610 K. The HAZ farthest reaches 900 K, and would not experience melting. For all the six (6) cases i.e., Figures 4.7(a) to 4.7(f), the laser cuts through the material depth.

Hole profiles vary with varying peak power. The resulting hole profiles as generated from the temperature profiles are as shown in Fig. 4.8(a) for 1 kW to 3 kW peak powers and Fig. 4.8(b) for 4 kW to 6 kW peak powers respectively.

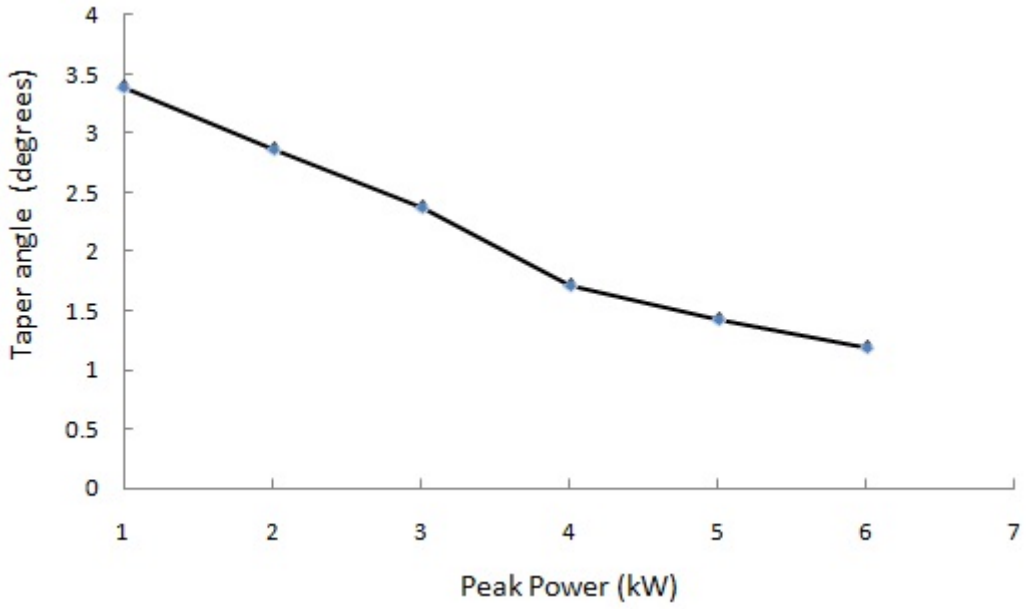

Figure 4.9: Influence of laser peak power on taper angles

Figure 4.9 shows the influence of laser peak power on taper angles. The taper angles

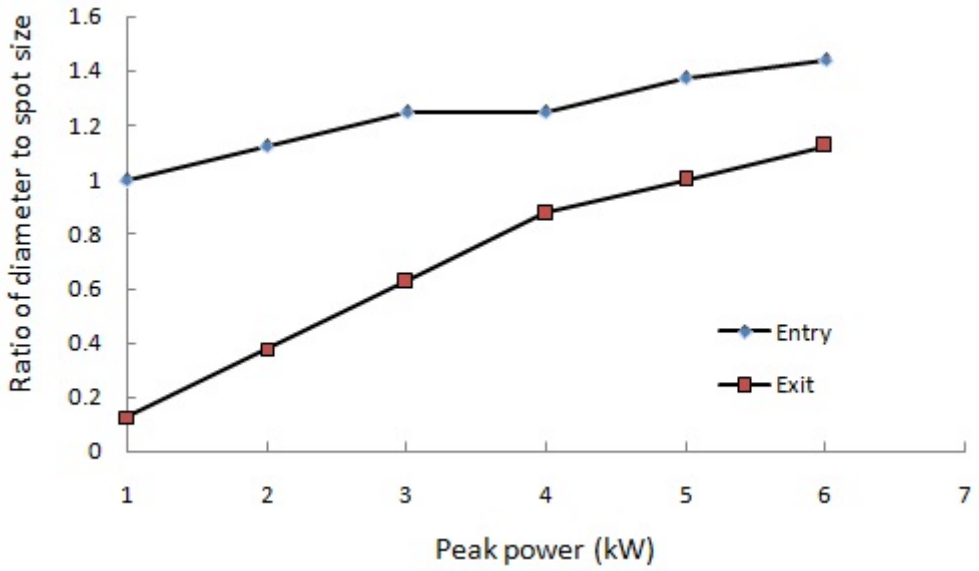

Figure 4.10: Influence of laser peak power on hole diameters

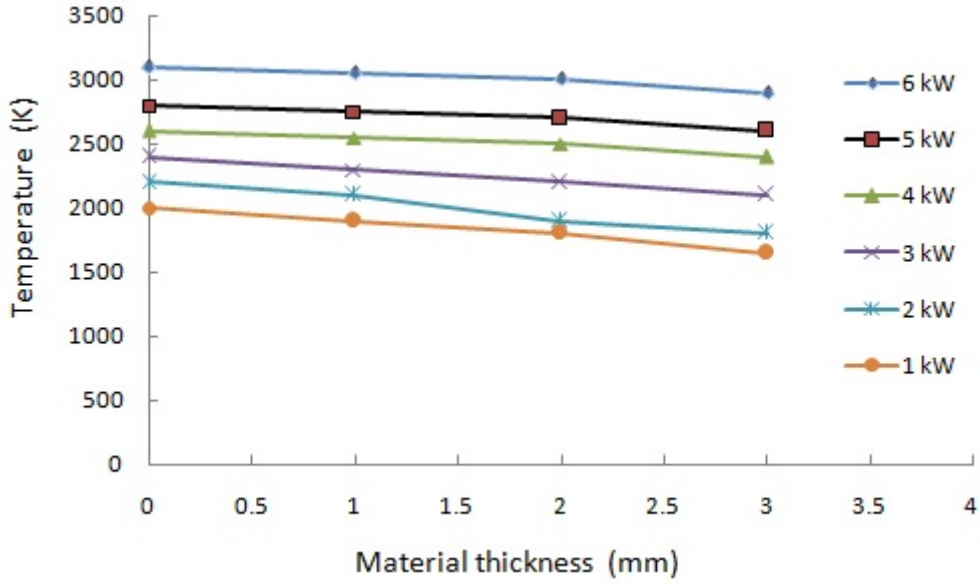

Figure 4.11: Temperature profile along the material thickness for different peak powers

are seen to generally reduce as the peak power increases. The tapering is to be expected since the exit hole would be smaller than the entry hole.

Figure 4.10 shows the influence of laser peak powers on the entry and exit diameters. The hole diameters are seen to generally increase as the peak power increases. This

increase is to be expected since the beam intensity at a spot increased with increasing power.

Figure 4.11 shows the temperature profile along the material depth for different peak powers. The temperature is seen to generally reduce through the depth of the work piece. This reduction is to be expected since heat conduction takes place in the material.

As peak power increases, more energy is transferred into the material creating more vapour above the workpiece surface. The large amount of vapour then causes a large recoil pressure above the melt liquid layer and enhances the liquid removal. High peak power can be achieved by either increasing the pulse energy or by reducing the pulse width. However, if a lower peak power is required, then it is recommended to adjust pulse energy rather than pulse width. At high laser pulse energy the exit diameter increases due to pressure exerted by the vaporization of the material in the hole.

4.2.2 Effect of laser pulse duration on hole geometry

Figure 4.12 shows the temperature profile along the material thickness for the various laser pulse durations. Pulse duration was varied from 1 ms to 3.5 ms at a constant peak power of 3 kW.

For the pulse duration of 1 ms, Figure 4.12(a), the temperature of the material below the beam spot (heating zone) reaches over 1960 K. The whole depth of the material below the heating zone is molten. This zone therefore experiences melting since the temperatures reached here surpass the Inconel 718 melting point of 1610 K. The HAZ closest reaches temperature of 1200 K, while the HAZ farthest reaches 420 K. These

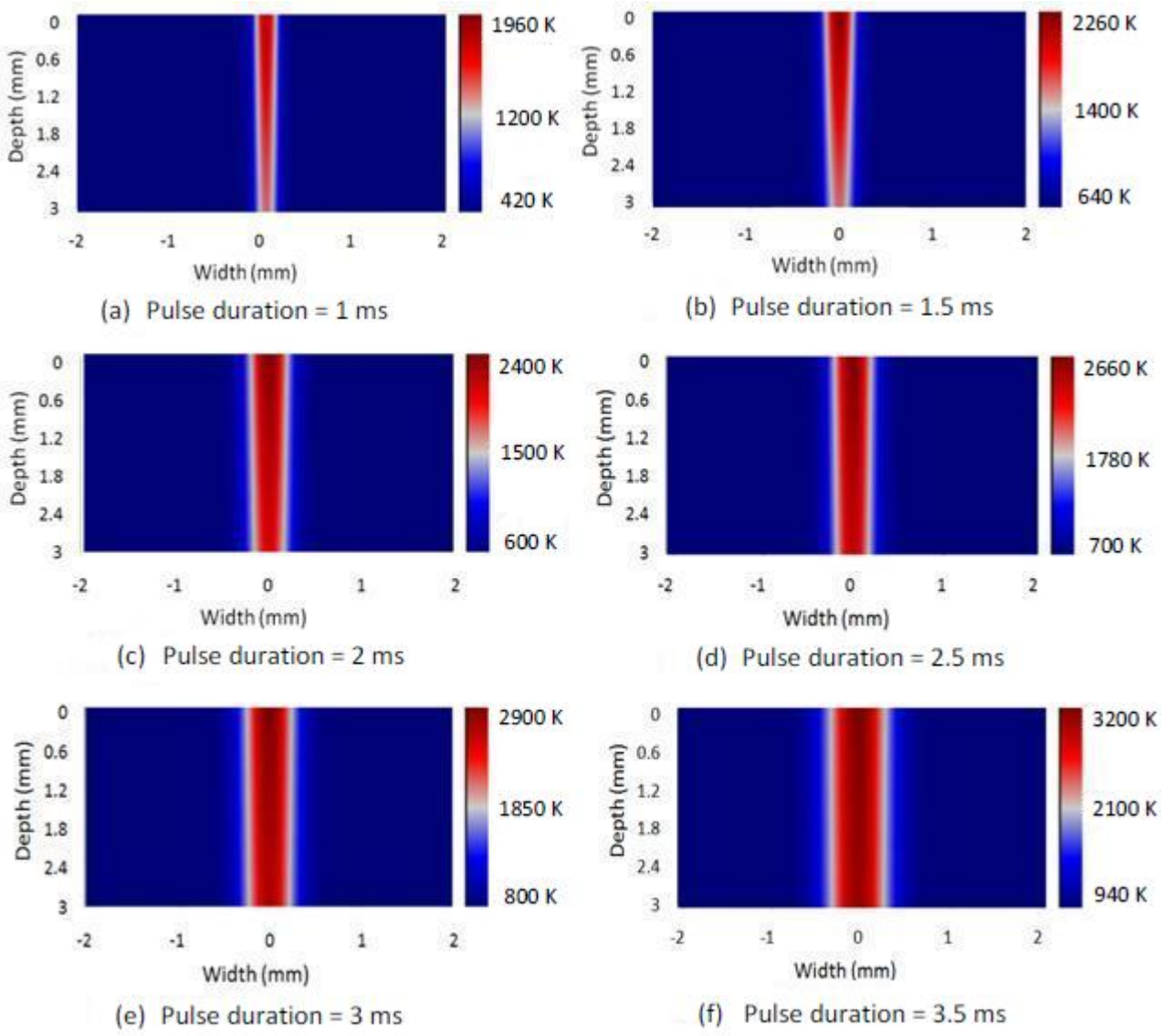

Figure 4.12: Temperature distribution along the material thickness for different pulse durations

two zones do not experience melting.

Figure 4.12(b) shows the temperature profile for the pulse duration of 1.5 ms. The temperature of the material below the heating zone reaches over 2260 K. The whole depth of the material below the heating zone is molten. This zone therefore experiences melting since the temperatures reached here surpass the Inconel 718 melting point of

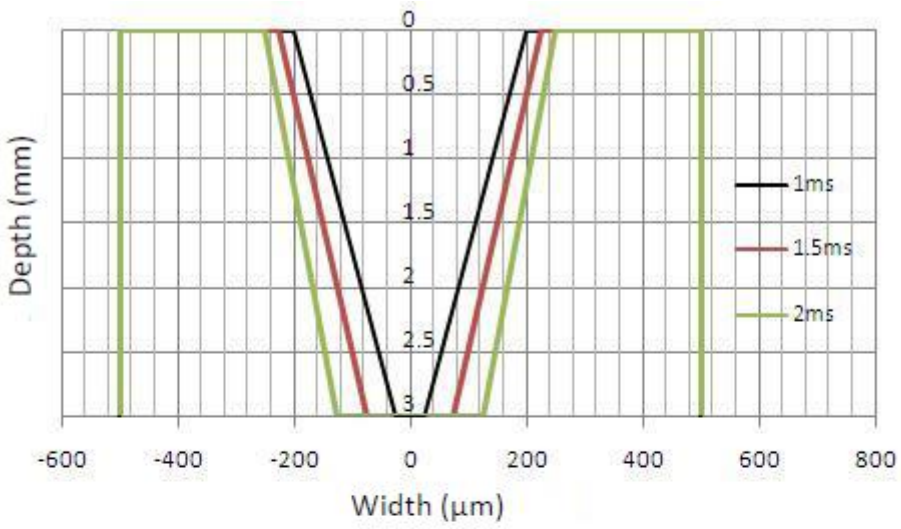

(a) Pulse duration = 1-2 ms

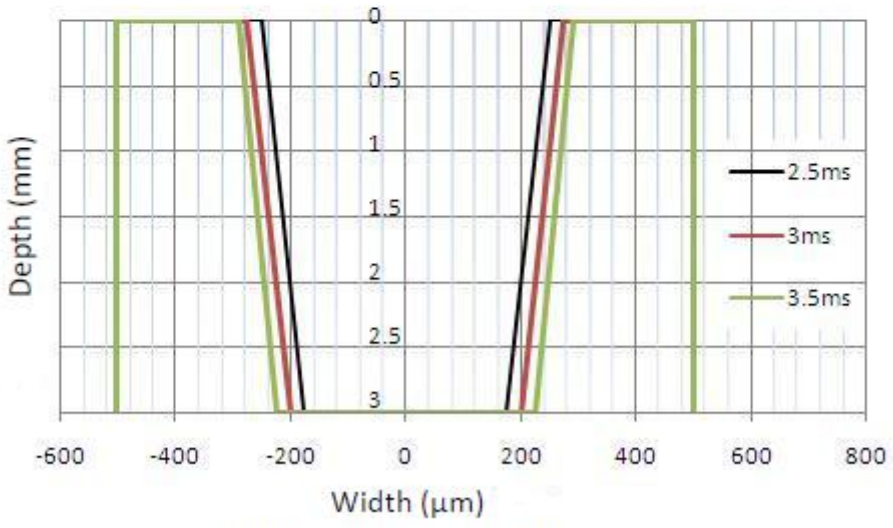

(b) Pulse duration = 2.5-3.5 ms

Figure 4.13: Hole profile along material thickness for different laser pulse durations

1610 K. The HAZ closest reaches temperature of 1400 K, while the HAZ farthest reaches 640 K. These two zones do not experience melting.

For the pulse duration of 2 ms, Figure 4.12(c), the temperature of the material below the heating zone reaches over 2400 K. The whole depth of the material below the heating zone is molten. This zone therefore experiences melting since the temperatures

reached here surpass the Inconel 718 melting point of 1610 K. The HAZ closest reaches temperature of 1500 K, while the HAZ farthest reaches 600 K. These two zones do not experience melting.

Figure 4.12(d) shows the temperature profile for the pulse duration of 2.5 ms. The temperature of the material below the heating zone reaches over 2660 K. The whole depth of the material below the heating zone is molten. The HAZ closest reaches temperature of 1780 K. These two zones experience melting since the temperatures reached here surpass the Inconel 718 melting point of 1610 K. The HAZ farthest reaches 700 K, and would not experience melting.

For the pulse duration of 3 ms, Figure 4.12(e), the temperature of the material below the heating zone reaches over 2900 K. The whole depth of the material below the heating zone is molten. The HAZ closest reaches temperature of 1850 K .These two zones experience melting since the temperatures reached here surpass the Inconel 718 melting point of 1610 K. The HAZ farthest reaches 800 K, and would not experience melting.

Figure 4.12(f) shows the temperature profile for the pulse duration of 3.5 ms. The temperature of the material below the heating zone reaches over 3200 K. The whole depth of the material below the heating zone is molten. The HAZ closest reaches temperature of 2100 K .These two zones experience melting since the temperatures reached here surpass the Inconel 718 melting point of 1610 K. The HAZ farthest reaches 940 K, and would not experience melting. For all the six (6) cases i.e., Figures 4.12(a) to 4.12(f)), the laser cuts through the material depth.

Hole profiles vary with increasing pulse duration. The resulting hole profiles as gener-

ated from the temperature profiles are as shown in Fig. 4.13(a) for 1 ms to 2 ms pulse durations and Fig. 4.13(b) for 2.5 ms to 3.5 ms pulse durations respecitvely.

Figure 4.14 shows the influence of laser pulse duration on taper angles. The taper angles are seen to generally reduce as the pulse width increases. The exit hole diameter increases at a higher rate than the entrance diameter hence leading to the reduction in hole taper with increase in pulse duration.

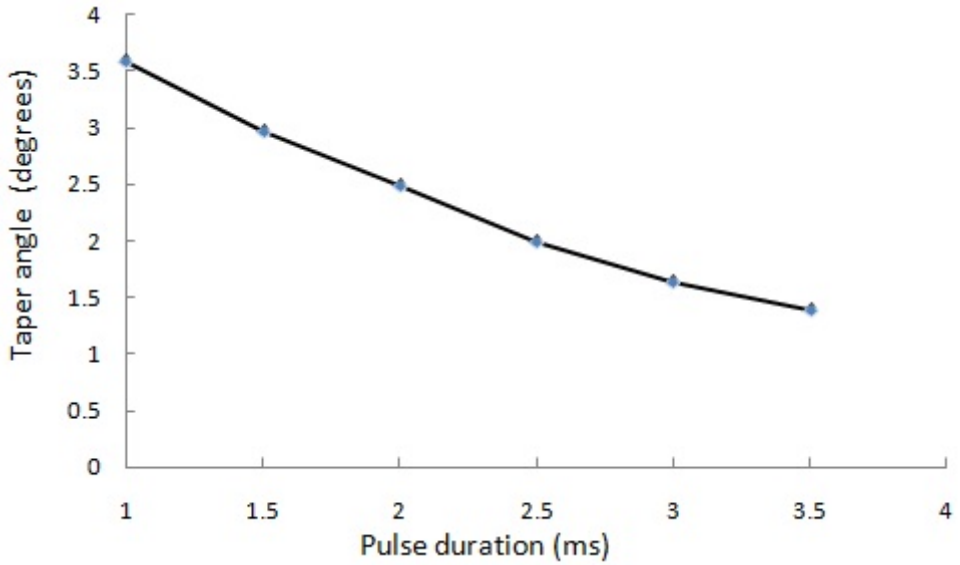

Figure 4.14: Influence of laser pulse duration on taper angles

Figure 4.15 shows the influence of laser pulse durations on the diameters at entry and exit. The hole diameters are seen to generally increase as the pulse width increases. This increase is to be expected since the energy delivered at the spot increased with increasing pulse width.

Figure 4.16 shows the temperature profile along the material depth for different pulse durations. The temperature is seen to generally reduce through the depth of the work piece. This reduction is to be expected since heat conduction takes place in the material.

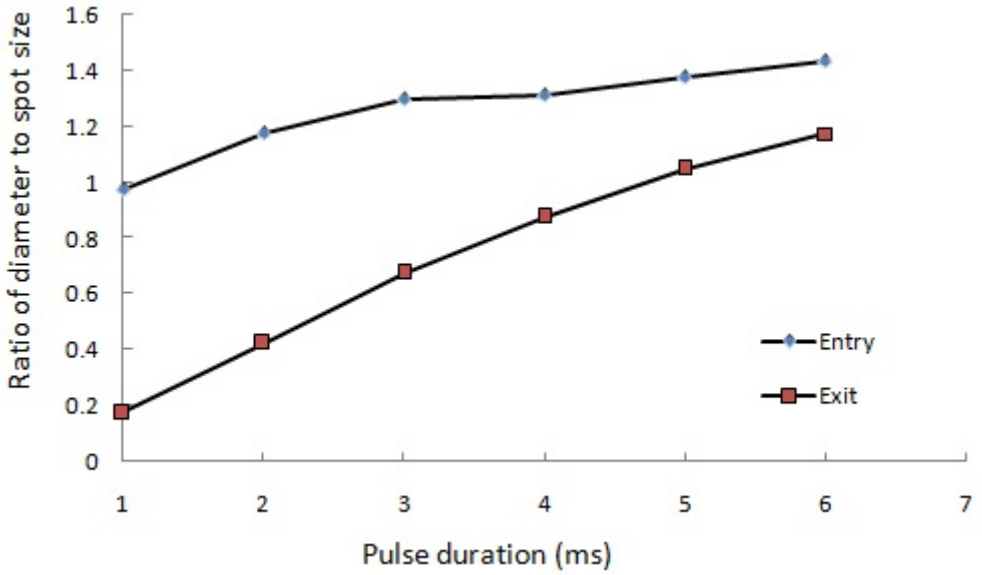

Figure 4.15: Influence of laser pulse duration on diameters

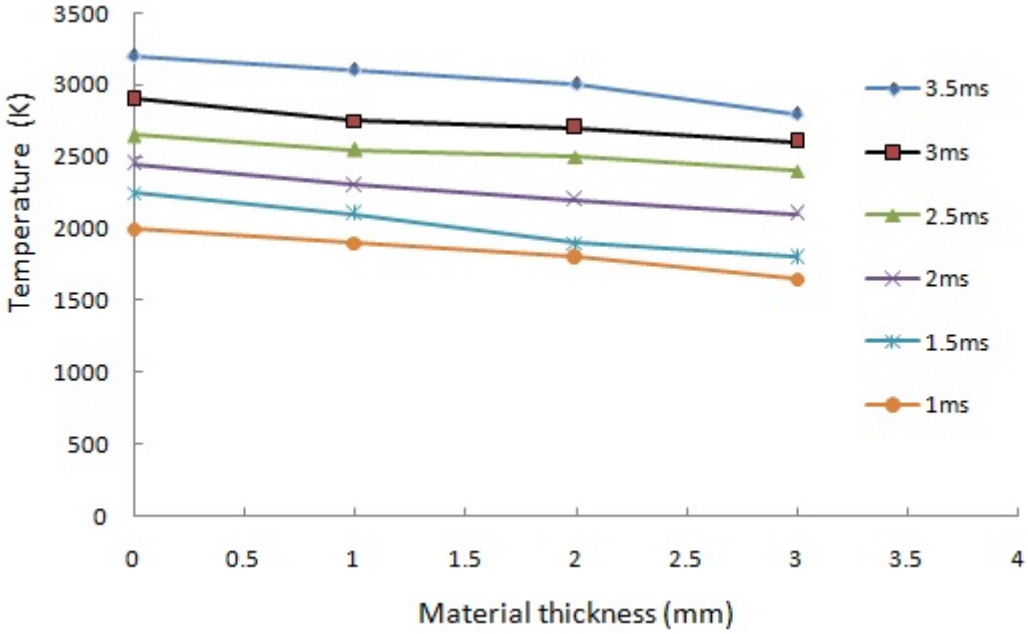

Figure 4.16: Temperature profile along the material thickness for different pulse durations

Longer pulse results in larger diameter and the deeper holes. However, too long pulse duration may be unable to produce the through hole. Short pulse duration improves hole circularity and process repeatability, and causes less heat affected zones (HAZ)

defects.

4.3 Performance of the neuro-fuzzy controller on the laser drilling process

The developed ANFIS based controller is analysed in the following section.

The effectiveness of the controller was tested by comparing the controller results with results from the developed laser drilling model. Output data from the model was used as the input to the controller. The data included the values for taper angle and exit diameter while varying the peak power at a fixed pulse duration of 2 ms.

The controller simultaneously controlled laser peak power and pulse duration. Figure 4.17 shows the variation of hole diameters with laser peak power. The diameters are seen to generally increase as the power increases. This increase is to be expected since the laser beam intensity at a spot increases with increasing power. For exit hole diameters ranging from 50 μm to 450 μm, the optimum laser peak power was found to be 2.082 kW.

The variation of hole taper with laser peak power is shown in Figure 4.18. The taper is seen to generally reduce as the power increases. For hole taper angles ranging from 1.2° to 3.4°, the optimum laser peak power was found to be 2.082 kW.

Figure 4.19 shows the variation of hole diameters with laser pulse duration. The diameters are seen to generally increase as the pulse duration increases. This increase is to be expected since the energy delivered at the spot increases with increasing pulse width. For exit hole diameters ranging from 50 μm to 450 μm, the optimum laser pulse

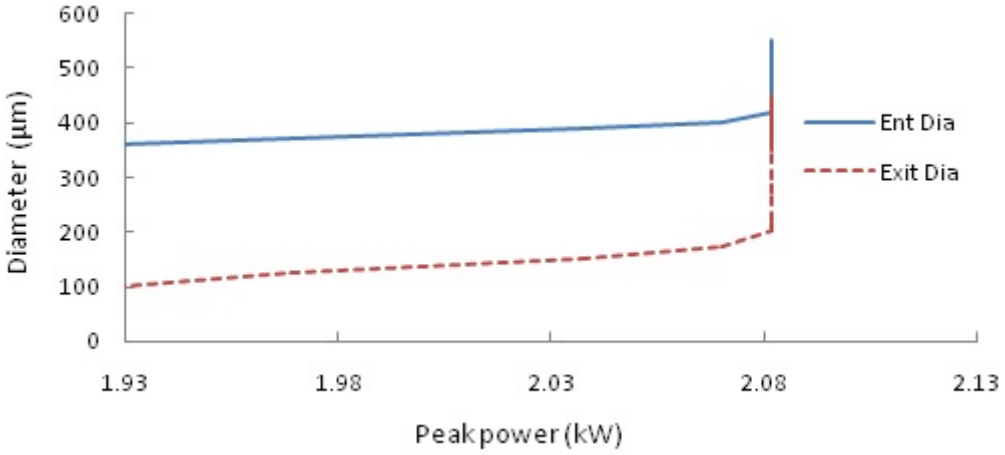

Figure 4.17: Effect of laser peak power on hole diameters

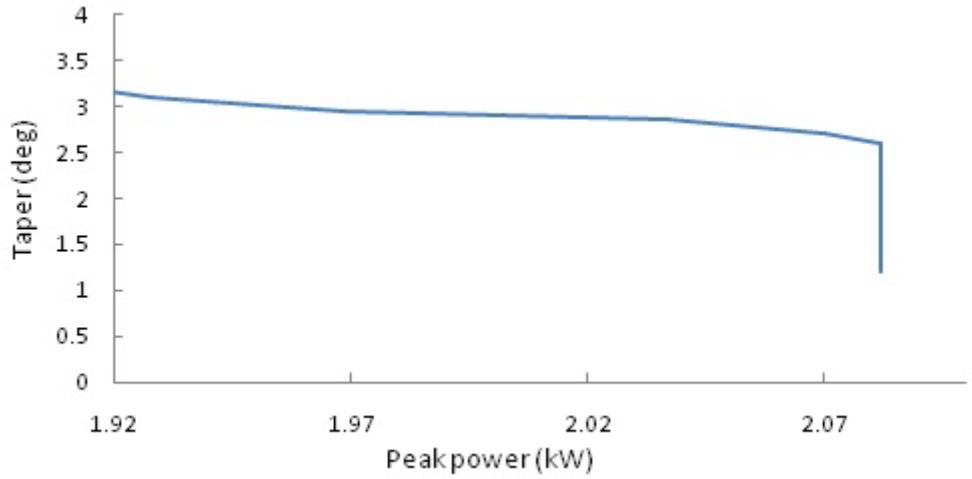

Figure 4.18: Effect of laser peak power on hole taper

duration was found to be 1.669 ms.

The variation of hole taper with laser pulse duration is shown in Fig. 4.20. The taper is seen to generally reduce as the pulse duration increases. For hole taper angles ranging from 1.2° to 3.4°, the optimum laser pulse duration was found to be 1.669 ms.

From Figures 4.21 and 4.22, it can be deduced that while drilling using the neuro-fuzzy controller, the laser peak power and pulse duration can be simultaneously varied in order to acquire optimal hole parameters. The Figures show values of peak power and

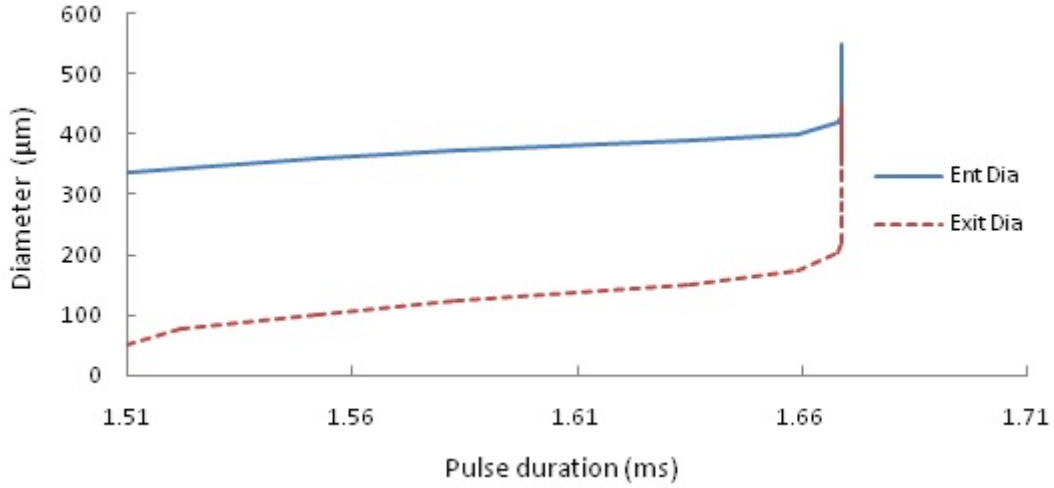

Figure 4.19: Effect of laser pulse duration on hole diameters

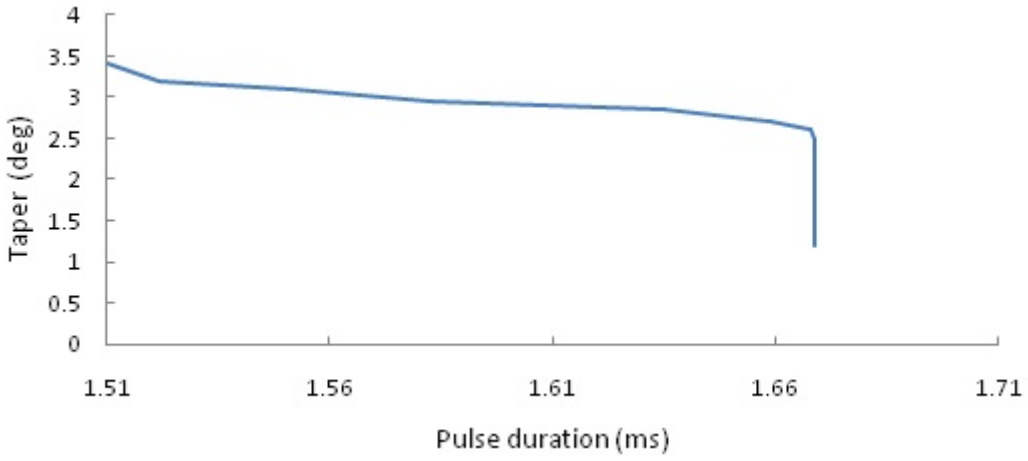

Figure 4.20: Effect of laser pulse duration on hole taper

pulse duration computed by the controller given values for hole taper and hole entrance diameters as the inputs. The ANFIS based neuro-fuzzy contoller read the input values from a spreadsheet file. Using the learning capabilty of artificial neural networks, the controller was able to compute the optimum values for laser peak power and pulse duration. Artificial neural networks have excellent capabality for approximation of process performance.

While drilling without the controller, the hole diameters increase with increasing laser

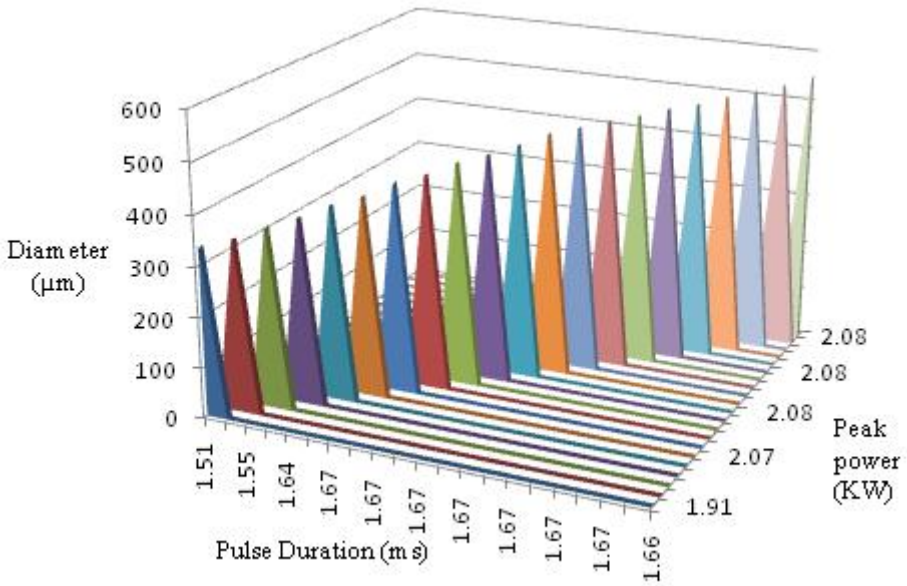

Figure 4.21: Surface map for entrance hole diameters

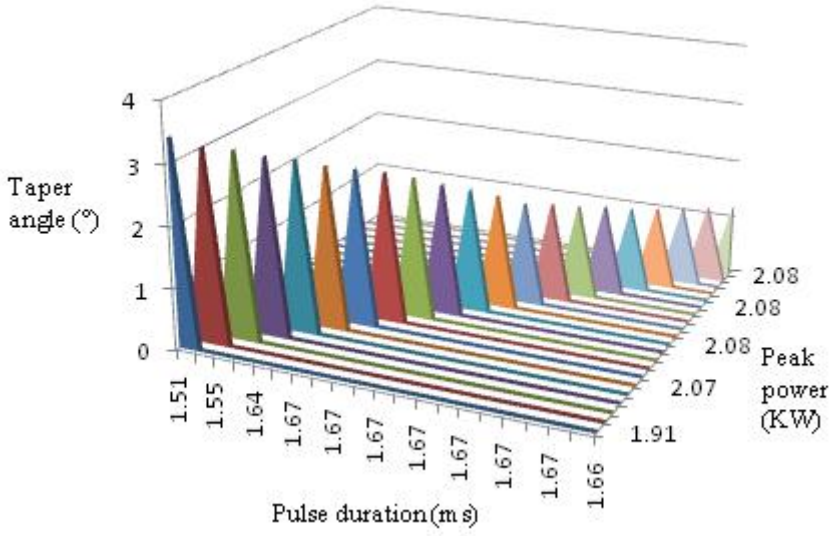

Figure 4.22: Surface map for hole taper angles

peak power and pulse duration. Increasing laser peak power at a fixed pulse duration increases the laser beam intensity at the drilling spot.

Figures 4.23 and 4.24 show the rates of change of hole diameters and taper with increase in peak power at a constant pulse duration. The entrance diameter increases at a rate of 0.0336 mm/kW while the exit diameter increase at a rate of 0.0814 mm/kW. The

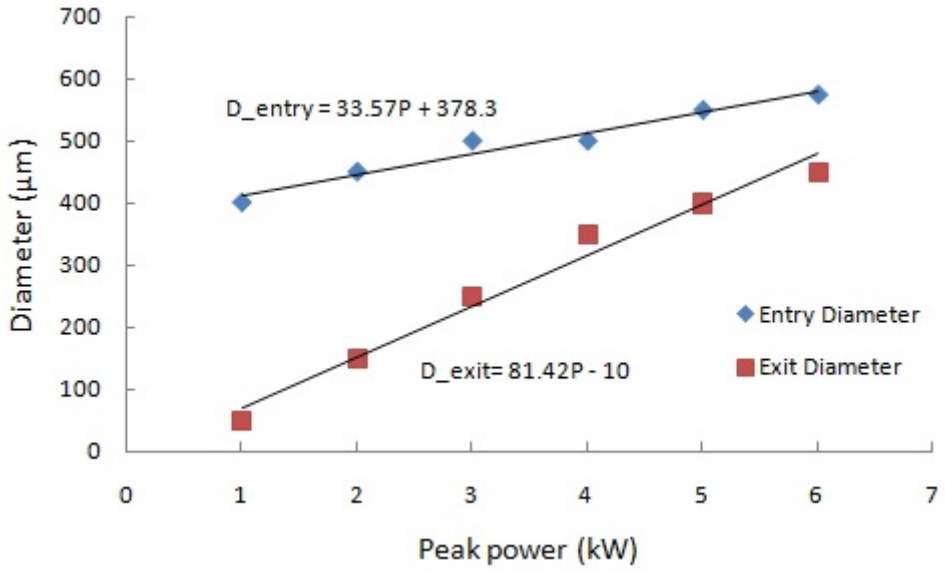

Figure 4.23: Rate of change of hole diameters with peak power (without controller)

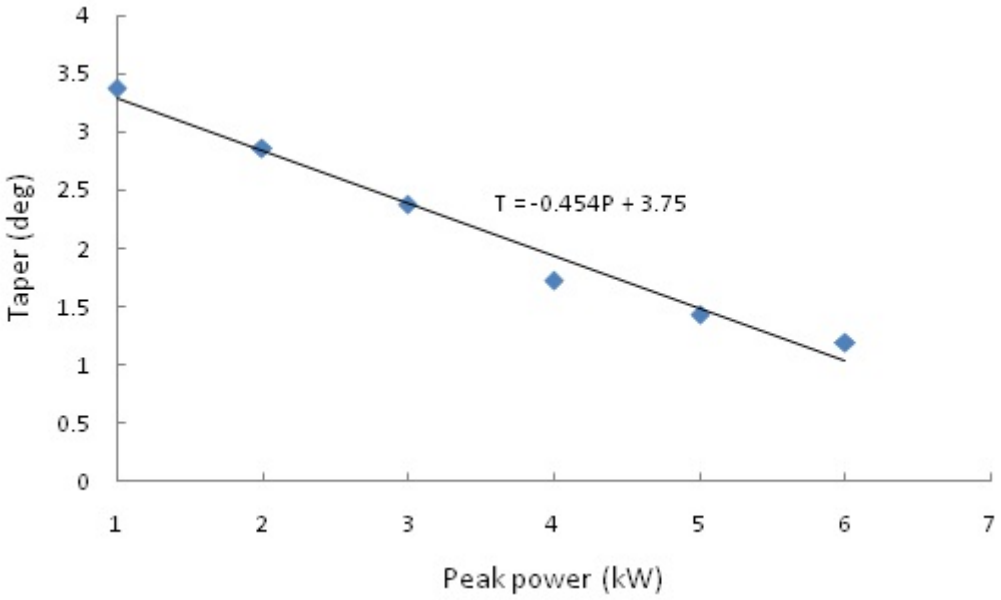

Figure 4.24: Rate of change of hole taper with peak power (without controller)

hole taper decreases at a rate of 0.45 deg/kW.

Increasing the pulse width at fixed peak power effectively increases energy per pulse of the laser beam. This will generate high vapor pressure built up inside the hole and ejecting more material. Figures 4.25 and 4.26 show the rates of change of hole

diameters and taper with increase in pulse duration at a constant peak power. The entrance diameter increases at a rate of 0.0334 mm/ms while the exit diameter increase at a rate of 0.0809 mm/ms. The hole taper decreases at a rate of 0.881 deg/ms.

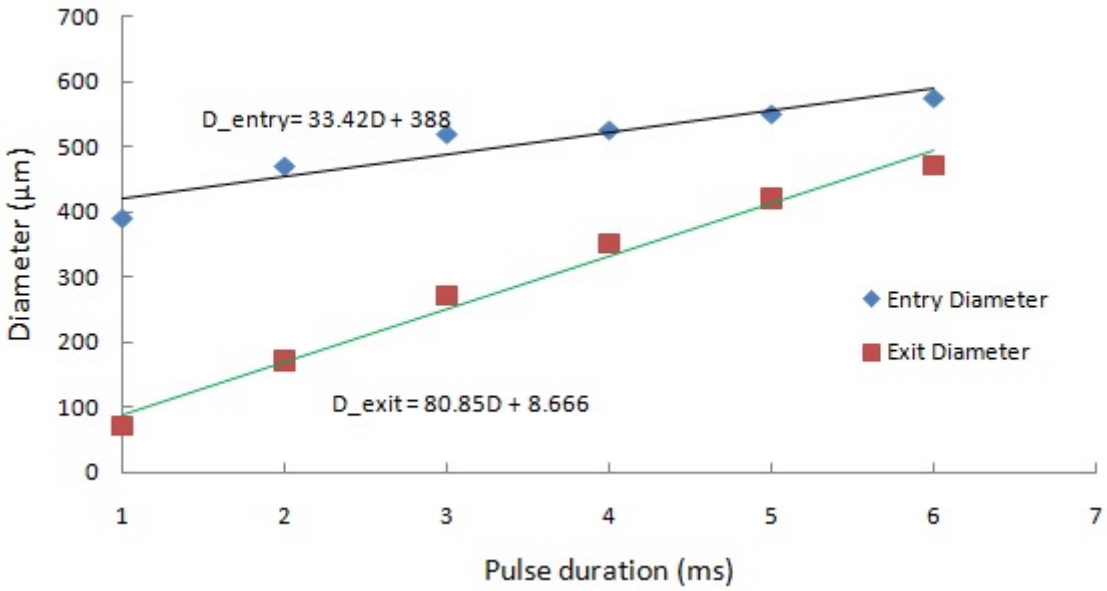

Figure 4.25: Rate of change of hole diameters with pulse duration (without controller)

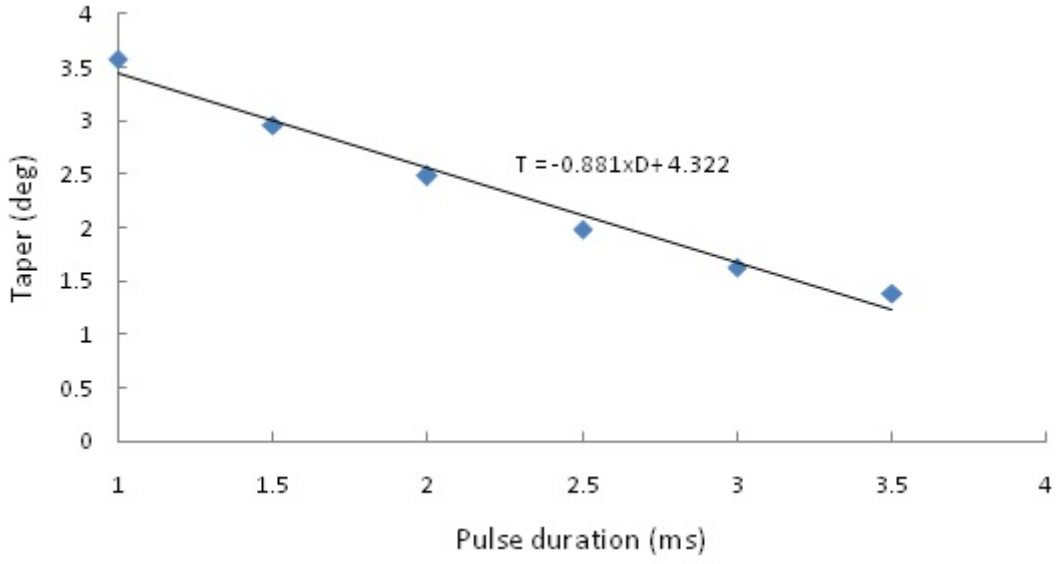

Figure 4.26: Rate of change of hole taper with pulse duration (without controller)

While using the controller, the hole diameters increase with increase in peak power

and pulse duration upto an optimum level beyond which the peak power and pulse duration remain constant as the diameters increase. The hole taper decreases with increase in peak power and pulse duration upto optimum level beyond which the peak power and pulse duration remain constant as the taper decreases. Thus, the controller helps maintain the peak power and pulse duration at optimum levels. Peak power and pulse duration bear a great influence on the laser energy incident on the material. The laser energy is responsible for the production of hole. Optimal combinations of the two parameters is thus of great importance for the process.

From Figures 4.17 through 4.20,the rates of change of hole diameters and taper with increase in peak power and pulse duration were computed. The hole entrance diameters increase at an average rate of 0.4 mm/kW and 0.5 mm/ms while the exit hole diameters increase at an average rate of 0.7 mm/kW and 0.89 mm/ms upto the optimum level of peak power and pulse duration. The hole taper decreases at an average rate of 4.55 deg/kW and 3.6 deg/ms upto the optimum level of peak power and pulse duration.

4.4 Summary

In this chapter, the results from model simulation and neuro-fuzzy controller have been presented. Simulation results have been validated by comparison to experimental results as reported by Wei [4]. The model satisfactorily predicted the expected hole diameters at the entrance and exit and also the taper angles for various values of laser peak power and pulse duration. It was also demonstrated that a neuro-fuzzy based controller effectively controls the hole diameters and taper through in-process adjustments of laser power and pulse duration. The controller helps maintain the peak power and pulse duration at optimum levels.

CHAPTER FIVE

5.0 CONCLUSION AND RECOMMENDATIONS

5.1 Conclusion

In this study, the effects of laser machining parameters, namely laser power and pulse duration, were investigated. A model for predicting the optimal laser parameters for quality drilling of Nickel based super alloy-Inconel 718 was successfully developed. Finite Element Method was used to evaluate the temperature distribution. Using mathematical formulations for the laser percussion drilling process, a simulation model was developed on $COMSOL^R$ platform and analysis done using an image analyzer platform. A neuro-fuzzy controller was then developed based on $MATLAB^R$ and $LabVIEW^R$ platforms. The controller was used to control the laser percussion drilling by simulating a drilling environment.

Validation of the model was through experimental results from literature. The models satisfactorily predicted the expected hole tapers and diameters for the laser parameters studied. The result showed that both laser power and pulse duration have great influence on the hole geometric parameters. Hole taper reduces with increase in both laser pulse duration and laser power. Hole diameters increase with increase in both laser power and pulse duration. The neuro-fuzzy based controller effectively controls the hole diameters and taper through in-process adjustments of laser power and pulse duration. While using the controller, the hole diameters increase with increase in peak power and pulse duration upto an optimum level beyond which the peak power and pulse duration remain constant as the diameters increase. The hole taper decreases with increase in peak power and pulse duration upto optimum level beyond which the

peak power and pulse duration remain constant as the taper decreases. The hole entrance diameters increase at an average rate of 0.4 mm/kW and 0.5 mm/ms while the exit hole diameters increase at an average rate of 0.7 mm/kW and 0.89 mm/ms upto the optimum level of peak power and pulse duration. The hole taper decreases at an average rate of 4.55 deg/kW and 3.6 deg/ms upto the optimum level of peak power and pulse duration. Thus, the controller helps maintain the peak power and pulse duration at optimum levels.

5.2 Recommendations

To improve the model and the neuro-fuzzy controller for the laser percussion drilling of nickel based super-alloys, the following are areas that could be further addressed.

1. Plume/vapor screening effect of laser drilling which was not included in the laser drilling model should be investigated.

2. The effects of assist gas on the laser drilling process were not considered in the model. These include the cooling effect, and exothermic and oxidation reactions. These should therefore be investigated since they have a great influence on the drilled hole quality.

3. The effects of non-linear temperature distribution in the solid, starting from the solid-liquid interface to the thermal diffusion depth should be investigated.

4. Validation of the model was through experimental data from literature. Experimental work on drilling of Inconel 718 should therefore be done in order to validate the model

5. The controller was implemented in a simulation environment and not tested experimentally due to unavailability of the laser facility. Actual machining environment should be therefore be investigated.

REFERENCES

[1] Sizov M.A., *Air-film cooling through laser drilled holes*, Eindhoven University of Technology, Netherlands, 2007.

[2] Narendra B.D., Sandip P.H., *Laser Fabrication and Machining of Materials*,New York, USA, 2007.

[3] Steen W.M., *Laser material processing*, Springer-Verlag, London, 1991.

[4] Wei H., *Computational and experimental investigations of laser drilling and welding for microelectronic packaging*, Ph.D thesis, Worcester Polytechnic Institute, 2004.

[5] Jan C., Johannes V., *Modelling Laser Percussion Drilling*, Eindhoven University, 2004.

[6] Patrick H.W., *Artificial Intelligence*, Pearson Education (Singapore), Third Edition, 2004.

[7] Witold P., *Fuzzy control and Fuzzy systems*, Research Studies Press ltd, Second extended edition, 1993.

[8] Naeem M., Mike W., *Laser percussion drilling of coated and uncoated aerospace materials with a high beam quality and high peak power lamp pumped pusled nd: yag laser*, Paper 305, pp. 111-119, 2005.

[9] Okasha M.M., Mativenga P.T. ,Driver N., Li L., *Sequential laser and mechanical micro-drilling of Ni superalloy for aerospace application*, Journal of Manufacturing Technology 59, pp. 199-202, 2010.

[10] Sushant D., Nishant S., Purohit R., *A review on laser drilling and its Techniques*, Proceedings: International Conference on Advances in Mechanical Engineering, 2006.

[11] Prasad G. et al., *Laser cutting of metallic coated sheet steels*, Journal of Materials Processing Technology, vol 74. pp. 234-242, 1998.

[12] Thamir K.I., Rahman M.M., Ahmed N.A., *Improvement of gas turbine performance based on inlet air cooling systems: A technical review*, International Journal of Physical Sciences Vol. 6(4), pp. 620-627, 2011.

[13] Shen. Z. H., Zhang. S. Y., Lu. J., *Mathematical modeling of laser induced heating and melting in solids*,Optics and Laser Technology, vol.33, pp.533-537, 2001.

[14] Ravindra H.P.,*Thermal modeling of laser drilling and cutting of engineering materials*, MSc. Thesis, University of Pune, India, 2005.

[15] John F. R.,*Industrial applications of lasers*, Academic Press (USA), second edition, 1997.

[16] Khan. A. H., Celotto. S., Tunna. L., Neill. W., and Sutcliffe. C. J., *Influence of Microsupersonic Gas Jets on Nanosecond Laser Percussion Drilling*, Optics and Laser in Engineering, vol. 45, pp. 709-178, 2007.

[17] Low D.K.Y., Li L., and Byrd P.J., *The Influence of Temporal Pulse Train Modulation during Laser Percussion Drilling*, Optics and Lasers in Engineering, vol. 35, pp. 149-164, 2001.

[18] Peters C., French P.W, Hand D.P., Shannon G.J., Byrd P., Steen W.M., *Investigation of the Nd:YAG laser percussion drilling process using high speed filming*, Department of Physics, Heriot Watt University, 1998.

[19] Ghoreishi M., Low D.K.Y., Li L., *Statistical modelling of laser percussion drilling for hole taper and circularity control*,Proceedings of the Institution of Mechanical Engineers, Part B: Journal of Engineering Manufacture, pp. 307-319, 2002.

[20] Low. D. K., Li. L., and Byrd. P. J., *The Effects of Process Parameters on Spatter Deposition in Laser Percussion Drilling*, Optics and Laser Technology, vol. 32, pp. 347-354, 2000.

[21] Hamilton D.C., Pashby I.R., *Hole drilling studies with a variable pulse length CO_2 laser*, Journal of Optics and Laser Technology, vol 11(4), Pages 183-188, 1979.

[22] Han W., Pryputniewicz J.R., *Investigations of Laser Percussion Drilling of Small Holes on Thin Sheet Metals*, Proceedings of SPIE, pp. 31-40, 2004.

[23] Roos S.O., *Laser Drilling with Different Pulse Shapes*, Journal of Applied Physics, vol. 51, pp. 5061-5063, 1998.

[24] Tan B., *Deep Micro Hole Drilling in a Silicon Substrate Using Multi-Bursts of Nanosecond UV Laser Pulses*, Journal of Micromechanics and Microengineering, vol. 16, pp. 109-112, 2006.

[25] Low D.K.Y., Li L., *Effects of Inter-Pulse and Intra-Pulse Shaping during Laser Percussion Drilling*, Proceedings of SPIE, pp. 191-194, 2002.

[26] Semak V. V., *Role of beam absorption in plasma during laser welding*,Journal of Physics, vol. 33(10), 2000.

[27] Lazare S., Tokarev V.N., *A Laser Beam Model for High Performance Micro-drilling*,Journal of Physics: Conference Series, vol. 59, pp. 32-35, 2007.

[28] Leigh S., Sezer K., Li L., Grafton-Reed C., Cuttell M., *Recast and oxide formation in laser-drilled acute holes in CMSX-4 nickel single-crystal super-alloy*, Proceed-

ings of the Institution of Mechanical Engineers, Part B: Journal of Engineering Manufacture 224, pp. 1005-1016, 2010.

[29] Kamalu J., Byrd P.J., *Statistical design of laser drilling experiments*, Proceedings of the International Conference on Applications of Lasers and Electro-Optics (ICALEO '98), Section B, pp. 264-273, 1998.

[30] S.Bandyopadhyay, J.K.S. Sundar, G.Sundararajan, and S.V.Joshi, *Geometrical Features and Metallurgical Characteristics of Nd:YAG Laser Drilled Holes in Thick IN718 and Ti-6Al-4V Sheets*, Journal of Materials Processing Technology, vol. 127, pp. 83-95, 2002.

[31] Kuar A.S. et al., *Modeling and analysis of pulsed Nd:YAG laser machining of zirconia (ZrO2)*, International Journal of Machine Tools and Manufacture. vol 46(12), pp. 1301-1310, 2006.

[32] Sivarao, Shukor, Anand, Ammar, *DOE based statistical approaches in modeling of laser processing - review and suggestion*, International Journal of Engineering and Technology IJET-IJENS, Vol 10(4), 2010.

[33] Joonghan S., *Measurement and numerical simulation of high temperature laser material processing*, Thesis, University of Michigan, 2010.

[34] Lawrence Y., Hongqiang C., *Thermal Aspects in Laser Material Removal*, NSF Workshop on Research Needs in Thermal Aspects of Material Removal Processes, pp. 247-256, 2003.

[35] Tam S.C. et al., *Application of Taguchi method in the optimization of the laser-cutting process*, Journal of Materials Processing Technology, vol 29, pp. 63-74, 1992.

[36] Seema C., Mitra R., Kumar V., *A Neuro-fuzzy Learning and its Application to Control system*, World Academy of Science, Engineering and Technology 34, 2007.

[37] Kurzwell R., *The age of intelligent machines*, MIT Press, Third edition, 1992.

[38] Fakhreddine O.K., Clarence S., *Soft Computing and Intelligent Systems Design*, Pearson Education (UK), 2004.

[39] Ali Z., Mohammad J., *Intelligent Control Systems Using Soft Computing Methodologies*, CRC Press, 2001.

[40] Alexander M.M., James S.A., *Intelligent systems, Architecture, Design, and control*, John Wiley & Sons, Inc (New York), 2002.

[41] Clarence W.S., *Intelligent control, fuzzy logic applications*, CRC press, 1995.

[42] Yang J.R., *ANFIS: Adaptive-Network-Based Fuzzy Inference System*, IEEE Trans. on systems, man, and cybernetic,vol. 23, no.3, pp. 665-685, May 1993.

[43] Nakhjavani O.B., Ghoreishi M., Aghanajafi S., *Optimization of laser percussion drilling by using neural network for stainless steel 304*, Department of Mechanical Engineering, IAzad University of Technology Science and Research Branch, 2004 .

[44] Sivarao et al, *Neural network modeling and validation for micro quality evaluation in laser processing*, International Journal of Intelligent Information Technology Application, pp. 84-90, 2009.

[45] Collins. J., and Gremaud. P., *A Simple Model for Laser Drilling*, Mathematics and Computers in Simulation, vol. 81, pp. 1541-1552, 2011.

[46] Xie.J. and Kar. A., *Mathematical Modeling of Melting during Laser Materials Processing*, Journal of Applied Physics, vol. 81, pp. 3015-3022, 1997.

[47] Zhang. v, Salama. I. S., Quick. N. R., and Kar. A., *One-Dimensional Transient Analysis of Volumetric Heating for Laser Drilling*, Journal of Applied Physics, vol. 99, pp. 113530-1-113530-10, 2006.

[48] Zhang.Y., and Faghri. A., *Vaporization, Melting and Heat Conduction in the Laser Drilling Process*, International Journal of Heat and Mass Transfer, vol. 42, pp. 1775-1790, 1999.

[49] Shin. S., and Chung. H., *Modeling of Melting, Evaporating, and Resolidifying Procedure in Laser-Induced Metal Processing*, ASME, vol. 131, pp. 024501-1-024501-5, 2009.

[50] Alexiades. V., and Solomon. A. D., *Mathematical Modeling of Melting and Freezing Processes*, Washington: Hemisphere Publishing Corporation, 1993.

[51] Zeng. D., Latham. W. P., and Kar. A., *Two-Dimensional Model for Melting and Vaporization during Optical Trepanning*, Journal of Applied Physics, vol. 97, pp. 104912-1-7, 2005.

[52] Yilbas. B. S., Mansoor. S. B., Shuja. S. Z., and Abualhamayel. H., *Laser Pulse Heating and Vapor Front Generation*, AIChE Journal, vol. 54, pp. 627-638, 2008.

[53] Shin.S. and Chung. H., *Modeling of Melting, Evaporating, and Resolidifying Procedure in Laser-Induced Metal Processing*, Journal of Manufacturing Science and Engineering, vol. 131, pp. 024501-1-024501-5, 2009.

[54] Ling. Z., Zhi-Rong. Z., and Jianglong. L., *Heat and Mass Transfer Model during Melting of Metal Induced by CW CO2 Laser Irradiation*, Key Engineering Materials, vol. 46-47, pp. 497-504, 1990.

[55] Smurov. I. Yu., Uglov. A. A., Lashin. A. M., Matteazzi. P., Tagliaferri. V., and Covelli. L., *Movement of Phase Boundaries of Metals Subjected to Surface Periodic Energy Pulses*, Journal of Applied Physics, vol. 69, pp. 8031-8036, 1991.

[56] Dowden. J. M., *The Mathematics of Thermal Modeling: An Introduction to the Theory of Laser Material Processing*, Florida: 2001.

[57] Sankaranarayanan. S., Emminger. H., and Kar. A., *Energy Loss in the Plasma during Laser Drilling*, Journal of Physics D: Applied Physics, vol. 32, pp. 1605-1611, 1999.

[58] Ng. G. K. L., Crouse. P. L., and Li. L., *An Analytical Model for Laser Drilling Incorporating Effects of Exothermic Reaction, Pulse Width and Hole Geometry*, International Journal of Heat and Mass Transfer, vol. 49, pp. 1358-1374, 2006.

[59] Semak. V., and Matsunawa. A., *The Role of Recoil Pressure in Energy Balance during Laser Materials Processing*, Journal of Physics D: Applied Physics, vol. 30, pp. 2541-2552, 1997.

[60] Low. D. K. Y., Li. L., and Byrd. P.J., *Hydrodynamic Physical Modeling of Laser Drilling*, ASME, vol. 124, pp. 852-862, 2002.

[61] Satapathy B.B., Rana J., and Maity P.K., *Quality Optimization of Micro-Hole In Laser Drilling*, IOSR Journal of Engineering,Vol.2(3) pp:382-388, Mar. 2012.

APPENDIX A

A.1 NEURO-FUZZY DATA

. Sample data generated from the Neuro-fuzzy controller is shown in Table A.1.

Table A.1: Controller data

Peak Power (KW)	**Pulse Duration** (ms)	**Ent Dia** (μm)	**Exit Dia** (μm)	**Taper** (deg)
1.911	1.51	335.2	50	3.4
1.913	1.522	344.4	76	3.2
1.928	1.552	360	100	3.1
1.969	1.583	371.4	124	2.95
2.037	1.635	389	150	2.85
2.07	1.659	400	174	2.7
2.082	1.668	420	202	2.6
2.082	1.669	429.6	220	2.5
2.082	1.669	447	250	2.35
2.082	1.669	457.4	273	2.2
2.082	1.669	470	298	2.05
2.082	1.669	486.2	327	1.9
2.082	1.669	492.5	350	1.7
2.082	1.669	500.3	362	1.65
2.082	1.669	504.9	375	1.55
2.082	1.669	512.7	387	1.5
2.082	1.669	517	400	1.4
2.082	1.669	526.1	413	1.35
2.082	1.669	532.9	424	1.3
2.082	1.669	540	435	1.25
2.082	1.669	550.5	450	1.2

APPENDIX B

B.1 INTELLIGENT SYSTEMS

Intelligent systems generally have a capacity to acquire and apply knowledge in an intelligent manner and have the capabilities of perception, reasoning, learning, and making inferences (or decisions) from incomplete information [37].

An intelligent machine consists of a knowledge system and a structural system. The knowledge system effects and manages intelligent behavior of the machine, analogous to the brain, and consists of various knowledge sources and reasoning strategies [37,38]. The structural system consists of physical hardware and devices that are necessary to perform the machine objectives yet do not necessarily need a knowledge system for their individual functions [39].

The method of knowledge-based systems (KBS), is one artificial intelligence paradigm which has found widespread application. This technique can represent a controller or a decision support system according to a number of architectures, and is able to handle heuristics and empirical knowledge [39].

There are four basic components as shown in Figure B.1: the knowledge base (or knowledge source), database, inference engine, and the system interface [37, 38]. The knowledge base contains knowledge and expertise in the specific domain, particularly domain-specific facts and heuristics useful for solving problems in the domain. The database is primarily a short-term memory. The database contains the current status of the problem, inference states, and the history of solutions to date. The inference engine is the driver program of a knowledge-based system. Depending on the data in the database, the inference engine applies and operates on the knowledge in the

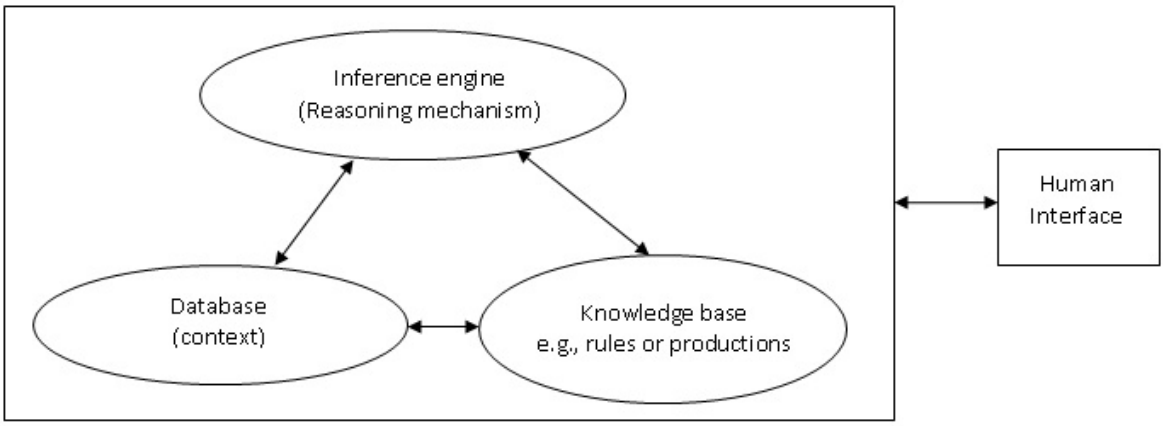

Figure B.1: The structure of a knowledge-based system

knowledge source to solve problems and arrive at conclusions. [6,38]. The fourth basic component of a KBS is the system interface (or user interface), which is provided for the external world (or user) to interact with the overall system, to browse through the knowledge source, to edit the knowledge (e.g., rules) and for many other interactive tasks.

Fuzzy logic, probability theory, artificial neural networks, and genetic algorithms are cooperatively used in soft computing for knowledge representation and for mimicking the reasoning and decision-making processes of a human [6, 38]. Of interest in this study are the fuzzy logic and neural networks.

ARTIFICIAL NEURAL NETWORKS (ANN)

An artificial neural network (ANN) is typically composed of a set of parallel and distributed processing units, called nodes or neurons [6]. These are usually ordered into layers, appropriately interconnected by means of unidirectional (or bi-directional in some cases) weighted signal channels, called connections or synaptic weights, as shown in Figure B.2 [38].

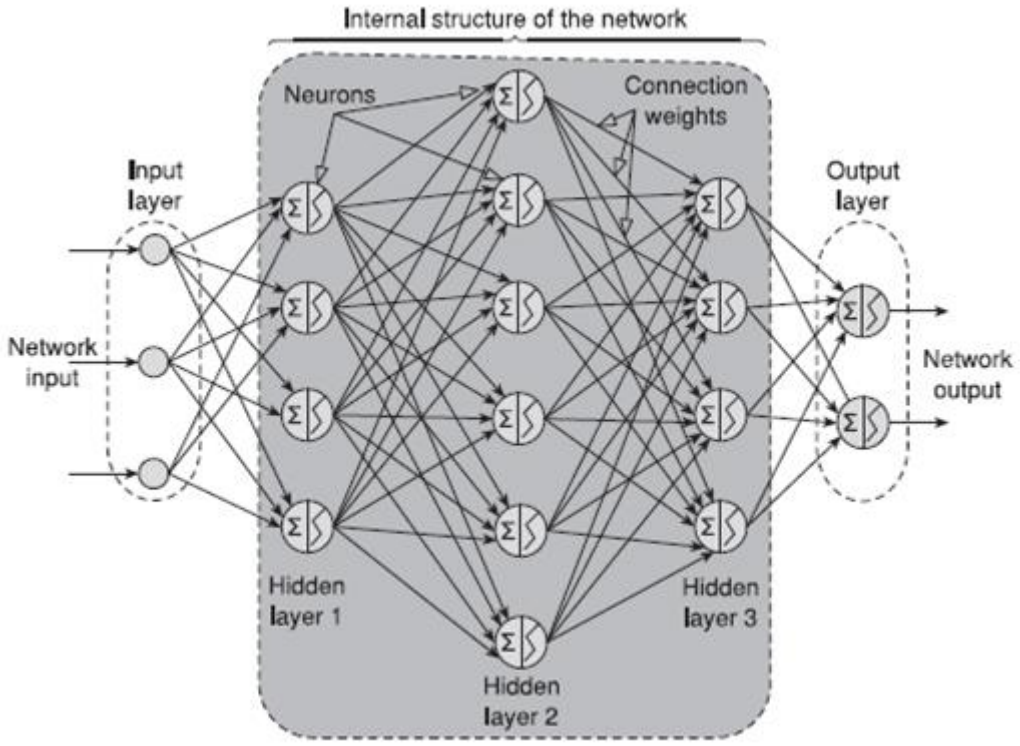

Figure B.2: Typical representation of a feedforward (unidirectional) artificial neural network with three inputs and two outputs

NEURAL NETWORK TOPOLOGIES

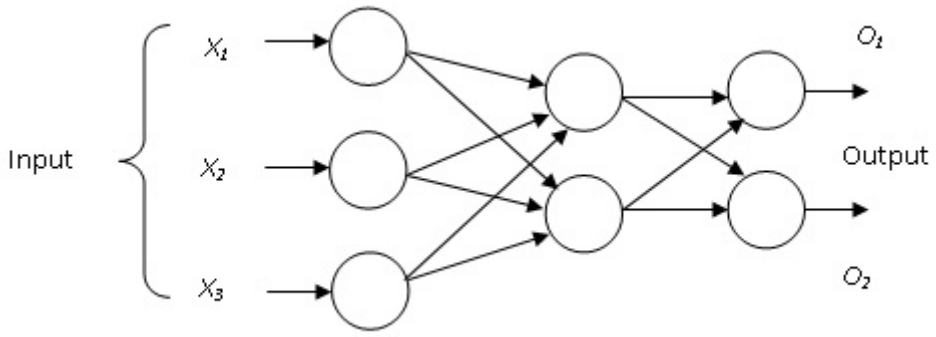

Figure B.3: Feedforward topology

These correspond to the ordering and organization of the nodes from the input layer to the output layer of the network. The two well-known ANN topologies are the feedforward and the recurrent architectures [39].

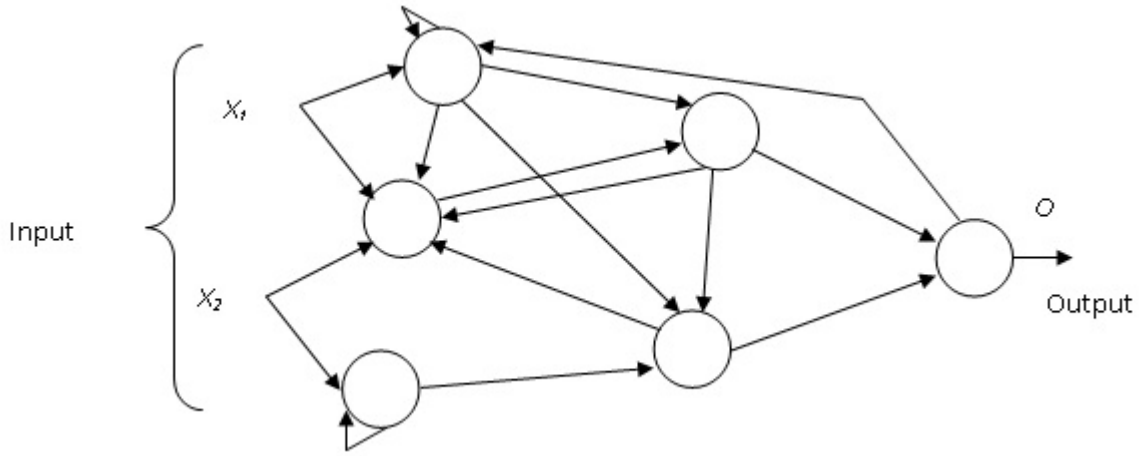

Figure B.4: Recurrent networks

A network with a feedforward (FF) architecture has its nodes hierarchically arranged in layers starting with the input layer and ending with the output layer. In between, a number of internal layers, also called hidden layers, provide most of the network computational power. The nodes in each layer are connected to the next layer through unidirectional paths [37, 38]. This means that the outputs of a given layer feed the nodes of the following layer in a forward path as shown in Figure B.3.

Unlike feedforward networks, recurrent networks (RN) allow for feedback connections among their nodes as illustrated in Figure B.4. Such networks include the Hopfield network and the time delayed neural networks (TDNN) [6, 38].

NEURAL NETWORK LEARNING ALGORITHMS

Learning algorithms are used to update the weight parameters at the interconnection level of the neurons during the training process of the network. There are three learning mechanisms namely; supervised learning mechanisms, unsupervised learning mechanisms (UL), and reinforced learning mechanisms (RL) [38].

The main feature of the supervised (or active) learning mechanism is the training by examples. This means that an external teacher provides the network with a set of input stimuli for which the output is a priori known. Supervised learning is particularly useful for feedforward networks [38].

Unlike supervised learning, unsupervised or self-organized learning does not involve an external teacher and relies instead upon local information and internal control. The training data and input patterns are presented to the system, and through predefined guidelines, the system discovers emergent collective properties and organizes the data into clusters or categories [6, 38].

For reinforced learning mechanisms, the network connections are modified according to feedback information provided to the network by its environment. This information simply instructs the system on whether or not a correct response has been obtained. In the case of a correct response, the corresponding connections leading to that output are strengthened otherwise they are weakened [6, 38].

FUZZY LOGIC

Fuzzy logic is useful in representing human knowledge in a specific domain of application and in reasoning with that knowledge to make useful inferences or actions.

In fuzzy logic, the knowledge base is represented by if-then rules of fuzzy descriptors. An example of a fuzzy rule would be, 'If the laser power is high and the pulse duration is long, then the taper angle is moderate', which contains the fuzzy descriptors high, long, and moderate. A fuzzy descriptor may be represented by a membership function. This function gives a membership grade between 0 and 1 for each possible value of the fuzzy descriptor it represents [38].

Zadeh developed the mathematics of fuzzy set theory and by extension fuzzy logic in 1965. He proposed new operations for the calculus of logic, and in principle, a generalization of classical logic. The theory proposed making the membership (or the values False and True) operate over the range of real numbers *[0, 1]*. The notion central to fuzzy systems is that truth values in fuzzy logic or membership values in fuzzy sets are indicated by a value in this range, with 0 representing absolute Falseness and 1 representing absolute Truth [41].

Fuzzy logic control is a technique of embodying human thinking into a control system. The controllers (FLC) are designed to emulate human deductive thinking, i.e., the process people use to infer conclusions from what they know [6].

A fuzzy logic system is a non-linear mapping from the input to the output space. An input is first fuzzified, that is converted from a crisp number to a fuzzy set, and subsequently processed by an inference engine that retrieves knowledge in the form of fuzzy rules contained in a rule-base. The fuzzy sets that are computed by the fuzzy inference as the output of each rule are then combined and defuzzified, that is, converted from a fuzzy set to a crisp number [41].

FUZZY INFERENCE SYSTEMS

Fuzzy inference systems are also known as fuzzy-rule-based systems, fuzzy models, fuzzy associative memories (FAM), or fuzzy controllers when used as a controller [7, 38, 41]. The system is composed of five functional blocks as shown in Figure B.5.

These are;

1. A rule base which contains a number of fuzzy IF-THEN rules.

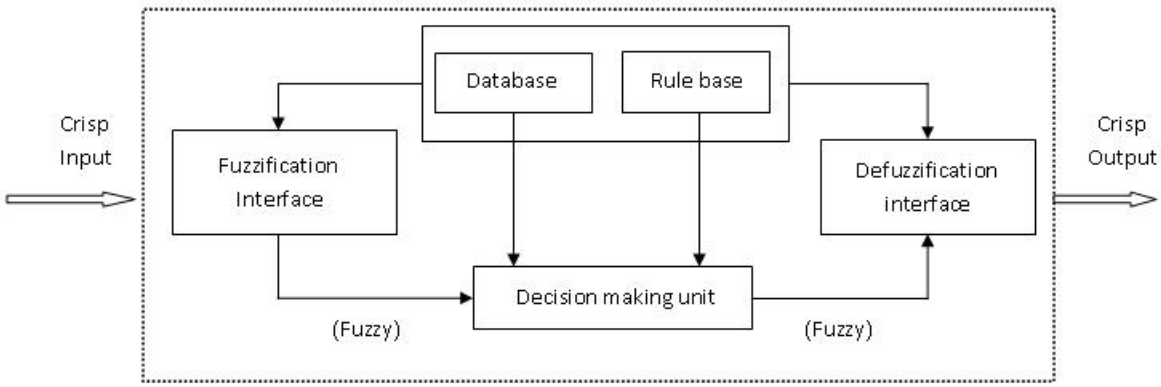

Figure B.5: Fuzzy inference system

2. A database which defines the membership functions of the fuzzy sets used in the fuzzy rules.
3. A decision-making unit which performs the inference operations on the rules.
4. A fuzzification interface which transforms the crisp inputs into degrees of match with linguistic values.
5. A defuzzification interface which transforms the fuzzy results of the inference into a crisp output.

The rule base and the database are jointly referred to as the knowledge base. The steps of fuzzy reasoning (inference operations upon fuzzy IF-THEN rules) performed by fuzzy inference systems are [7]:

1. Comparison of the input variables with the membership functions on the premise part to obtain the membership values of each linguistic label, a process called fuzzification.
2. Combination of the membership values on the premise part to get firing strength or weight of each rule through a specific T-norm operator.
3. Generation of the qualified consequent of each rule depending on the firing strength.

4. Aggregatation of the qualified consequents to produce a crisp output.

Mamdani and Takagi-sugeno inference mechanisms are the most widely used inference mechanisms. Takagi-sugeno is used in non-linear control due to its ability to model non-linear processes. Mamdani inference mechanism is used where there is need to capture human knowledge [7].

Fuzzy logic systems considerably improve machining processes, ensuring less human intervention. The systems have benefits of replicating all desired features of human input, while maintaining all the advantages of closed-loop automation control. Fuzzy systems have the following advantages [7, 38];

1. They can simulate human experience, human intelligence and experimental information for controlling a process.
2. They can be used to control very complex and uncertain processes that have the properties such as multiple-input multiple-output (MIMO) and non-linearity among others.
3. They can be used for real-time control of a process. This is because the computational task and time can be enormously reduced as compared to classical or modern control theory.